

ABSTRACT

Title of Document: SEISMIC PUSHOVER ANALYSIS OF STEEL
INTEGRAL ABUTMENT BRIDGE

Xinya Liu
Master of Science, 2018

Directed By: Professor Chung C. Fu
Department of Civil and Environmental
Engineering

Integral abutment bridges (IABs) have a continuous deck monolithically encased into abutment stem. A lack of information on their seismic design and performance may discouraged their usage in high seismic zones.

In this study, current research and implementation of IABs are comprehensively reviewed. The properties and typical construction details are presented. Three real-life IABs with steel-concrete girders provided by NYDOT are chosen as prototypes for intensive seismic study. Three-dimensional finite element models of IABs for nonlinear seismic analysis are elaborated to capture the behavior of components of steel-concrete superstructure, abutment stem, piles, backfill, etc.

Pushover analyses are carried out to obtain the capacity curve. To evaluate the seismic performance of the three IABs, capacity spectrum method from the ATC-40 specification is studied and executed by CSiBridge[®] software. By parametric studies, the effects of bearing and skew are outlined. Conclusions and some recommendations are made for seismic evaluation and design practice.

SEISMIC PUSHOVER ANALYSIS OF STEEL INTEGRAL ABUTMENT BRIDGE

By

Xinya Liu

Thesis submitted to the Faculty of the Graduate School of the
University of Maryland, College Park, in partial fulfillment
of the requirements for the degree of
Master of Science
2018

Advisory Committee:
Dr. Chung C. Fu, Chair/Advisor
Dr. Amde Amde
Dr. Brian Phillips

© Copyright by
Xinya Liu
2018

ACKNOWLEDGEMENTS

I would like to express my special thanks to my advisor, Dr. Chung C. Fu, for his knowledge and guidance during my studies. His insightfulness and encouragement are indispensable parts towards the completion of this thesis, and help me all the time when I was stuck in different challenges when doing research and writing this thesis.

Secondly I would also like to thank Dr. Amde and Dr. Philips for their valuable time serving on my thesis committee.

I am also deeply indebted to the BEST Center group members, Chaoran Xu, who helped me learning the CSiBridge software, Yunchao Ye, Yifan Zhu and Kuang-yuan Hou for providing assistance during my study.

I am also grateful to the NYDOT for providing the design drawing of bridges used in this study as example cases.

TABLE OF CONTENTS

ACKNOWLEDGEMENTS	ii
TABLE OF CONTENTS	iii
List of Tables.....	iv
List of Figures	v
CHAPTER 1: INTRODUACTION.....	1
1.1 Integral abutment bridge and its application	1
1.2 Literature review	4
1.3 Research scope of the thesis.....	5
CHAPTER 2: PROPERTIES OF INTEGRAL ABUTMENT BRIDGES AND TYPICAL CONSTRUCTION DETAILS.....	8
2.1 Categories of IAB classification by different characteristics	8
2.2 Construction details for integral and semi-integral abutment bridges.....	12
2.3 Integral bridge design in American practice	13
2.3.1 Case-1 Single span: Arthur road over I-87 S.B.	15
2.3.2 Case 2-Single skew span: NY Route 415 over Meads Creek.....	17
2.3.3 Case 3-Three-span I-87 SB Bridge over Megsville road/ black river	20
CHAPTER 3: STRUCTURAL MODELING AND DYNAMIC MODES OF INTEGRAL BRIDGES 24	24
3.1 Modeling of superstructure	25
3.2 Modeling of substructure	27
3.3 Modeling of soil-structural interaction.....	29
3.3.1 Pile-soil interaction	29
3.3.2 Abutment -soil interaction	36
3.4 Eigenvalue analysis results.....	40
CHAPTER 4: PUSHOVER ANALYSIS.....	45
4.1 Principle of pushover method.....	45
4.2 Plastic hinge assignment	45
4.3 Pushover results	47
4.4 Capacity Spectrum method	59
4.5 Evaluation by time-history analysis	65
CHAPTER 5: PARAMETRIC STUDY	69
5.1 Comparison of fully integral abutment and semi-integral abutment bridges	69
5.2 Comparison of skew and non-skew bridges.....	75
CHAPTER 6: CONCLUSIONS	84
6.1 Conclusions	84
6.2 Future work	88
REFERENCE.....	90

List of Tables

Table 2.1- Main features of the bridges in 3 cases	15
Table 3.1 - Superstructure properties of cases 1, 2 and 3	26
Table 3.2 - Framing size of cases 1, 2 and 3.....	26
Table 3.3- Properties of the piles at abutment	28
Table 3.4 - Soil properties at piles according to general notes	32
Table 3.5 - Pile-soil spring parameters of case 1	33
Table 3.6 - Pile-soil spring parameters of case 2	34
Table 3.7 - Pile-soil spring (for piles at abutment) parameters of case 3	35
Table 3.8- Pile-soil spring (for piles at pile cap) parameters of case 3.....	36
Table 3.9-Soil properties at abutments according to general notes	38
Table 3.10- Abutment-soil spring parameters of case 1	39
Table 3.11-Abutment-soil spring parameters of case 2	39
Table 3.12-Abutment-soil spring parameters of case 3	40
Table 3.13 - Modal frequencies and periods of three cases.....	44
Table 4.1 -Locations of plastic hinges.....	51
Table 4.2 - Numbers of hinges occurred in stages (case1-x).....	51
Table 4.3 - Numbers of hinges occurred in stages (case1-y).....	52
Table 4.4 - Numbers of hinges occurred in stages (case2-x).....	52
Table 4.5 - Numbers of hinges occurred in stages (case2-y).....	53
Table 4.6 - Numbers of hinges occurred in stages (case3-x).....	53
Table 4.7 - Numbers of hinges occurred in stages (case3-y).....	54
Table 4.8- Performance point data	65
Table 4.9 - Comparison of Pushover and NLTH results.....	68
Table 5.1- Comparison of IAB (Case 1) and SIAB on single span bridges	70
Table 5.2- Comparison of IAB and SIAB (Case 2) on single span skew bridges	70
Table 5.3 - Comparison of IAB and SIAB (Case3) on 3-span bridges.....	71
Table 5.4 – Performance point value of single span IAB and SIAB (Case1).....	74
Table 5.5 - Performance point value of single skew IAB and SIAB (Case2).....	74
Table 5.6 - Performance point value of 3-span IAB and SIAB (Case3).....	74
Table 5.7- Comparison of dynamic modes between skew and non-skew bridges	76
Table 5.8- Comparison of the locations of plastic hinges in skew and non-skew cases.....	76
Table 5.9- Numbers of hinges occurred in stages (non-skew bridge-x)	78
Table 5.10 - Numbers of hinges occurred in stages (non-skew bridge-y)	79
Table 5.11 -Performance point value of skew and non-skew bridges	81

List of Figures

Figure 1.1 -Schematic of a typical Integral Abutment Bridge.....	2
Figure 2.1 -Abutment details of IAB and SIAB	9
Figure 2.2-Construction details of concrete IABs and steel-concrete composite IABs	10
Figure 2.3- Layout of non-skew, skew and curved bridge	11
Figure 2.4- Construction Detail of fully-integral abutment bridges.....	12
Figure 2.5- Construction detail of Semi-Integral abutment bridges.....	13
Figure 2.6-Seismic zones and maximum magnitude for the Central, Eastern and North Eastern parts of US (Figure from source: USGS 2008)	14
Figure 2.7- Plan view of Arthur Road Bridge over I-87 S.B.....	16
Figure 2.8-Elevation view of Arthur road over I-87 S.B.....	16
Figure 2.9-Cross section of Arthur Road Bridge over I-87 S.B.	16
Figure 2.10- Pile layout of Arthur Road Bridge over I-87 S.B.	17
Figure 2.11- Abutment detail of Arthur Road Bridge over I-87 S.B.	17
Figure 2.12- Planform of NY Route 415 over Meads Creek.....	18
Figure 2.13- Elevation view of NY Route 415 bridge over Meads Creek	19
Figure 2.14- Deck cross section of NY Route 415 bridge over Meads Creek.....	19
Figure 2.15- Pile layout at beginning abutment of NY Route 415 bridge over Meads Creek.....	19
Figure 2.16- Semi-abutment detail of NY Route 415 bridge over Meads Creek	19
Figure 2.17- Planform of I-87 S.B. Bridge over Meigsville Rd.....	21
Figure 2.18- Elevation view of I-87 S.B. Bridge over Meigsville Rd.....	21
Figure 2.19- Proposed cross section I-87 S.B. over Meigsville Rd.....	21
Figure 2.20- Piles layout of I-87 S.B. over Meigsville Rd.....	22
Figure 2.21- Semi-integral abutment detail of I-87 S.B. over Meigsville Rd.	22
Figure 2.22- Pier details of I-87 S.B. over Meigsville Rd.....	23
Figure 2.23- Pile layout at pier 1 and pier 2.....	23
Figure 3.1 - Bridge finite element models.....	25
Figure 3.2 - Framing plans of cases 1, 2 and 3.....	27
Figure 3.3 - Cross section of piles in case 1	28
Figure 3.4 - Simplified P-y curve of pile-soil interaction.....	30
Figure 3.5- Schematic diagram of earth pressure along depth	31
Figure 3.6 - Simplified P-y curve of abutment-soil interaction.....	37
Figure 3.7-Force-displacement relationship of frictional resistance	38
Figure 3.8-The first five mode shapes of case 1.....	41
Figure 3.9-The first five mode shapes of case 2.....	42
Figure 3.10-The first five mode shapes of case 3.....	43
Figure 4.1 - Pile section and PM curve	46
Figure 4.2 - Moment-curvature model	46
Figure 4.3 - Steel hinge properties	47
Figure 4.4 - Order of occurrence of plastic hinges in the global x direction (Case1).....	48
Figure 4.5 - Order of occurrence of plastic hinges in the global y direction (Case1).....	48

Figure 4.6 - Order of occurrence of plastic hinges in the global x direction (Case2).....	49
Figure 4.7 - Order of occurrence of plastic hinges in the global y direction (Case2).....	49
Figure 4.8 - Order of occurrence of plastic hinges in the global x direction (Case3).....	50
Figure 4.9 - Order of occurrence of plastic hinges in the global y direction (Case3).....	50
Figure 4.10 - Case1 hinge results	55
Figure 4.11 - Case2 hinge results	55
Figure 4.12 - Case 3 hinge results	56
Figure 4.13-Case1 x-direction pushover curve with the mark of hinges yielding.....	57
Figure 4.14-Case1 y-direction pushover curve with the mark of hinges yielding.....	57
Figure 4.15-Case2 x-direction pushover curve with the mark of hinges yielding.....	58
Figure 4.16-Case2 y-direction pushover curve with the mark of hinges yielding.....	58
Figure 4.17-Case3 x-direction pushover curve with the mark of hinges yielding.....	59
Figure 4.18-Case3 y-direction pushover curve with the mark of hinges yielding.....	59
Figure 4.19 - Design response spectrum of bridge site	62
Figure 4.20 - Case1 curve results in the longitudinal direction (kips, ft)	62
Figure 4.21 - Case1 curve results in the transverse direction (kips, ft)	63
Figure 4.22 - Case2 curve results in the longitudinal direction (kips, ft)	63
Figure 4.23 - Case2 curve results in the transverse direction (kips, ft)	63
Figure 4.24 - Case 3 curve results in the longitudinal direction (kips, ft)	64
Figure 4.25- Case 3 curve results in the transverse direction (kips, ft)	64
Figure 4.26- Performance point of Case1	66
Figure 4.27- Performance point of Case2	66
Figure 4.28- Performance point of Case3	66
Figure 4.29 - Plot of time-history record with scaled 0.4g PGA.....	67
Figure 5.1-Pushover curve comparison in the x-direction of case1	72
Figure 5.2 - Pushover curve comparison in the y-direction of case1	72
Figure 5.3 - Pushover curve comparison in the x-direction of case2	72
Figure 5.4- Pushover curve comparison in the y-direction of case2	73
Figure 5.5- Pushover curve comparison in the x-direction of case3	73
Figure 5.6- Pushover curve comparison in the y-direction of case3	73
Figure 5.7-3D model of non-skew bridge	75
Figure 5.8-Order of occurrence of plastic hinges in the global x direction (non-skew bridge)....	77
Figure 5.9- Order of occurrence of plastic hinges in the global y direction (non-skew bridge)....	77
Figure 5.10-Pushover curves of skew and non-skew bridge in the x direction.....	80
Figure 5.11-Pushover curves of skew and non-skew bridge in the y direction	80
Figure 5.12-Pile displacement comparison (x-direction)	82
Figure 5.13- Pile displacement comparison (y-direction)	83
Figure 6.1-Flow chart of seismic design procedure for IABs based on capacity spectrum method	87

CHAPTER 1: INTRODUACTION

1.1 Integral abutment bridge and its application

Traditionally, bridges are always built with expansion joints to release longitudinal displacement due to temperature variations. However, it is the expansion joints which will affect smooth ride ability and make passages for water, salt, and deicing chemicals permeable to beam ends, bearing assemblies, beam seats, and substructures. As a result, this type of damage is repetitive in nature, requiring substantial maintenance funds to rectify and causing serious disruption to the travelling public.

To overcome such problems, the idea of integral abutment bridge (IABs) has been brought forth for a long time. By literature review, the early practice of integral abutment bridges can be traced back to the 1930s in US (Wolde-Tinsae, A., Klinger, J., 1987). But until recently, its application potentials have been widely recognized in many countries.

Integral bridges are designed without any expansion joints between spans or between spans and abutments. Resistance to longitudinal thermal movements and braking loads is provided by the stiffness of the soil abutting the end supports and, in some cases by the stiffness of the intermediate supports. A typical integral abutment bridge is illustrated in Figure 1.1.

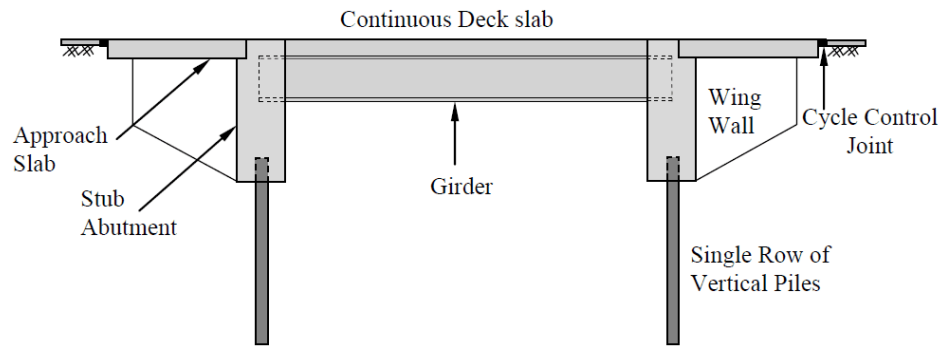


Figure 1.1 -Schematic of a typical Integral Abutment Bridge

In general, integral abutment bridges have many advantages over conventionally articulated bridges in that

- (1) Expansion joints between bridge deck and abutment may cause track irregularities, while jointless deck will provide smoother ride.
- (2) Expansion joints are the most vulnerable components in bridge deck system, and the replacement job will disrupt traffic. In contrast, integral abutment bridges will lower the maintenance efforts and minimize the traffic interruption.
- (3) Monolithic construction increases the degree of indeterminacy, which avoids the unseating during earthquake action.
- (4) Integrated bridge deck surfacing will be beneficial to blocking water ingress, and therefore minimizing the maintenance cost caused by deterioration.
- (5) Construction cost can be minimized by no use of expansion joints and bearings.

However, it has to be confessed that the application of integral abutment bridges

is not so widely accepted as conventional bridges with expansion joints. The following are among the major reasons.

- (1) The overall length of an integral abutment bridge shall be limited to a certain extent (usual no longer than 200m) to allow for thermal deformation tolerance.
- (2) The details and stiffness of the integral abutment and piles should be well engineered to ensure the structure is strong enough to resist lateral pressures that could build up behind the abutment, and yet flexible enough to accommodate movement, otherwise cracking will be occurred in abutment due to overdue or unexpected deformation.
- (3) The seismic analysis of the integral abutment bridges should be elaborately conducted to take soil-abutment interaction into consideration.

In the 1930s and 1940s, Ohio, South Dakota, and Oregon were the first to explore the area of concrete bridge. In the mid-1950s, California followed suit and began to use a non-telescopic bridge. With the advent of the international superhighway construction boom in the late 1950s and early 1960s, the construction of the jointless bridge really began its growth. By the mid-1960s, Tennessee and five other states would have a non-telescopic bridge that would be used as a standard structure (Paraschos, et.al, 2011).

In the 1970s, Britain began to study the non-expansion joints of the whole bridge. At present, in the UK, a bridge structure with no expansion joints is widely adopted in the road bridge which is within 65m. For using filler juncture of integral abutment Bridges,

British maintains permissible displacement of 25 mm is good for highway bridges, and 40 mm for railway bridges. So in the UK within 100 m of highway Bridges, within 120 m of railway Bridges may consider adopting bridge expansion joint structure.

1.2 Literature review

IABs are usually considered as a prime alternative to conventional jointed bridges. IABs have recently become very popular in North America and Europe as they provide many economical and functional advantages (Bhowmick 2003; Spyrakos and Loannidis 2003; Ahn et al. 2011; Zordan et al. 2011; Scott et al. 2013; Franchin and Pinto 2014; Briseghella and Zordan 2015). More than 10,000 IBs are in service today in the US (Maruri and Petro 2005; Fayyadh et al. 2011). In the last decade, many research studies have been conducted on IABs. Most of these research studies are concentrated on the performance of IABs under thermal loads (Faraji et al. 2001; Kalayci et al. 2012), live load distribution among the components of IABs (Dicleli and Erhan 2011), soil–structure interaction effects in IABs (Petursson and Kerokoski 2013) as well as state of art and practice of IAB design (Arockiasamy et al. 2004; Erhan, S. and Dicleli, M., 2017).

Modern IABs are known to have performed well in recent earthquakes due to the increased redundancy, larger damping resulting from cyclic soil–pile-structure interaction, smaller displacements and elimination of unseating potential (Itani and Sedarat, 2000). The monolithic construction of IABs also provides better transfer of seismic loads to the backfill and pile foundations.

In 2005, the integral abutment-backfill behavior on sand soil was study by pushover analysis on a 2-D model. A study of earthquake resistance of IABs was conducted by Purdue University in 2009, in which a time-history analysis was done on a 2-D model. In 2015, a study by Narges Easazadeh Far, Shervin Maleki and Majid Barghian combined seismic and actual thermal loads at the time of an earthquake is considered in the analysis of 2-D IAB model (Maleki, Barghian, 2015). In 2017, a study (Semih Erhan and Murat Dicleli, 2017) investigating the effect of various structural and geotechnical properties and parameters on the seismic performance of IABs and proposing practical modelling tools for their seismic analysis.

However, a research of seismic capacity of the IABs based on 3-D finite model and pushover analysis has not been provided. Accordingly, this research study is aimed at investigating the seismic capacity using capacity curves resulted from the pushover analysis. The effect of different parameters such as the properties of nonlinear materials, plastic hinges, soil springs and $M-\phi$ curves of cross section is also discussed in this study.

The results of this parametric study are then used to propose appropriate structural configurations and geotechnical properties for IABs to enhance their seismic performance.

1.3 Research scope of the thesis

The scope of this study is to investigate the capacity of the integral abutment bridges under the seismic and provide a procedure of seismic design of integral

abutments based on capacity spectrum method.

The study presents an overview of integral abutment bridges and discusses their evolution, advantages compare to conventional bridges and their limitations. The literature review includes the popular points of research of the IABs in recent years. The research utilizes three-dimensional nonlinear finite element models using the commercial structural software CSiBridge; each model incorporates the entire bridge structure, which includes the bridge superstructure, substructure and foundation as well as the soil behind the abutments and around the piles. In the nonlinear structural models, the soil–bridge interaction effects are modelled by nonlinear soil springs. The nonlinear behavior of the concrete pier columns and steel piles at the abutments are modelled using appropriate M-curvature ($M-\phi$) rules available in the CSiBridge[®] and XTRACT. The pushover analysis are conducted using displacement control and the maximum displacement is the 2% of the height of structures.

One of the main points of this study is to evaluate the seismic capacity of the IABs through capacity curves obtained from pushover analysis. In the parametric study, the effect of various structural properties on the seismic performance of IABs is investigated by varying the properties of bearings and layout plan. The other main point is to evaluate whether the structure can meet the target performance by capacity spectrum method. Nonlinear time-history analysis was also conducted as a verification of the results from pushover analysis.

The analyses results are then used to provide suggestions for the structural

properties of IABs so as to improve their seismic performance.

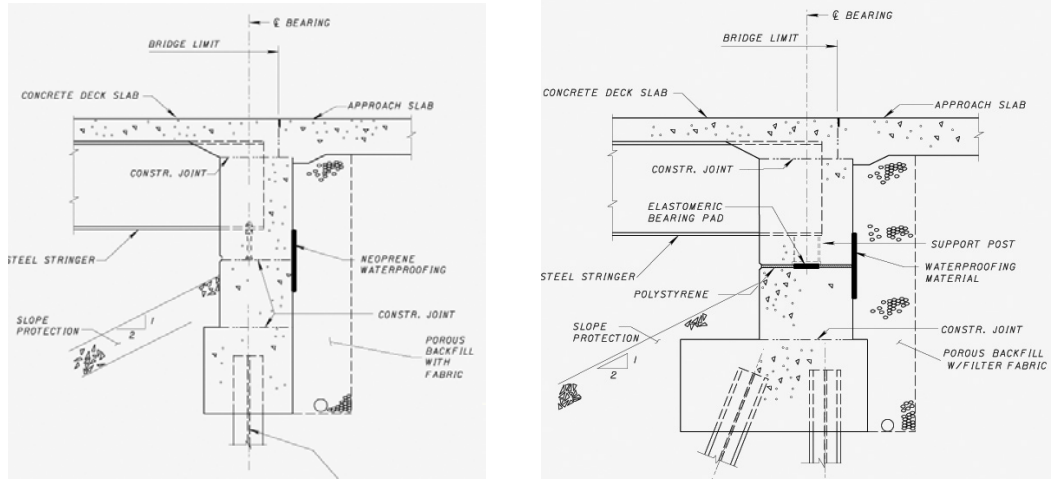
CHAPTER 2: PROPERTIES OF INTEGRAL ABUTMENT BRIDGES AND TYPICAL CONSTRUCTION DETAILS

As has been stated, integral abutment bridges have the superstructure constructed monolithically with the abutments, encasing the ends of the superstructure within the backwall. The main characteristics of integral bridges are their jointless construction and flexible abutment foundations. In principle, the system is structurally continuous, and the abutment foundation is flexible longitudinally. However, there are alternatives on general arrangement and detail construction, which will be elaborated in this chapter.

2.1 Categories of IAB classification by different characteristics

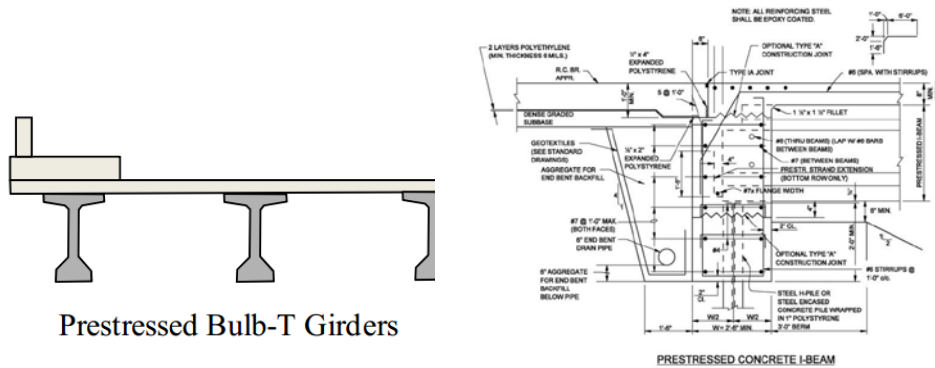
Jointless bridges can be classified into different categories by different characteristics.

- 1) From the movability of articulation, IABs can be classified into fully-integral and semi-integral bridges (SIAB). The key point of whether a bridge is fully integral or not is that the superstructure is restrained longitudinally with the pile cap or abutment stem, as shown in Figure 2.1.



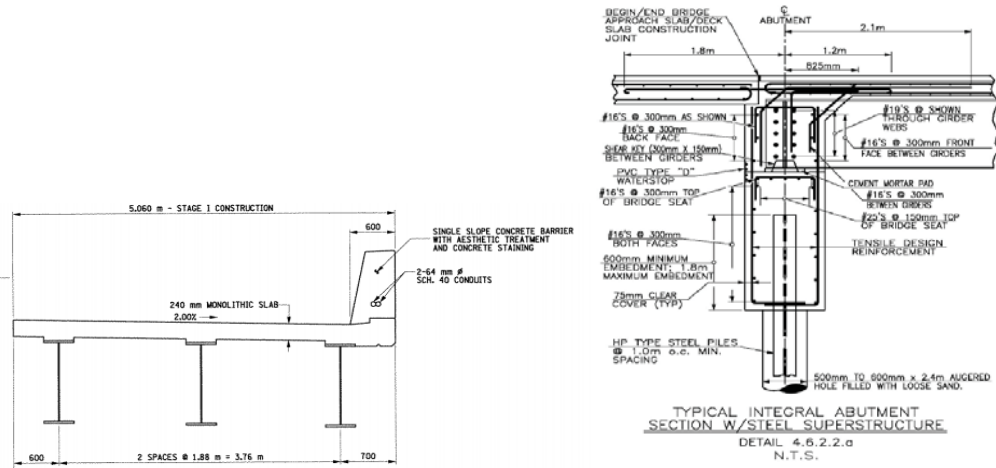
(a) Fully-integral abutment (b) Semi-integral abutment
 Figure 2.1 - Abutment details of IAB and SIAB

2) From the type of materials of deck, they can be classified into concrete IABs and steel-concrete composite IABs. The cross section and abutment connection details of concrete IABs and steel-concrete composite IABs are shown respectively in Figure 2.2.



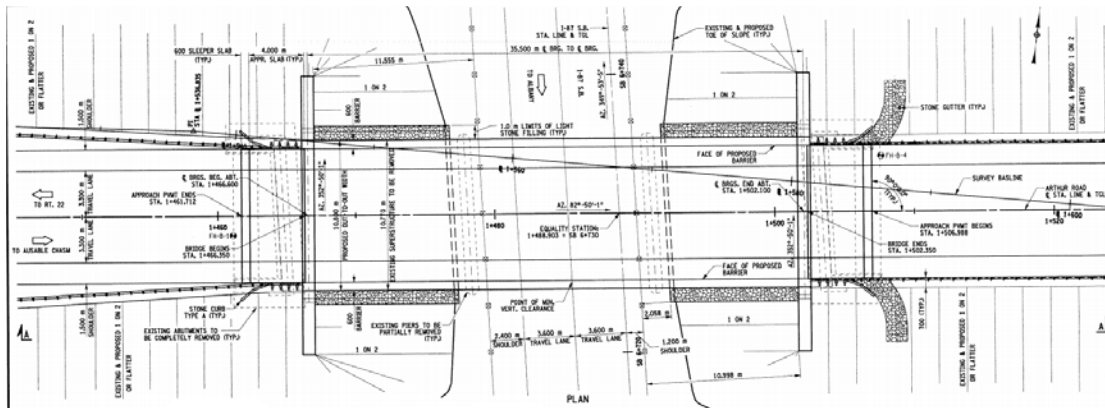
Prestressed Bulb-T Girders

(a) Concrete slab cross section and abutment details

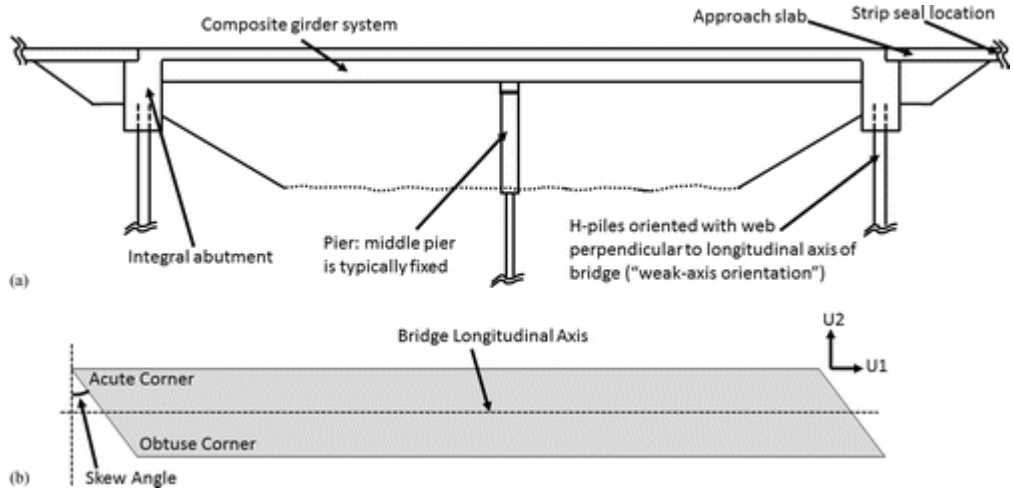


(b) Steel-concrete composite slab cross section and abutment details
 Figure 2.2-Construction details of concrete IABs and steel-concrete composite IABs

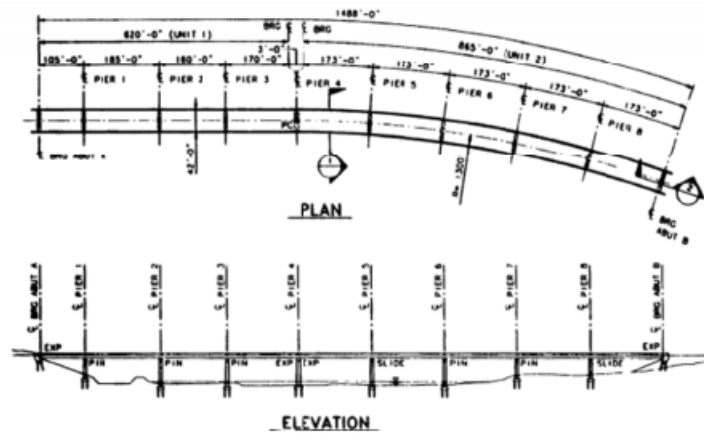
3) From the Planar layout, integral abutment bridges can be classified as non-skew IAB, skew IAB and curved IAB, as shown in Figure 2.3.



(a) Typical non-skew IAB sketch



(b) Typical skew IAB sketch



(c) Typical curved IAB sketch

Figure 2.3- Layout of non-skew, skew and curved bridge

The skew degree of integral bridges is a concern to structural engineers. Research indicates that higher skew angles result in lateral displacements of the abutment wall towards the acute side of the bridge. As a result, high stresses in the superstructure and substructure develop near the obtuse corners of skewed integral abutment bridges (Paraschos, 2016).

2.2 Construction details for integral and semi-integral abutment bridges

(A) Integral Abutment Bridge

Integral abutment bridges have the superstructure constructed monolithically with the abutments, encasing the ends of the superstructure within the backwall, as shown in Figure 2.4.

The jointless construction of the integral bridge and the superstructure requires the special design of the abutment and supporting piles. According to the survey, the integral abutment with steel pile supports is the most common form of abutment. In structural behavior, moments and shears are transferred between superstructure and abutment piles.

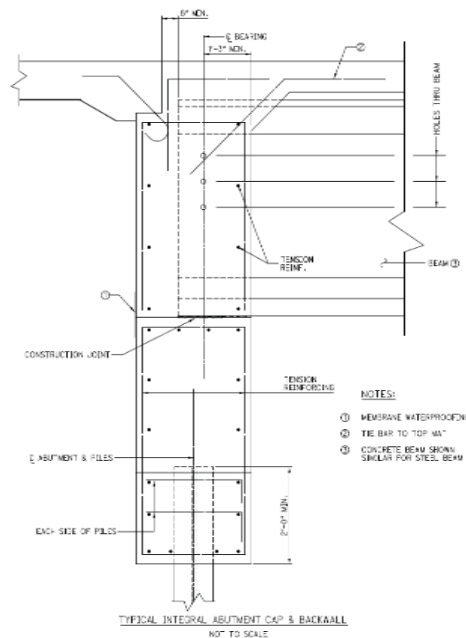
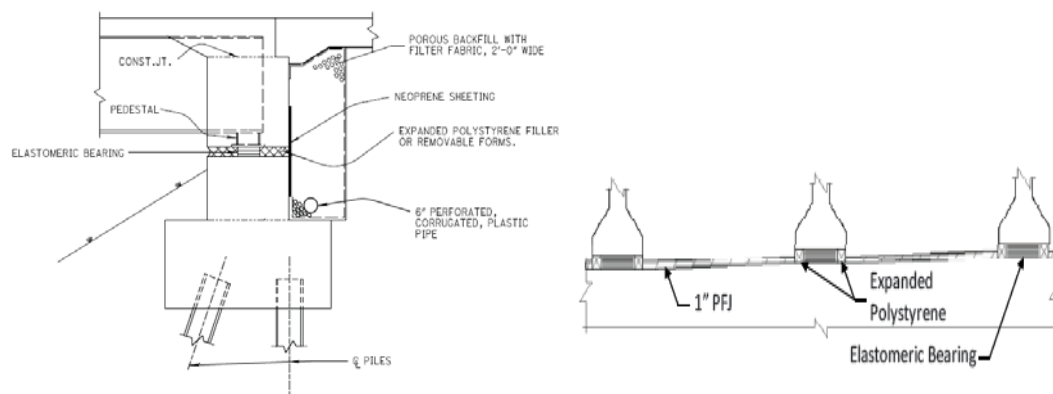


Figure 2.4- Construction Detail of fully-integral abutment bridges

(B) Semi-integral bridges

Semi-integral bridges are defined as having an end diaphragm that serves as the abutment backwall and that is cast encasing the superstructure ends. In this system, the superstructure rests on expansion bearings, and the end diaphragm is not restrained longitudinally with respect to the pile cap or abutment stem. The deck may be sliding or casted monolithically with the backwall, but it does not have a joint above the abutment. The foundation is rigid longitudinally, where superstructure movement is accommodated through bearings. Different from integral abutment bridge, moments and/or shears are not transferred between superstructure and abutment piles in semi-integral system. The semi-integral abutment is usually used for non-typical design, such as high ramp and single soil condition. The construction detail of typical semi-Integral abutment bridges is shown in Figure 2.5.



(a) Semi-abutment elevation (b) girder with pedestal

Figure 2.5- Construction detail of semi-Integral abutment bridges

2.3 Integral bridge design in American practice

The integral abutment bridge is now widely used in the United States. Most of

States reported designing and building integral abutment bridges. In this study, three IABs designed by NYDOT are shown as examples for case study.

The Figure 2.6 shows the maximum earthquake magnitude distribution in part of US; the location of the bridges studied were marked with red points. It can be observed that the location has the highest magnitude in the range of central, eastern and north eastern parts of US. Thus, to learn the seismic behavior of the bridges here is of great significance.

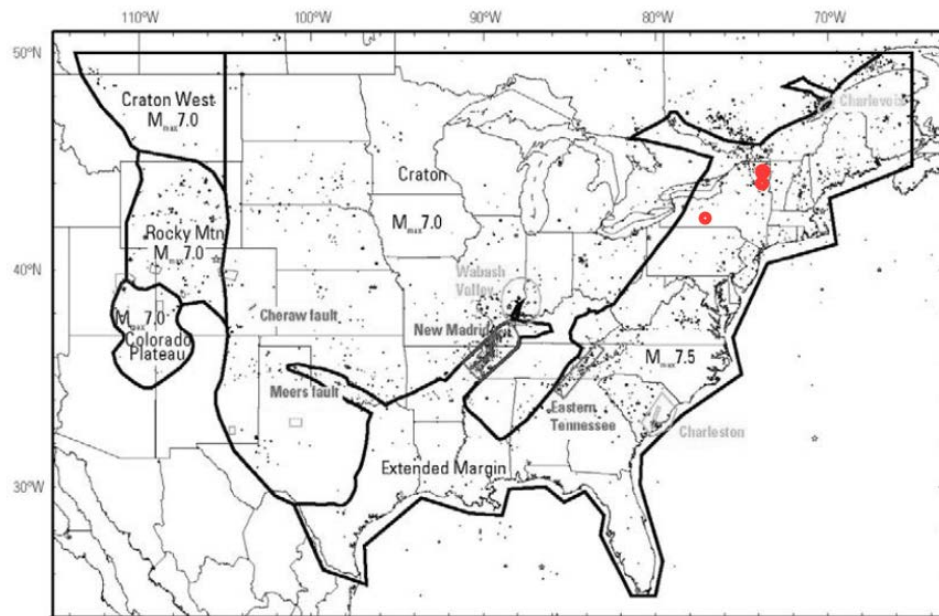


Figure 2.6-Seismic zones and maximum magnitude for the Central, Eastern and North Eastern parts of US (Figure from source: USGS 2008)

The main features of the bridges are listed in the Table 2.1 and the details of each case are stated in section 2.3.1-2.3.3.

Table 2.1- Main features of the bridges in 3 cases

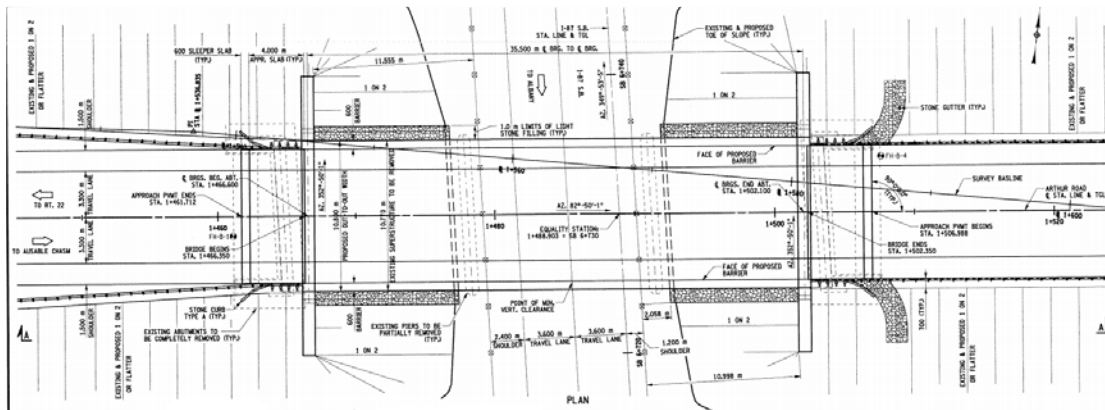
		case1	case2	case3
Planar Layout		Non-skew	Skew	Non-skew
Numbers of span		1	1	3
Span length(ft)		116.5	190	100+130+100
Girder type		Steel-concrete composite (steel I girder)		
Abutment type		integral	semi-integral	semi-integral
Bent number		/	/	2
Pile section	Shape	circle	HP-shape	
	Material	reinforced concrete	steel	

2.3.1 Case-1 Single span: Arthur road over I-87 S.B.

The Arthur Road Bridge over I-87 Southbound (44.540366N, -73.499410W) was renovated from a conventional bridge into an integral abutment one. It is a single span bridge with the span length of 35.5m (116.5ft), as shown in Figure2.7. Existing piers and abutments were removed as indicated in dash lines in Figure2.8. Also the deck was replaced from concrete slab into the steel-concrete composite one, which is shown in Figure2.9. The bridge deck is composed of a 240-mm (9.45-in.)-thick, 10.8-m(425-in)-width reinforced concrete slab supported by six I-shaped steel girders spaced at 8.83 ft. from center to center. The integral abutment are 0.9m (3ft) thick and 10.5m (34.44ft) long each, supported by 12 reinforced concrete piles with 0.324-m (1-ft)-diameter section. The layout of piles is shown in Figure2.10 and the abutment detail is shown in Figure2.11.



(a) Aerial view of the bridge site



(b) Plan view drawing

Figure 2.7- Plan view of Arthur Road Bridge over I-87 S.B.

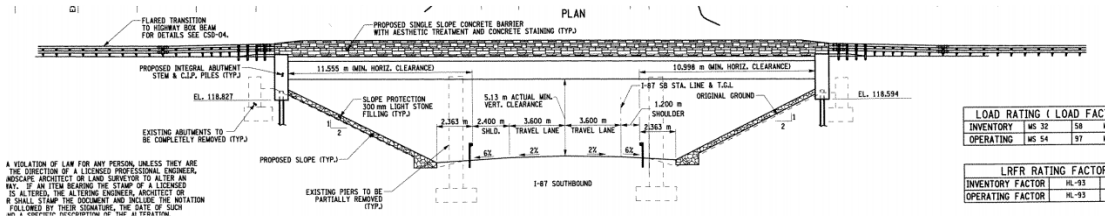


Figure 2.8-Elevation view of Arthur road over I-87 S.B.

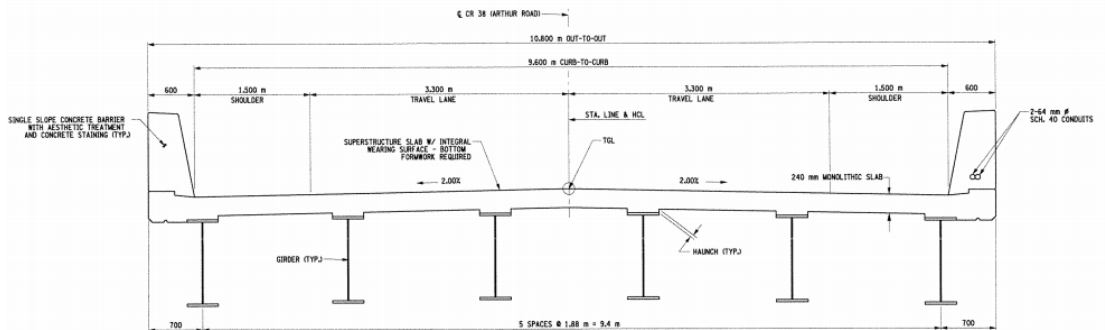


Figure 2.9-Cross section of Arthur Road Bridge over I-87 S.B.

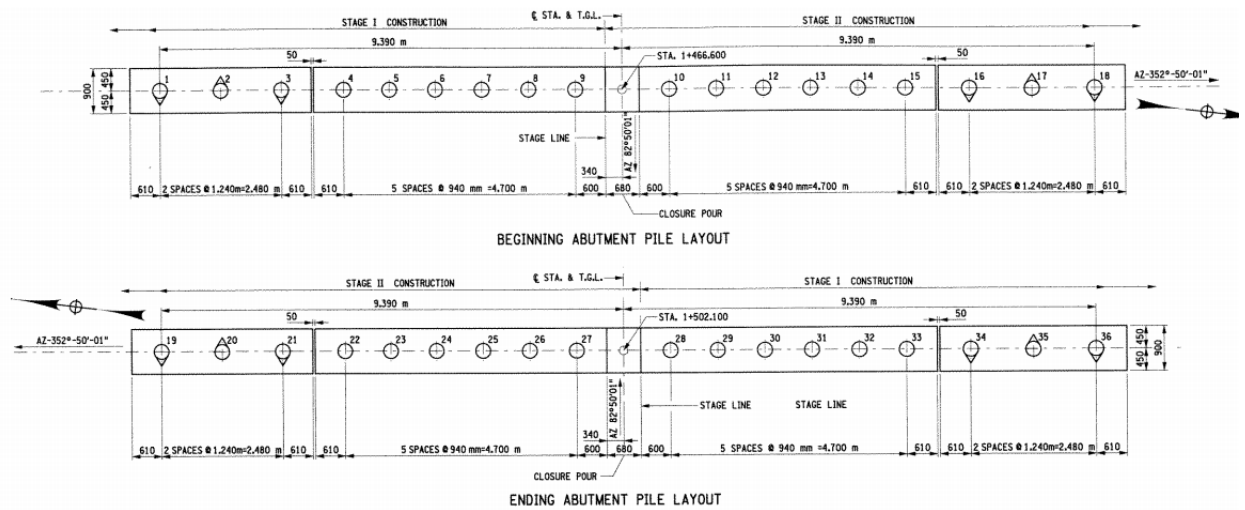


Figure 2.10- Pile layout of Arthur Road Bridge over I-87 S.B.

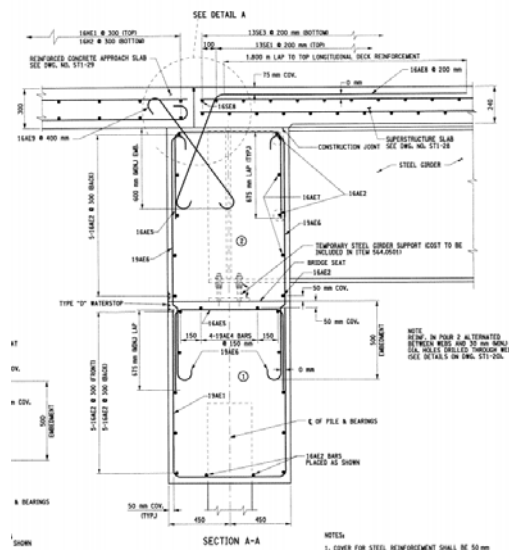


Figure 2.11- Abutment detail of Arthur Road Bridge over I-87 S.B.

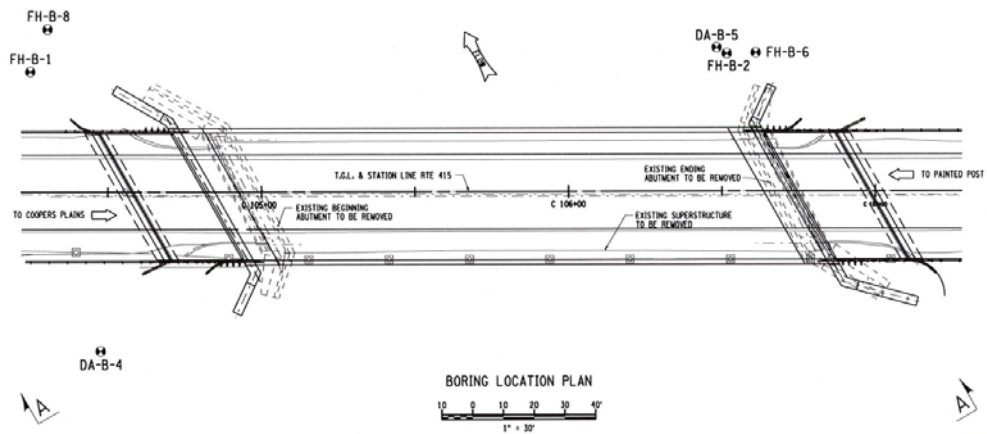
2.3.2 Case 2-Single skew span: NY Route 415 over Meads Creek

NY Route 415 over Meads Creek (42.175721N, -77.12136W) is a semi- integral abutment bridge in the NY state. It is a 190-ft long single span bridge with a skew angle of 30 degree. The bridge site is shown in Figure2.12 and the elevation view is shown in

Figure 2.13. The composite superstructure is constructed from five 6.85 ft. deep steel I girders, spacing at 112 in, and a 9.5 in. thick concrete slab with a total width of 44 ft., as shown in Figure 2.14. The abutments are 3-ft-thick and 51-ft-long each, supported by 11 HP12x84 piles in a single row spaced 56 in center to center. The layout of piles is shown in Figure 2.15 and the abutment detail is shown in Figure 2.16.



(a)



(b)

Figure 2.12- Planform of NY Route 415 over Meads Creek

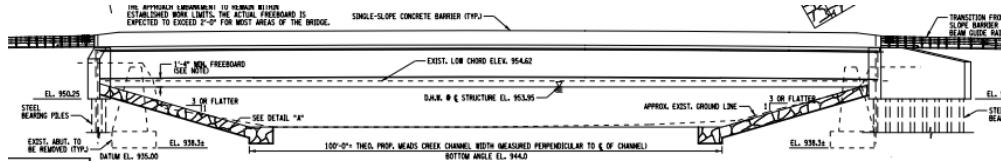


Figure 2.13- Elevation view of NY Route 415 bridge over Meads Creek

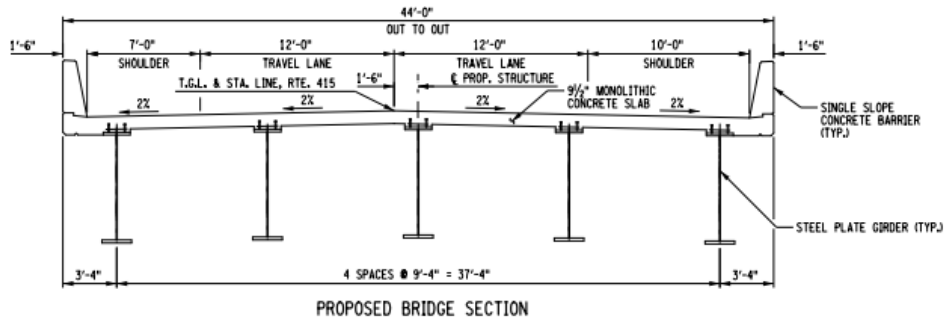


Figure 2.14- Deck cross section of NY Route 415 bridge over Meads Creek

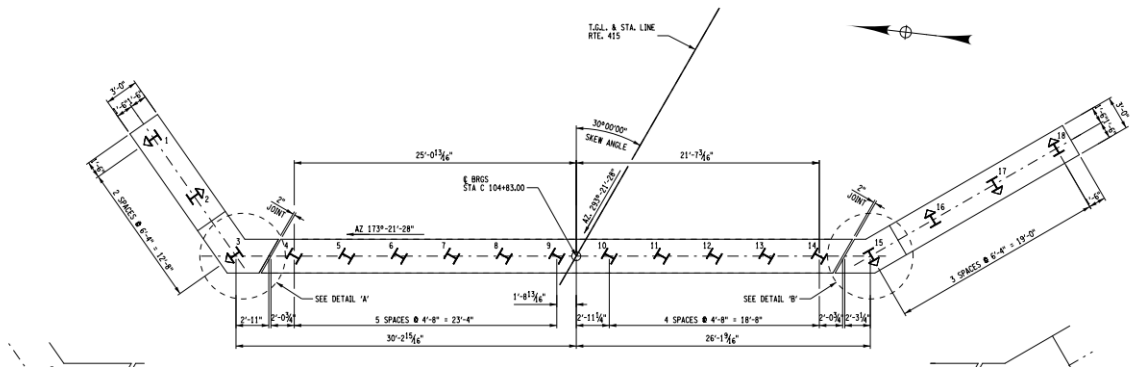


Figure 2.15- Pile layout at beginning abutment of NY Route 415 bridge over Meads Creek

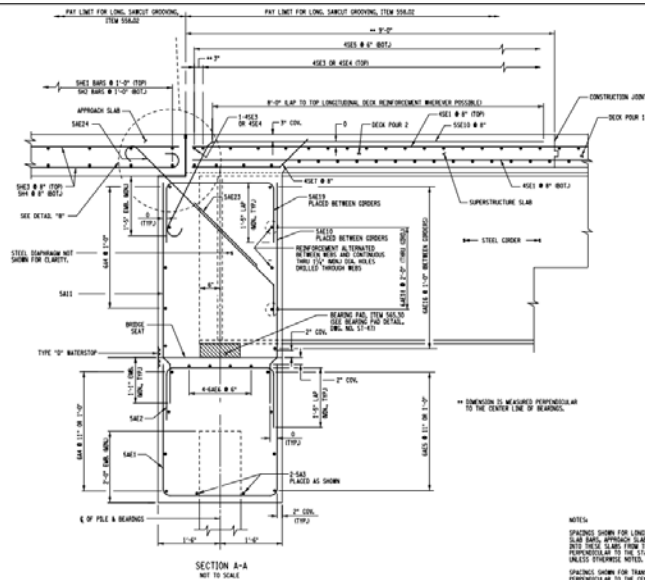


Figure 2.16- Semi-abutment detail of NY Route 415 bridge over Meads Creek

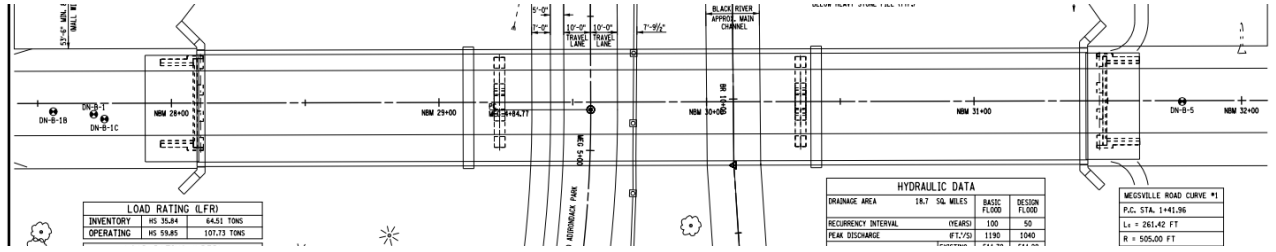
2.3.3 Case 3-Three-span I-87 SB Bridge over Megsville road/ black river

The I-87 South Bound Bridge over Megsville (44.197050N, -73.528862W) is a straight three-span semi-integral abutment bridge with a total length of 330ft and a central span of 130ft as shown in Figures 2.17 and 2.18. Similar to the previous ones, components of the bridge were retrofitted to turn a conventional bridge into a semi-integral abutment bridge.

The bridge deck is composed of a 9.5-in.-thick, 520-in-width reinforced concrete slab supported by 5 I-shaped steel girders spaced at 110in. from center to center as shown in Figure 2.19. The abutments are 3-ft-thick and 43.33-ft-long each, supported by eight HP12x84 piles in a single row spaced 69in center to center. The layout of piles at the beginning abutment is shown in Figure1.20 and the semi-abutment detail is shown in Figure1.21.



(a)



(b)
Figure 2.17- Planform of I-87 S.B. Bridge over Meigsville Rd.

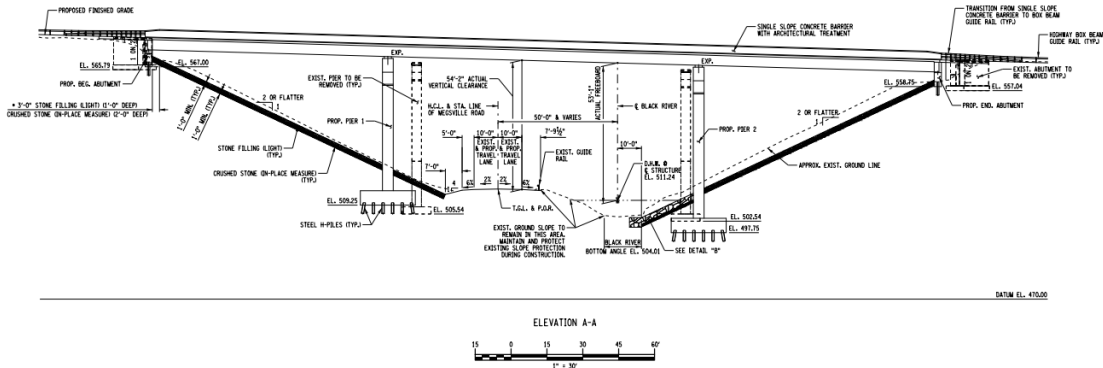


Figure 2.18- Elevation view of I-87 S.B. Bridge over Meigsville Rd.

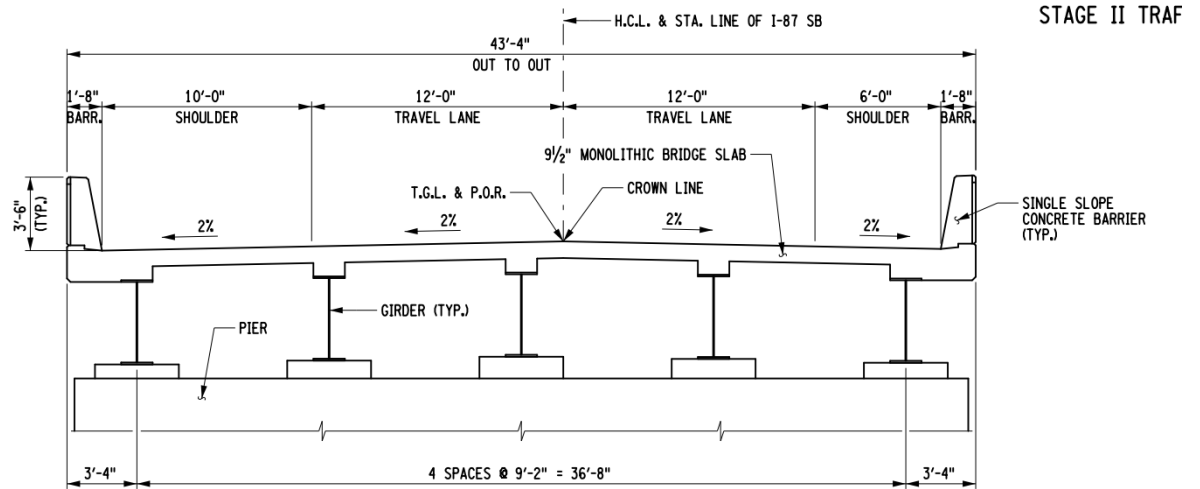


Figure 2.19- Proposed cross section I-87 S.B. over Meigsville Rd.

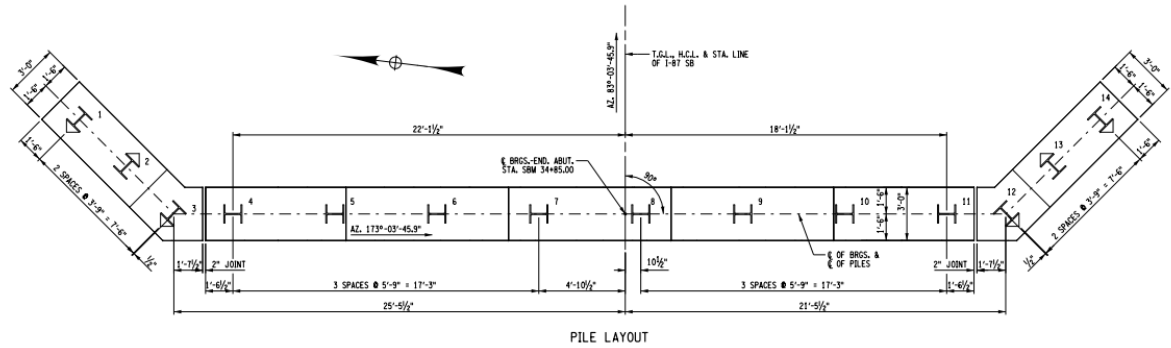


Figure 2.20- Piles layout of I-87 S.B. over Meigsville Rd.

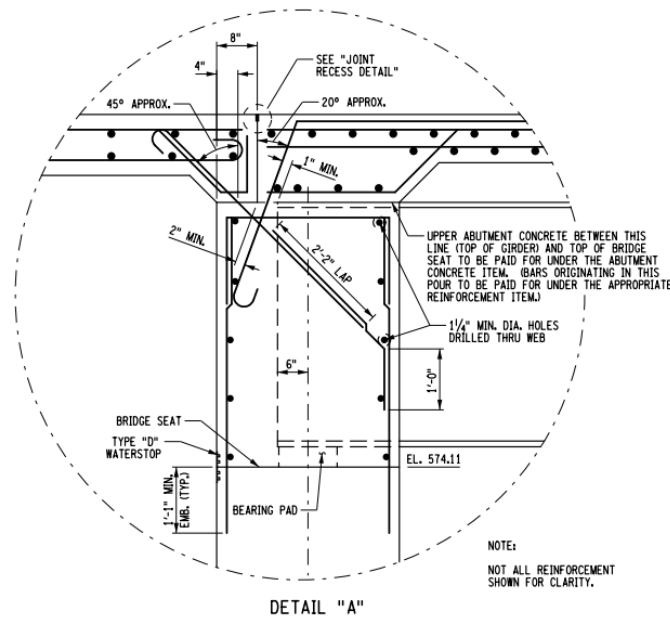
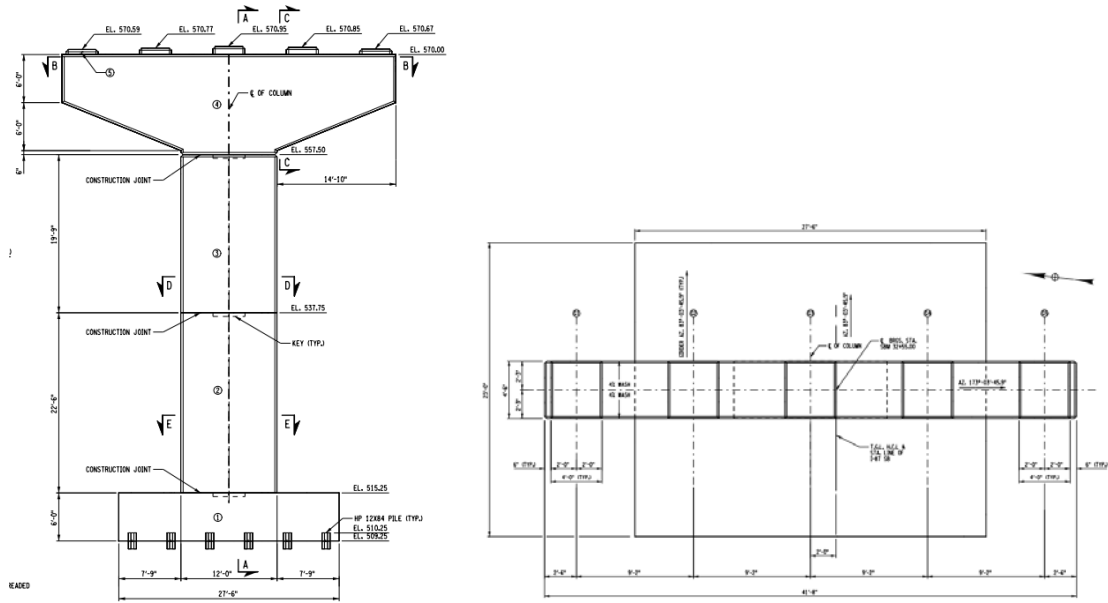


Figure 2.21- Semi-integral abutment detail of I-87 S.B. over Meigsville Rd.

The two piers are supported on single columns with a height of 50ft and 42ft, respectively. Figure 2.22 (a) and 2.22 (b) show the elevation view of the pier1 and cross section of cap, respectively. The layout of pile at piers is shown in Figure 2.23. It is shown that each pile cap is 330in by 276in and 72in thick and supported by 36 HP12x84 steel piles with the length of 50ft. All piles are in weak axis in longitudinal direction.



(a) Elevation view (b) Plan view
 Figure 2.22- Pier details of I-87 S.B. over Meigsville Rd.

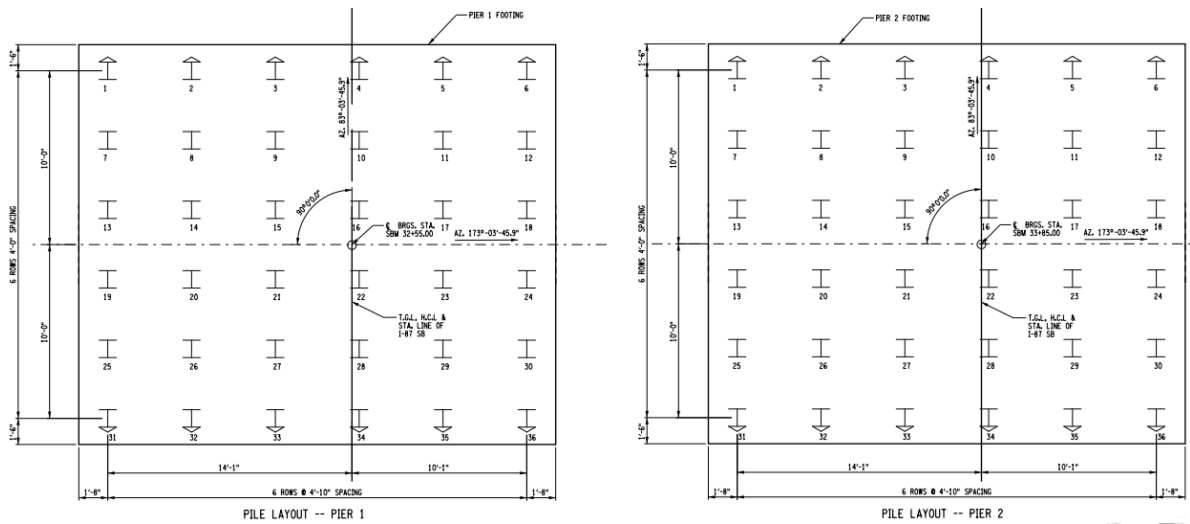
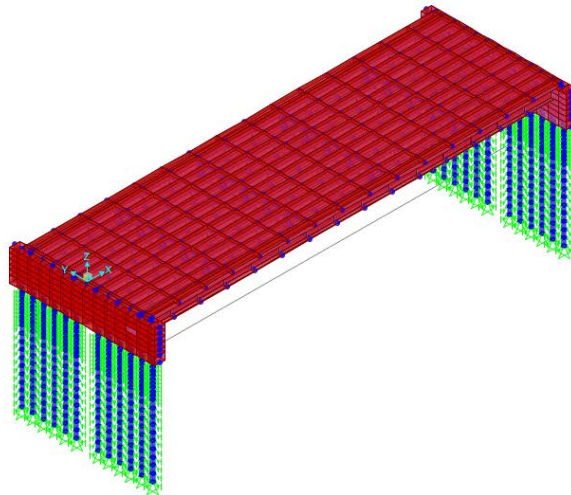


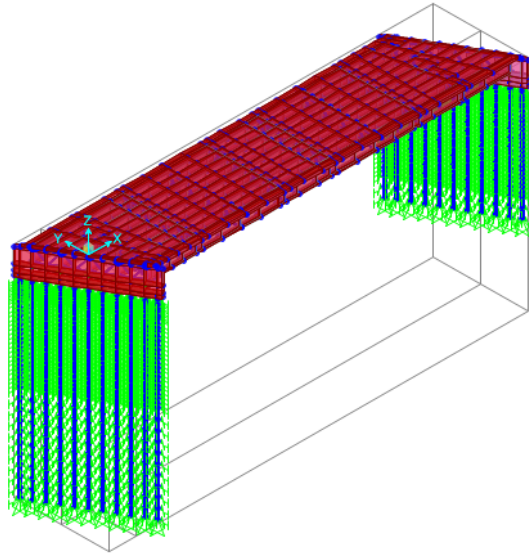
Figure 2.23- Pile layout at pier 1 and pier 2

CHAPTER 3: STRUCTURAL MODELING AND DYNAMIC MODES OF INTEGRAL BRIDGES

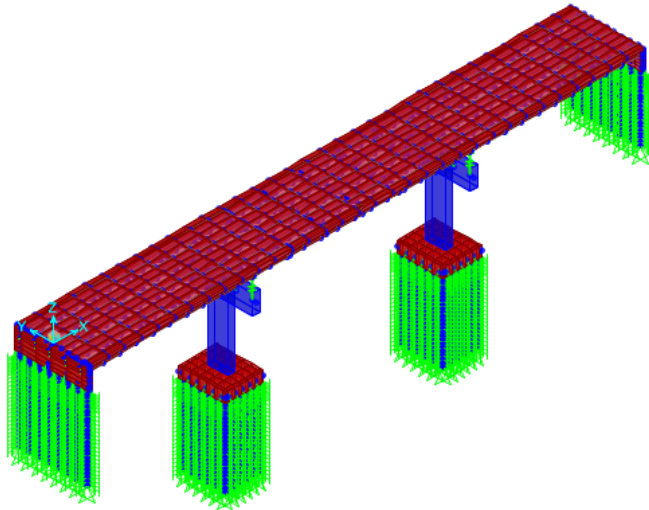
The three-dimensional nonlinear finite element models was established by CSiBridge[®]. Each model incorporates the entire bridge structure, including the bridge superstructure, substructure and foundation as well as the soil behind the abutments and around the piles. The entire models of three cases are shown in Figure 3.1.



(a) Model of case 1 - Simple span: Arthur road over I-87 S.B



(b) Model of case 2 - Simple skew span: NY Route 415 over meads creek



(c) Model of case 3 - Three-span I-87 SB over Megsville road/ black river

Figure 3.1 - Bridge finite element models

3.1 Modeling of superstructure

The bridge superstructure was modelled using 3-D shell elements. Full composite action between the slab and the girders was assumed.

Properties of the superstructure for three cases are listed in Table3.1.

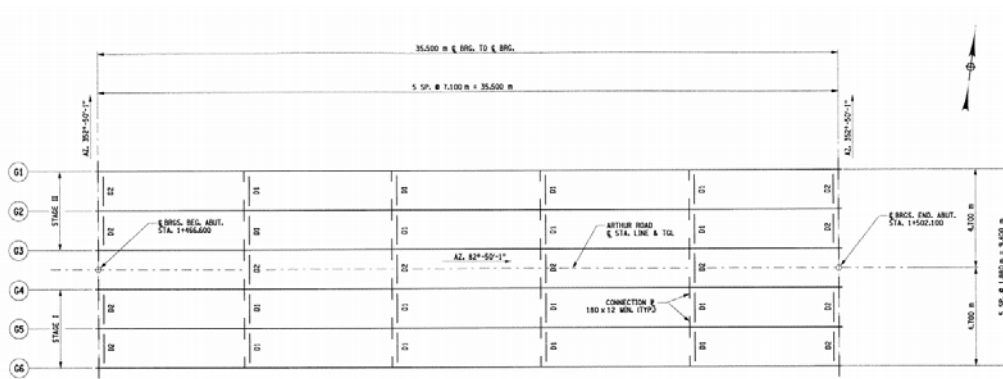
Table 3.1 - Superstructure properties of cases 1, 2 and 3

	total width(in)	concrete slab thickness (in)	concrete strength (psi)	steel girder					material
				top flange(in)	bottom flange(in)	web(in)	numbers	space(in)	
case 1	425	9.5	3000	18x1.25	22x1.57	43x0.4724	6	74	ASTM A709 G345W(50W)
case 2	528	9.5	3000	20x2	22x2.25	78x0.6875	5	110	ASTM A709 G50W
case 3	520	9.5	3000	18x1	18x1.125	46x0.5625	5	112	ASTM A709 G50W

Beam elements are used to model the diaphragms. The framing layout plan of cases 1, 2 and 3 are shown in Figure 3.2 and sizes of framing are listed in Table 3.2.

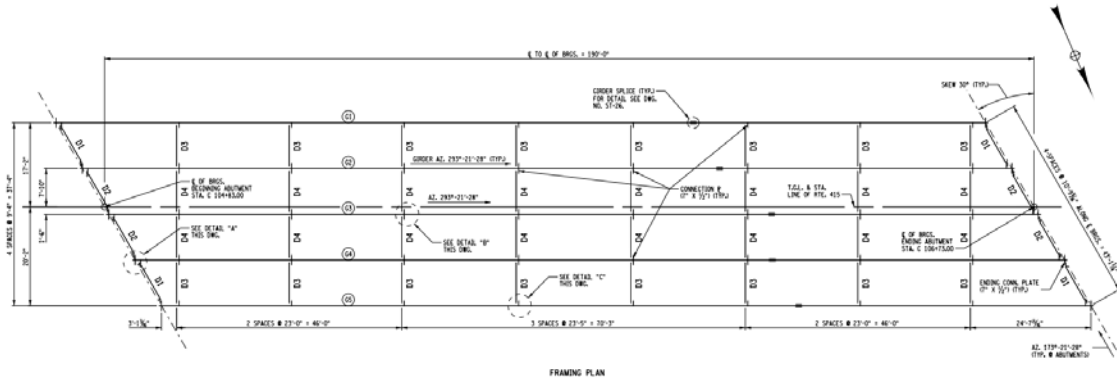
Table 3.2 - Framing size of cases 1, 2 and 3

	D1(D3)		D2(D4)		unit
	Top& Bottom cord	Brace	Top cord	Brace	
case 1	L76x76x9.5	L76x76x9.5	L76x76x9.5	L76x76x9.5	mm
case 2	L4x4x3/8	L4x4x3/8	L4x4x3/8	L4x4x3/8	in
case 3	L4x4x3/8	L3x3x3/8	L4x4x3/8	L3x3x3/8	in

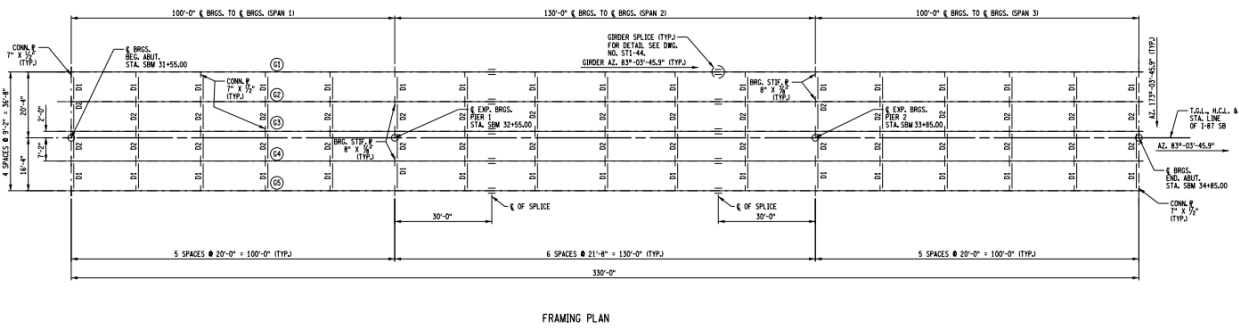


FRAMING PLAN

(a) Framing plan of case 1



(b) Framing plan of case 2



(c) Framing plan of case 3

Figure 3.2 - Framing plans of cases 1, 2 and 3

3.2 Modeling of substructure

Abutment -

Abutments are modeled by thick shell elements. For fully integral abutment in case 1, the fixed bolts are simulated by links that fixed all six DOFs. For the semi-integral abutment in cases 2 and 3, the bearing pads at abutment are simulated by links that fixed y and z translational DOFs.

Pile -

The piles in case 1 are reinforced concrete piles. They are 324mm (12.756in) in diameter with 7mm (0.276in) minimum wall thickness and 50mm (1.97in) cover as

shown is Figure 3.3. Six #19 (metric units, #6 in imperial units) longitudinal bars are equally spaced and the spiral bars are in the size of #10 (metric units, #3 in imperial units).

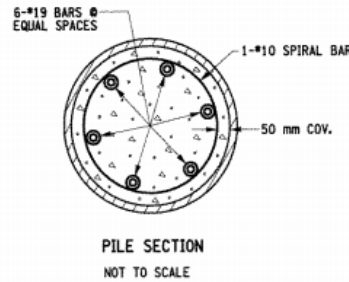


Figure 3.3 - Cross section of piles in case 1

The piles at abutments in cases 2 and 3 are HP12x84 steel piles located in the weak axis along the longitudinal direction. Properties of the piles at abutment in these three cases are listed in Table 3.3.

Table 3.3- Properties of the piles at abutment

pile	Size	Number	Space(in)	Material		Length(ft)	
						Beginning abutment	Ending abutment
case 1	324mm-diameter	12	37	concrete	3000psi	30	30
case 2	HP12x84	11	69	steel	ASTM A572 G50	100	60
case 3	HP12x84	8	69	steel	ASTM A572 G50	50	40

The piles are modeled by beam elements and subdivided into numbers of segment. The 2ft embedded length was considered in the model, allowing full moment transfer between piles and abutments. At the end of each pile, restrains that fix three translational DOFs are assigned.

At the nodes along piles, soil springs were assigned to simulate the lateral

pile-soil interaction, which will be discussed in section 3.3.

Pier and group piles in case 3:

Beam elements are used to model the piers and cap beams. The expansion bearings are simulated by links that released in the x direction.

The group piles are modelled by beam elements and the pile cap that supported by these piles are in shell elements. To link the pier and the cap, the constraint is used to connect the bottom of the pier column to the center of the planar pile cap. The piles are HP12x84 steel piles in the length of 50ft, located with strong axis in the longitudinal direction. The piles are fixed at the top with caps by common nodes and the piles are fixed at the bottom to the ground.

3.3 Modeling of soil-structural interaction

The soil-pile and soil-abutment interaction simulation is an important structural modeling part of seismic behavior analysis of IABs. The soil-pile interaction has significant effects on the overall structural dynamic characteristics.

3.3.1 Pile-soil interaction

The pile-soil interaction can be defined by a nonlinear force (P)-displacement(Y) curve, where P is the lateral resistance of soil and Y is the lateral displacement. In this study, the actual nonlinear P-Y curves of soil are simplified with an elastic-plastic force-displacement curve relating the ultimate resistance of the soil as shown in Figure

3.4. The pile-soil springs were modelled by non-linear joint link elements in CSiBridge®.

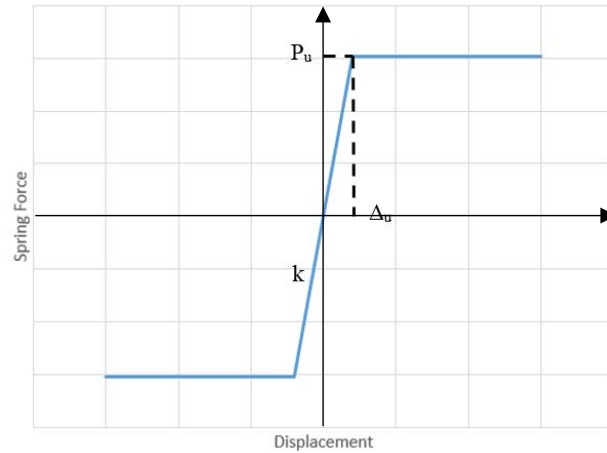


Figure 3.4 - Simplified P-y curve of pile-soil interaction

The soil around the piles is assumed sand according to the soil information used in the design given in the general notes. The Broms method (Broms, M, 1964) is used in this study to calculate the soil resistance. According to Broms method, the maximum soil resistance per unit length of pile in the less cohesive soils is assumed to be three times the Rankine passive earth pressure times the pile diameter. Thus, as shown in Figure 3.5, at a depth z below the ground surface, the soil resistance P_z (lb. /ft) can be obtained as follows:

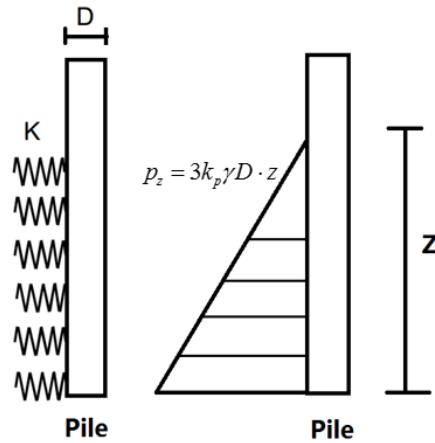


Figure 3.5- Schematic diagram of earth pressure along depth

$$p_z = 3k_p \gamma D \cdot z \quad (3-1)$$

The equivalent maximum force P_u (lb) for each spring is:

$$P_u = p_z \cdot s = 3k_p \gamma D \cdot z \cdot s \quad (3-2)$$

The soil spring stiffness k (lb/ft) at the depth of z :

$$k = n_h \cdot z \cdot s \quad (3-3)$$

The maximum displacement:

$$\Delta_u = \frac{P_u}{k} \quad (3-4)$$

Where:

$k_p = \tan^2(45^\circ + \frac{\phi}{2})$, which is the coefficient of passive earth pressure.

ϕ is the friction angle.

γ (lb/ft³) is the unit weight of soil

D (ft) is the width of diameter of pile

s (ft) is the space of soil springs

$$n_h = \frac{J\gamma}{1.35}$$

is the constant of the subgrade reaction

J =200 for loose sand ($\phi=30^\circ$)

=600 for medium sand ($\phi=35^\circ$)

=1500 for dense sand ($\phi=40^\circ$)

In the general notes of each drawing, values of unit weight of soil and friction angle are given as listed in Table 3.4; the passive earth pressure coefficient should be divided by 1.25.

Table 3.4 - Soil properties at piles according to general notes

	location	unit weight (lb/ft ³)	friction angle
case 1	piles support abutment	133	40
case 2	piles support abutment	120	30
case 3	piles support abutment	120	30
	piles support cap	120	35

The soil reaction is linearly increased with depth; for the soil spring stiffness k is proportional to Pu, the soil spring stiffness varies with depth.

For the piles in case 1, the soil springs spaced at 1 ft. for the top 10ft and at 2ft for the remaining 30ft for both beginning and ending abutment. The properties of the soil springs along the piles are listed in Table 3.5.

Table 3.5 - Pile-soil spring parameters of case 1

NO.	Z(ft)	S(ft)	Dense	
			k(Kips/in)	Pu(kips)
1	1	1.5	18.47	2.33
2	2	1	24.63	3.11
3	3	1	36.94	4.67
4	4	1	49.26	6.22
5	5	1	61.57	7.78
6	6	1	73.89	9.34
7	7	1	86.20	10.89
8	8	1	98.52	12.45
9	9	1	110.83	14.00
10	10	1.5	184.72	23.34
11	12	2	295.56	37.35
12	14	2	344.81	43.57
13	16	2	394.07	49.79
14	18	2	443.33	56.02
15	20	2	492.59	62.24
16	22	2	541.85	68.47
17	24	2	591.11	74.69
18	26	2	640.37	80.91
19	28	2	689.63	87.14
20	30	2	738.89	93.36

The maximum displacement: $\Delta_u = \frac{P_u}{k} = 0.126in$

For the piles in case 2, the soil springs spaced at 1 ft. for the top 10ft, at 2ft for the middle 40ft and at 5ft for the remaining 50ft at the beginning abutment; the soil springs spaced at 1 ft. for the top 10ft, at 2ft for the middle 40ft and at 5ft for the remaining 10ft at the ending abutment. The properties of the soil springs along the piles are listed in Table 3.6.

Table 3.6 - Pile-soil spring parameters of case 2

NO.	Z(ft)	s(ft)	Loose		NO.	Z(ft)	s(ft)	Loose	
			K(kips/in)	Pu(kips)				K(kips/in)	Pu(kips)
1	1	1.5	2.22	1.33	21	32	2	94.81	56.68
2	2	1	2.96	1.77	22	34	2	100.74	60.22
3	3	1	4.44	2.66	23	36	2	106.67	63.76
4	4	1	5.93	3.54	24	38	2	112.59	67.31
5	5	1	7.41	4.43	25	40	2	118.52	70.85
6	6	1	8.89	5.31	26	42	2	124.44	74.39
7	7	1	10.37	6.20	27	44	2	130.37	77.93
8	8	1	11.85	7.08	28	46	2	136.3	81.48
9	9	1	13.33	7.97	29	48	2	142.22	85.02
10	10	1.5	22.22	13.28	30	50	2	148.15	88.56
11	12	2	35.56	21.25	31	55	3.5	285.19	170.48
12	14	2	41.48	24.80	32	60	5	444.44	265.68
13	16	2	47.41	28.34	33	65	5	481.48	287.82
14	18	2	53.33	31.88	34	70	5	518.52	309.96
15	20	2	59.26	35.42	35	75	5	555.56	332.1
16	22	2	65.19	38.97	36	80	5	592.59	354.24
17	24	2	71.11	42.51	37	85	5	629.63	376.38
18	26	2	77.04	46.05	38	90	5	666.67	398.52
19	28	2	82.96	49.59	39	95	5	703.7	420.66
20	30	2	88.89	53.14	40	100	5	740.74	442.8

The maximum displacement: $\Delta_u = \frac{P}{k} = 0.598in$

For the piles at abutment in case 3, the soil springs spaced at 1 ft. for the top 10ft and at 2ft for the remaining 40ft at the beginning abutment; the soil springs spaced at 1 ft. for the top 10ft and at 2ft for the remaining 30ft at the ending abutment. Properties of the soil springs along the piles are listed in Table 3.7.

Table 3.7 - Pile-soil spring (for piles at abutment) parameters of case 3

No.	Z(ft)	s(ft)	Loose		No.	Z(ft)	s(ft)	Loose	
			K(kips/in)	Pu(kips)				K(kips/in)	Pu(kips)
1	1	1.5	2.22	1.33	16	22	2	65.19	38.97
2	2	1	2.96	1.77	17	24	2	71.11	42.51
3	3	1	4.44	2.66	18	26	2	77.04	46.05
4	4	1	5.93	3.54	19	28	2	82.96	49.59
5	5	1	7.41	4.43	20	30	2	88.89	53.14
6	6	1	8.89	5.31	21	32	2	94.81	56.68
7	7	1	10.37	6.20	22	34	2	100.74	60.22
8	8	1	11.85	7.08	23	36	2	106.67	63.76
9	9	1	13.33	7.97	24	38	2	112.59	67.31
10	10	1.5	22.22	13.28	25	40	2	118.52	70.85
11	12	2	35.56	21.25	26	42	2	124.44	74.39
12	14	2	41.48	24.80	27	44	2	130.37	77.93
13	16	2	47.41	28.34	28	46	2	136.3	81.48
14	18	2	53.33	31.88	29	48	2	142.22	85.02
15	20	2	59.26	35.42	30	50	2	148.15	88.56

The maximum displacement:
$$\Delta_u = \frac{P_u}{k} = 0.598in$$

For the piles at cap in case 3, the soil springs spaced at 1 ft. for the top 10ft and at 2ft for the remaining 40ft, whose properties are listed in Table 3.8.

Table 3.8- Pile-soil spring (for piles at pile cap) parameters of case 3

No.	Z(ft)	s(ft)	Medium		No.	Z(ft)	s(ft)	Medium	
			K(kips/in)	Pu(kips)				K(kips/in)	Pu(kips)
1	1	1.5	6.67	1.63	16	22	2	195.56	47.93
2	2	1	8.89	2.18	17	24	2	213.33	52.29
3	3	1	13.33	3.27	18	26	2	231.11	56.65
4	4	1	17.78	4.36	19	28	2	248.89	61.00
5	5	1	22.22	5.45	20	30	2	266.67	65.36
6	6	1	26.67	6.54	21	32	2	284.44	69.72
7	7	1	31.11	7.63	22	34	2	302.22	74.08
8	8	1	35.56	8.71	23	36	2	320.00	78.43
9	9	1	40.00	9.80	24	38	2	337.78	82.79
10	10	1.5	66.67	16.34	25	40	2	355.56	87.15
11	12	2	106.67	26.14	26	42	2	373.33	91.50
12	14	2	124.44	30.50	27	44	2	391.11	95.86
13	16	2	142.22	34.86	28	46	2	408.89	100.22
14	18	2	160.00	39.22	29	48	2	426.67	104.58
15	20	2	177.78	43.57	30	50	2	444.44	108.93

The maximum displacement: $\Delta_u = \frac{P_u}{k} = 0.245in$

3.3.2 Abutment -soil interaction

The abutment-soil interaction consists of two parts: compressive resistance in the longitudinal direction and friction of interface in the transverse direction.

Abutment-soil springs were added on the abutment elements as area springs. For the longitudinal springs, they simulated the compressive resistance generated by soil when the abutments move toward it and no tension forces when the abutments move away from soil. The elastic-plastic force-displacement characteristics are shown in Figure 3.6.

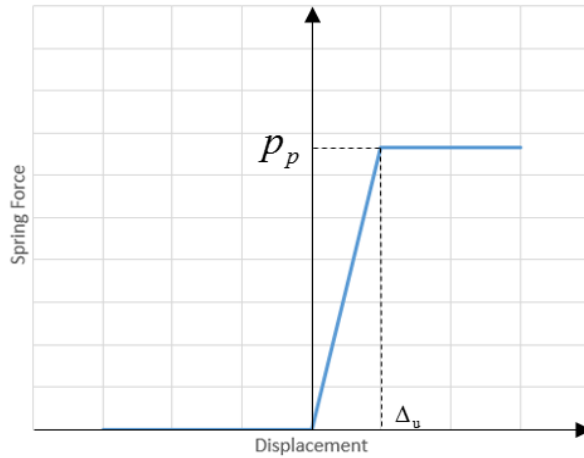


Figure 3.6 - Simplified P-y curve of abutment-soil interaction

According to the Rankine's earth pressure, the backfill horizontal-passive earth pressure at the depth of z is determined as:

$$p_p = \gamma z k_p \quad (3-5)$$

Where $k_p = \tan^2(45^\circ + \frac{\phi}{2})$, which is the coefficient of passive earth pressure. ϕ is the friction angle. γ (lb/ft³) is the unit weight of soil.

The magnitude of movement required to reach the passive state is commonly assumed as 2% of wall height (Robert J. Frosch, 2008). This value is also appears in the AASHTO Specifications.

Frictional resistance was modeled by joint springs with plastic property. According to the procedure proposed by Fang (1991), the coefficient of friction between soil and concrete was estimated as 0.6. The resistance was estimated in equation (3-6) per unit area. The force-displacement relationship is shown in Figure 3.7.

$$p_f = 0.6P_p \quad (3-6)$$

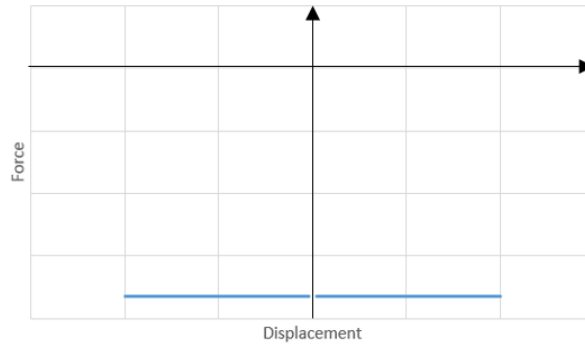


Figure 3.7-Force-displacement relationship of frictional resistance

Table 3.9 listed the parameters of soil at abutments from the general notes of cases 1, 2 and 3.

Table 3.9-Soil properties at abutments according to general notes

	Location	Unit weight γ (lb/ft ³)	Friction angle ϕ (degree)
Case 1	Abutment	120	30
Case 2	Abutment	120	30
Case 3	Abutment	120	30

The parameters of area soil springs of cases 1, 2 and 3 are shown in Tables 3.10-3.13. For case 1, the beginning and ending abutment have the same dimension; for cases 2 and 3, the heights of the beginning and ending abutments are different. In case 2, the area springs are perpendicular to the abutment planes, 30° deviate from the longitudinal direction, which is the results of combining the soil pressure of x and y directions. For the other two cases, the direction of soil springs is in the longitudinal direction.

Table 3.10- Abutment-soil spring parameters of case 1

Case1	Soil Springs	Depth	Passive pressure	Stiffness	Maximum displacement	Frictional resistance
	No.	Z(ft)	p_p (psi)	K(psi/in)	Δ_u (in)	p_f (psi)
First/Last abut.	1	0.66	1.31	0.63	2.094	0.79
	2	1.97	3.94	1.88		2.36
	3	3.61	7.22	3.45		4.33
	4	5.25	10.50	5.01		6.30
	5	6.89	13.78	6.58		8.27
	6	8.86	17.71	8.46		10.63

Table 3.11- Abutment-soil spring parameters of case 2

Case 2	Soil spring	Depth	passive pressure	Stiffness	Maximum displacement	Frictional resistance
	No.	z(ft)	p_p (psi)	K(psi/in)	Δ_u (in)	p_f (psi)
First abut.	1	1.25	2.50	0.82	3.0576	1.50
	2	3.75	7.50	2.45		4.50
	3	6.25	12.50	4.09		7.50
	4	9.12	18.24	5.97		10.94
	5	11.74	23.48	7.68		14.09
Last abut.	1	1.25	2.50	0.82	2.856	1.50
	2	3.75	7.50	2.45		4.50
	3	6.25	12.50	4.09		7.50
	4	8.7	17.40	5.69		10.44
	5	10.9	21.80	7.13		13.08

Table 3.12-Abutment-soil spring parameters of case 3

Case 3	Soil spring	Depth	passive pressure	Stiffness	Maximum displacement	Frictional resistance
	No.	Z(ft)	p_p (psi)	K(psi/in)	Δ_u (in)	p_f (psi)
First abut.	1	0.72	1.44	0.53	2.720	0.87
	2	2.17	4.33	1.59		2.60
	3	3.61	7.22	2.66		4.33
	4	5.58	11.17	4.11		6.70
	5	8.08	16.17	5.94		9.70
	6	10.33	20.67	7.60		12.40
Last abut.	1	0.72	1.44	0.61	2.360	0.87
	2	2.17	4.33	1.84		2.60
	3	3.61	7.22	3.06		4.33
	4	5.21	10.42	4.41		6.25
	5	6.96	13.92	5.90		8.35
	6	8.83	17.67	7.49		10.60

3.4 Eigenvalue analysis results

An eigenvalue analysis was conducted to determine the bridge natural period T_n of the bridges. For cases 1 and 2, the single span bridges, the third mode is in the longitudinal direction and the fourth in the transverse direction. For case 3, the 3-span bridge, the first mode is in the transverse direction and the second one in the longitudinal direction. The first five mode shapes of three cases are shown in Figures 3.8-3.10 and the frequencies and periods are listed in Table 3.14.

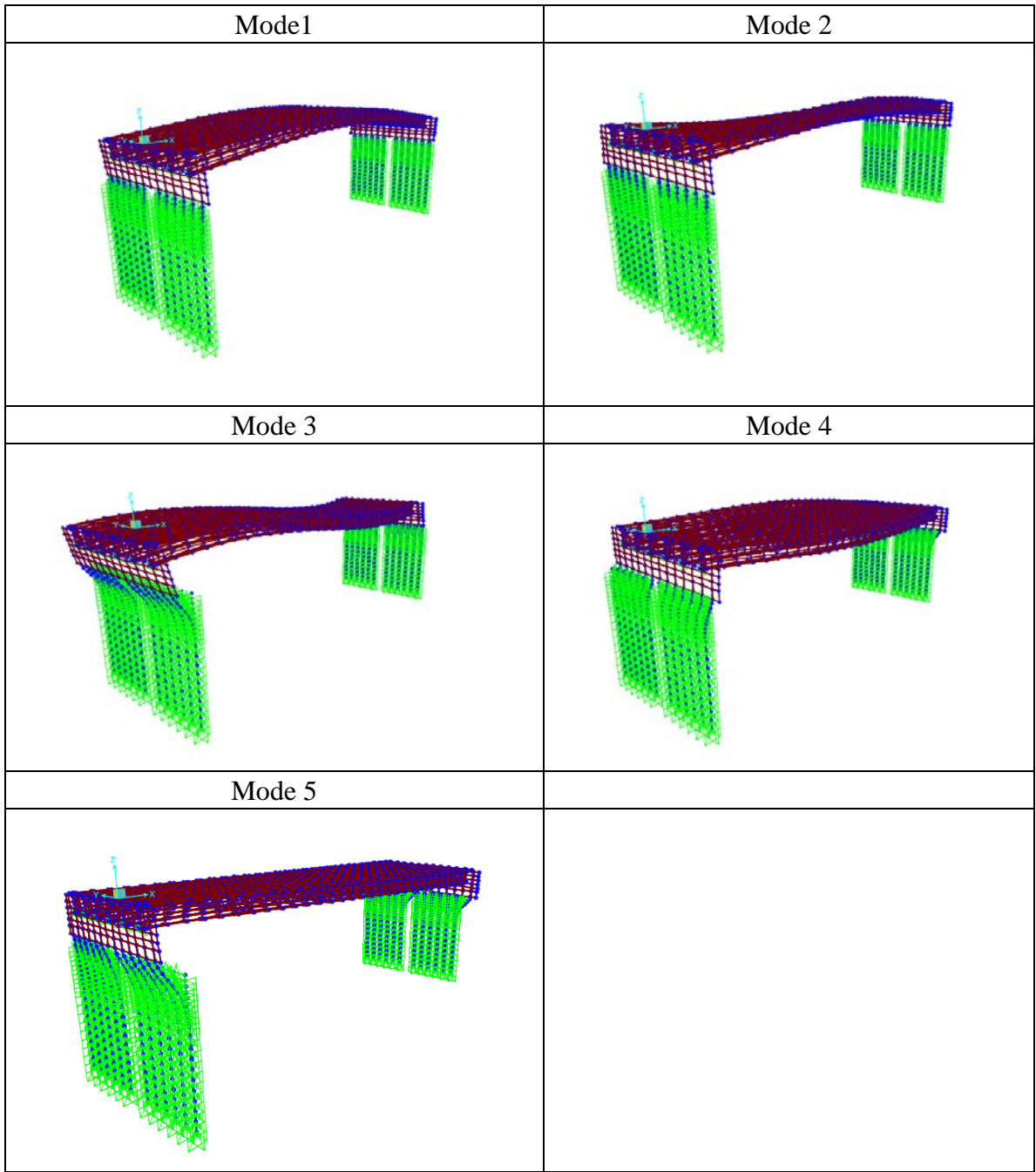


Figure 3.8-The first five mode shapes of case 1

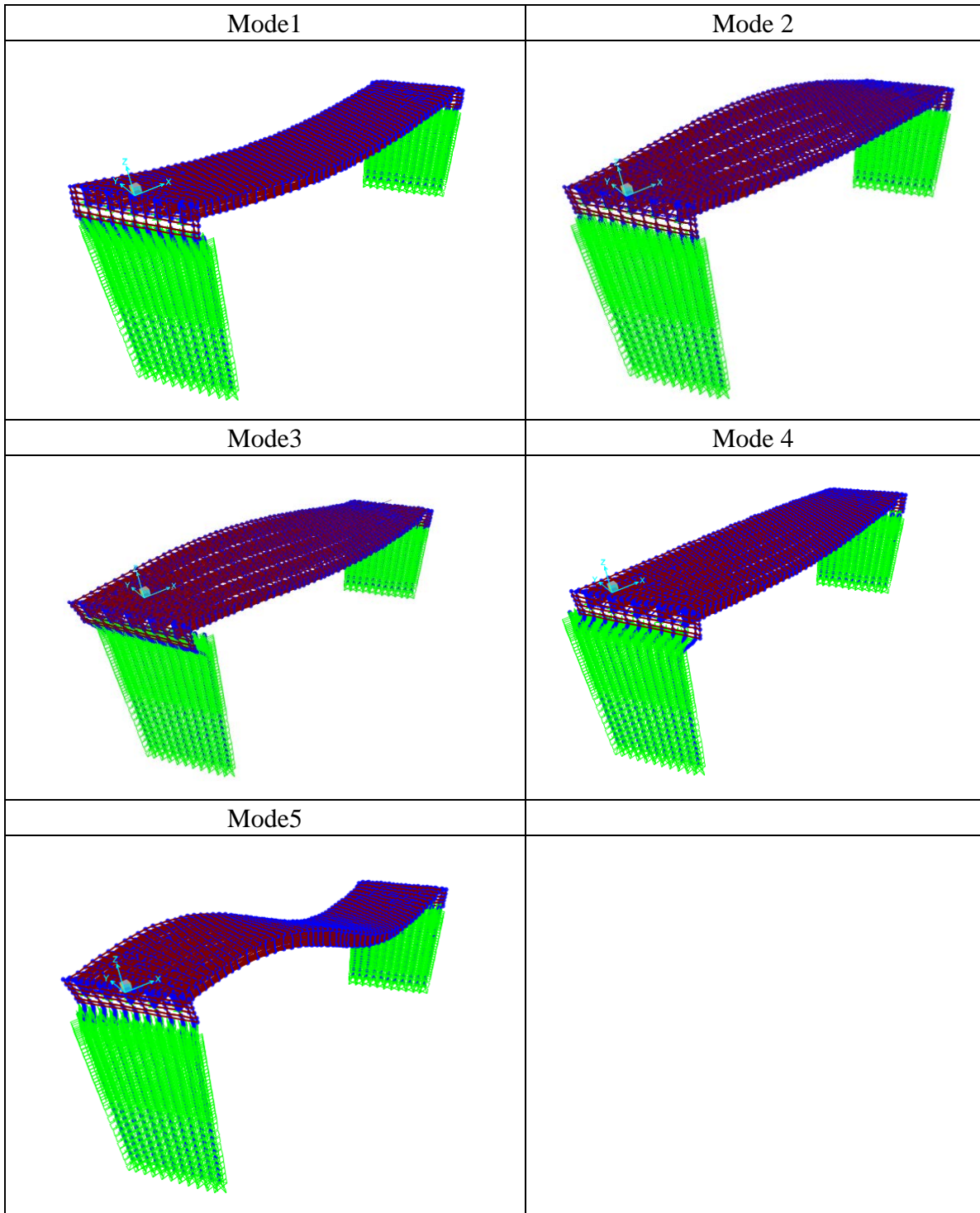


Figure 3.9-The first five mode shapes of case 2

Case3:

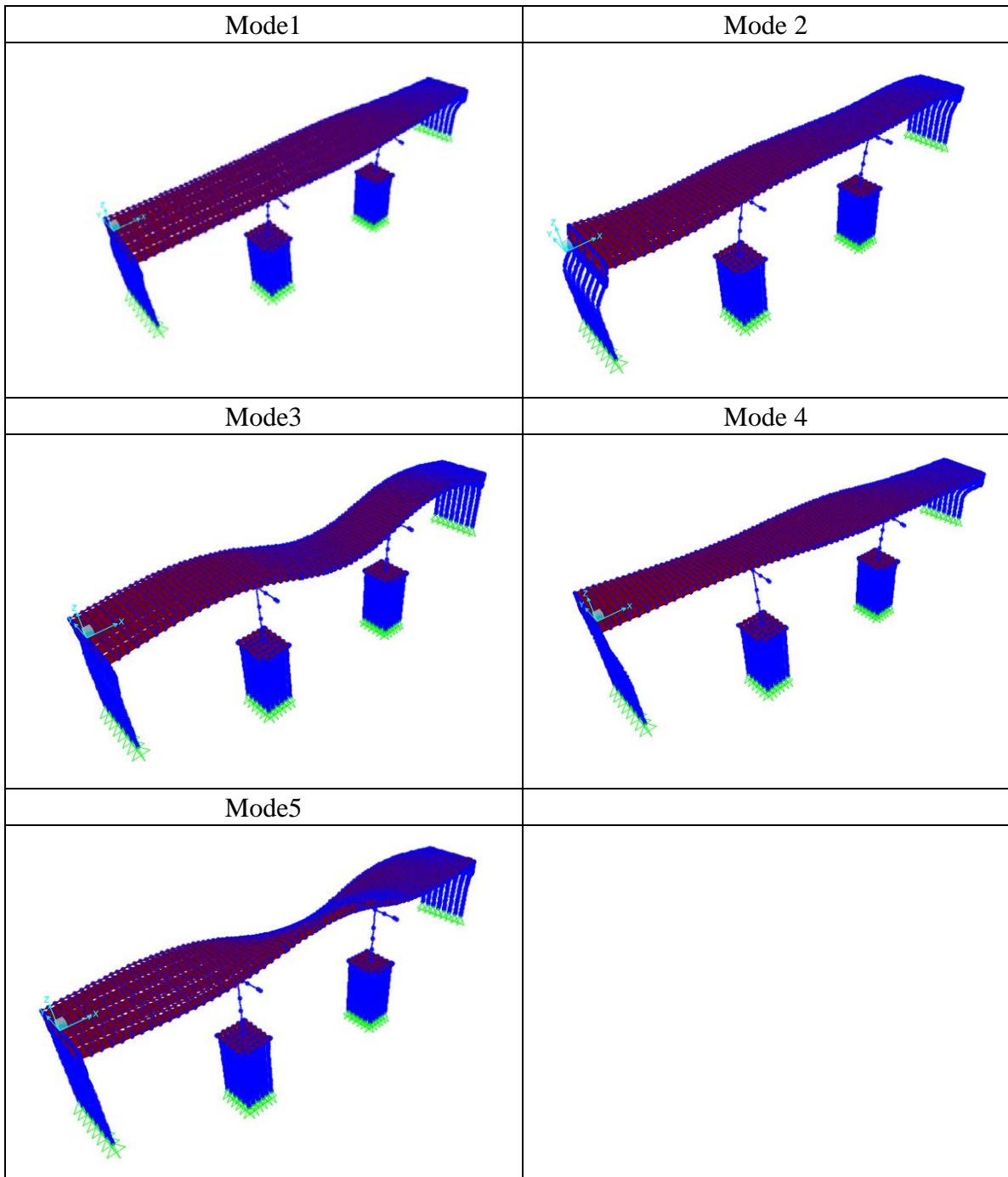


Figure 3.10-The first five mode shapes of case 3

The values of period and frequency of the first 10 modes are listed in Table3.13

Table 3.13 - Modal periods and frequencies of three cases

Modes	Case1		Case2		Case3	
	T(sec)	f(Hz)	Ts(sec)	fs(Hz)	Ts(sec)	fs(Hz)
1	0.3386	2.9536	0.5893	1.6968	0.6141	1.6283
2	0.2916	3.4293	0.5173	1.9331	0.6047	1.6538
3	0.257	3.8909	0.457	2.1883	0.4499	2.2225
4	0.2174	4.6001	0.4128	2.4224	0.4241	2.3581
5	0.1567	6.3832	0.3172	3.1523	0.4203	2.3793
6	0.1106	9.0387	0.1728	5.7873	0.2892	3.4581
7	0.1062	9.4202	0.1682	5.9455	0.2735	3.6559
8	0.1052	9.5073	0.1285	7.7813	0.2625	3.8091
9	0.0716	13.9714	0.1166	8.576	0.255	3.9222
10	0.0626	15.9753	0.1006	9.9402	0.2395	4.1752
11	0.0598	16.732	0.0974	10.2692	0.224	4.4642
12	0.0564	17.7395	0.0904	11.066	0.2184	4.5796

CHAPTER 4: PUSHOVER ANALYSIS

4.1 Principle of pushover method

Pushover analysis is an inelastic, incremental static analysis procedure aimed at defining the lateral force-resisting capacity of the bridge and the displacement demand on the bridge. It is used for determining that the available ductility is sufficient to ensure satisfactory seismic performance. Traditional linear analysis methods use lateral forces to represent a design condition. For nonlinear methods it is easier and more direct to use a set of lateral displacements as a design condition.

Nonlinear static pushover analysis is employed to a bridge model to determine the elastic capacity and the nonlinear behavior of bridge components, such as columns and piles in both longitudinal and transverse directions.

In this study, to conduct a pushover analysis, a uniform lateral load was applied on deck in the longitudinal and transverse directions, respectively; the displacement monitored node was located at the center of the deck in each bridge.

4.2 Plastic hinge assignment

Hinge properties are described in the following section.

1. Concrete pile-

The cross section of concrete piles in Case1 was calculated by Xtract, a structural software used for calculating the properties of cross sections. The P-M curve is shown in Figure 4.1 - The moment-curvature curves under different axial loads were obtained and

were transformed into the hinge backbone model as shown in Figure 4.2 (b). Figure 4.2 (a) shows the backbone model in CSiBridge®, where IO, LS and CP stand for immediate occupancy, life safety and collapse prevention, respectively.

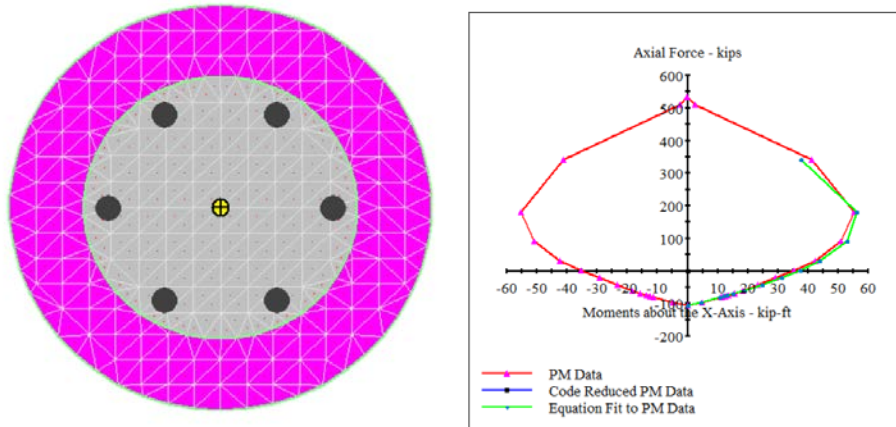


Figure 4.1 - Pile section and PM curve

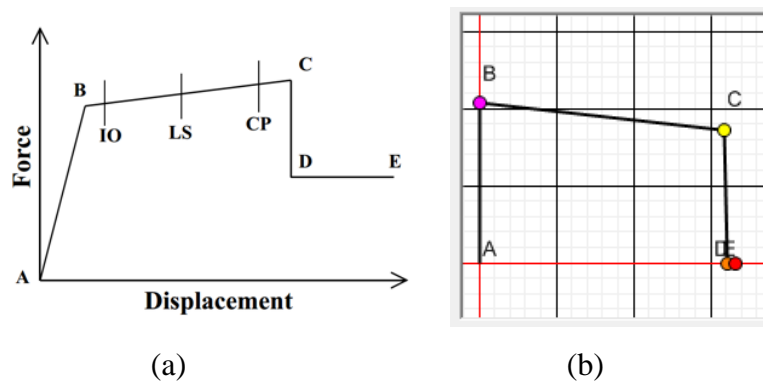
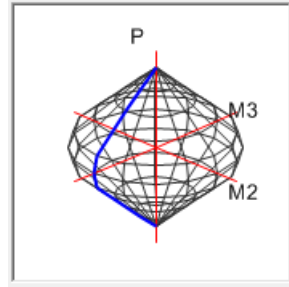


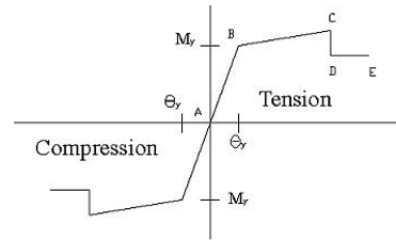
Figure 4.2 - Moment-curvature model

2. H-steel pile-

For the HP12x84 piles in Cases 2 and 3, default PMM, PM2 and PM3 plastic hinges were defined. The yield rotation factors are in accordance with ASCE 41-13 Table 9-6. The steel PM interaction curve shape is shown in Figure 4.3(a) and the moment-curvature backbone curve is shown in Figure 4.3(b).



(a) PM interaction curve shape



(b) moment-curvature backbone curve

Figure 4.3 - Steel hinge properties

3. Location-

The relatively high stiffness of integral abutments will attract most of the longitudinal and transverse seismic forces. The piles and piers in IABs are allowed to act as “weak links” during seismic events and limit the seismic forces. These piles will be subjected to large flexural moments that cause the section to yield and eventually form a plastic hinge (Monzon, E et al., 2014)..

The static pushover analysis was performed in the longitudinal and the transverse directions; then the plastic hinges were estimatedly assigned at the locations with the largest moment.

4.3 Pushover results

The plastic hinges occurred in sequence in the pushover analysis. The following Figures show the general order of occurrence of plastic hinges at different locations.

In case 1, the plastic hinges firstly occurred on the top of the piles, the location where the maximum positive moment occur, at both sides, then the location with maximum negative moment went into the plastic phase successively. The order of occurrence of plastic hinges is shown in Figures 4.4 and 4.5.

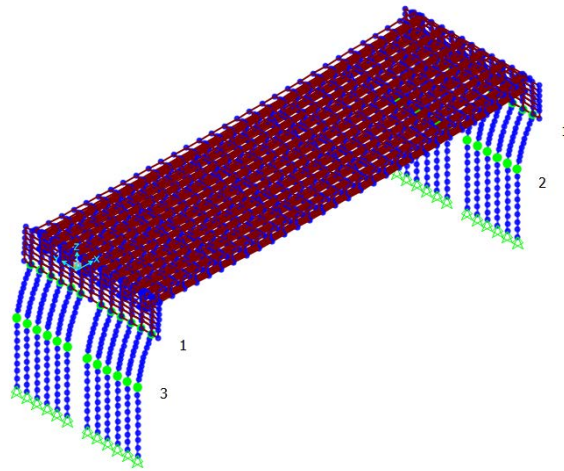


Figure 4.4 - Order of occurrence of plastic hinges in the global x direction (Case1)

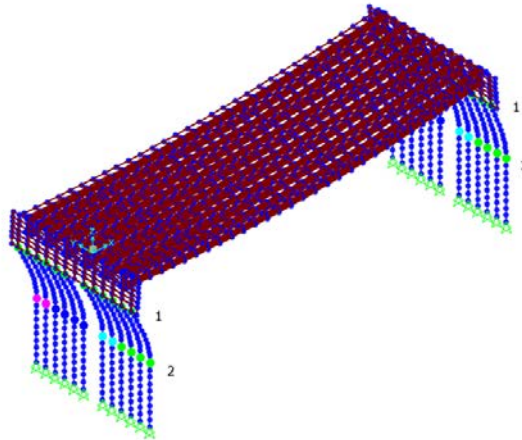


Figure 4.5 - Order of occurrence of plastic hinges in the global y direction (Case1)

In case 2, in general order, the plastic hinges occurred at the top of piles first and the location with maximum negative moment next. Due to the bridge is in skew and the piles at each side are not in the same length, the plastic hinges at the location of maximum negative moment did not occur at the same time. In the longitudinal direction, the piles at the abutment in obtuse angle went into plastic first as shown in Figure 4.6. In the transverse direction, other than the hinges at the top; plastic hinges then occurred at inflection points at the piles with shorter length as shown in Figure 4.7.

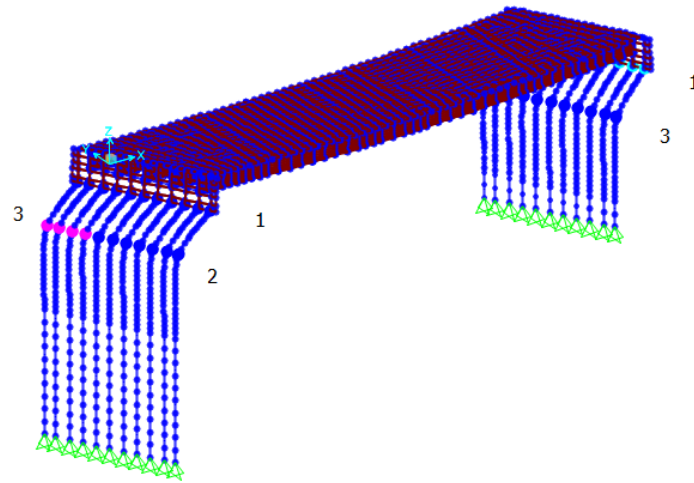


Figure 4.6 - Order of occurrence of plastic hinges in the global x direction (Case2)

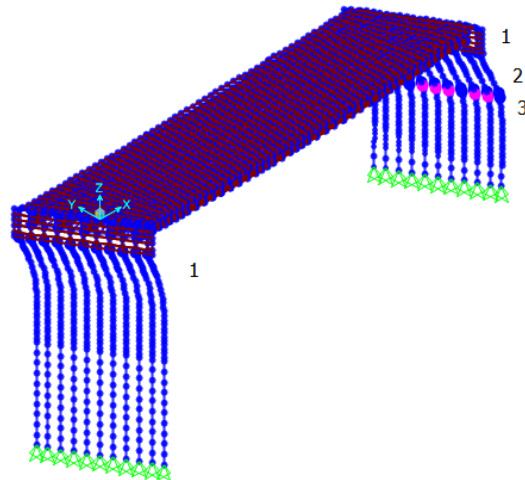


Figure 4.7 - Order of occurrence of plastic hinges in the global y direction (Case2)

The bridge piers in case 3 will be protected from seismic damage in the longitudinal direction by introducing expansion bearings at the top of piers. Expansion bearings act as structural weak links to limit the forces passed to the pier columns so that they can be designed to remain elastic. Thus, hinges will not form on the piers when the longitudinal pushover load applied on the deck. Plastic hinges were formed on piles in the longitudinal direction as shown in Figure 4.8. In the transverse direction, stiffness of

piers is relatively high, which attracts most of the pushover loads and formed plastic hinges at the bottom of the piers as shown in Figure 4.9. Also, because of different heights of piers, plastic hinges occurred in sequence when the pushover loads were symmetrically applied.

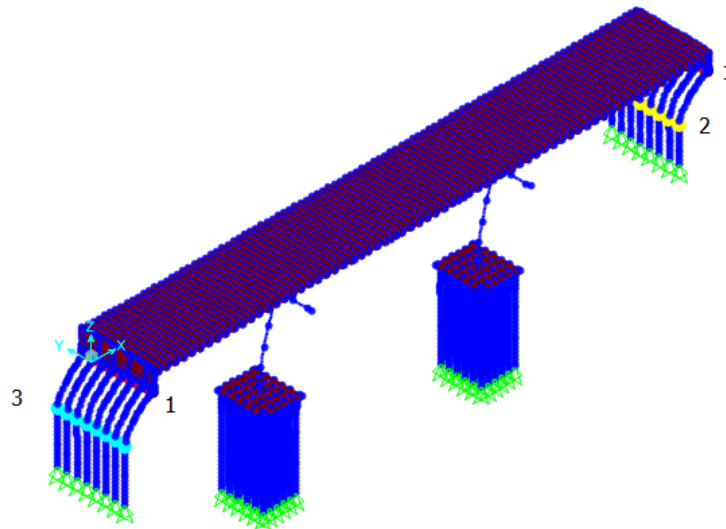


Figure 4.8 - Order of occurrence of plastic hinges in the global x direction (Case3)

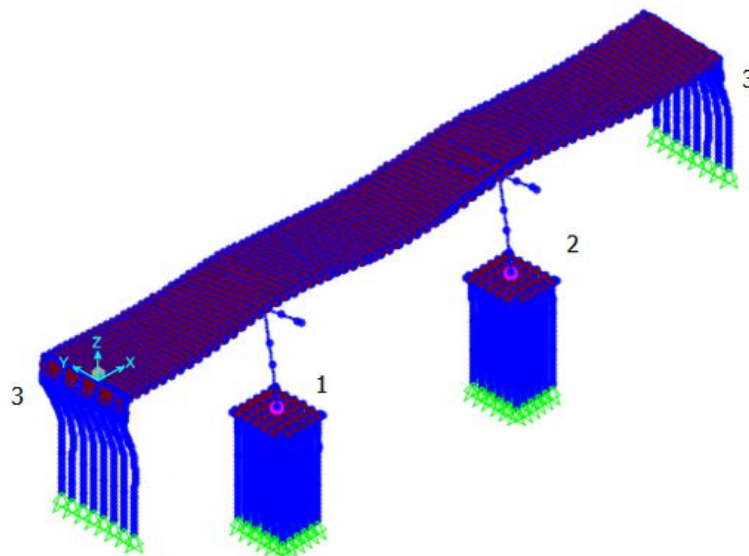


Figure 4.9 - Order of occurrence of plastic hinges in the global y direction (Case3)

A summary of locations of plastic hinges are listed in Table 4.1.

Table 4.1 -Locations of plastic hinges

		Case1	Case2		Case3					
		Pile	Pile		Pile				pier1	pier2
		First/Last abut.	First abut.	Last abut.	First abut.	Last abut.	pier1	pier2		
Location (distance in feet from the top of each pile)	x	0	0	0	0	0	-	-	-	-
		12	16	16	20	20	-	-	-	-
	y	0	0	0	-	-	-	-	Bot. of pier	Bot. of pier
		12	-	16						
-	-	18								

Numbers of hinges in different stages of every step are listed in Tables 4.2-4.7

below. The plastic hinges at top of the piles went into plastic stages first and when the section with maximum negative moment went into plastic, the ones at top went to the stage of further damage. In these tables, A, B, IO, LS, CP, C, D, E are as indicted in Figure 4.2(a).

Table 4.2 - Numbers of hinges occurred in stages (case1-x)

step	Disp.(ft)	Base Force(kips)	A-B	B-IO	IO-LS	LS- CP	CP- C	C-D	D-E	Beyond E	Total
0	0.00	0.00	48	0	0	0	24	0	0	0	72
1	0.02	159.86	48	0	0	0	24	0	0	0	72
2	0.04	363.37	48	0	0	0	24	0	0	0	72
3	0.04	363.08	48	0	0	0	24	0	0	0	72
4	0.07	500.72	48	0	0	0	24	0	0	0	72
5	0.13	686.83	48	0	0	0	24	0	0	0	72
6	0.21	804.78	48	0	0	0	24	0	0	0	72
7	0.23	854.28	24	24	0	0	24	0	0	0	72
8	0.27	881.57	24	0	24	0	24	0	0	0	72
9	0.34	967.26	0	0	0	0	72	0	0	0	72
10	0.35	974.22	0	0	0	0	72	0	0	0	72
11	0.40	1010.60	0	0	0	0	72	0	0	0	72
12	0.47	1031.95	0	0	0	0	72	0	0	0	72
13	0.54	1032.02	0	0	0	0	72	0	0	0	72
14	0.60	1032.08	0	0	0	0	72	0	0	0	72
15	0.66	1032.14	0	0	0	0	72	0	0	0	72

Table 4.3 - Numbers of hinges occurred in stages (case1-y)

step	Disp.(ft)	Base Force(kips)	A-B	B-IO	IO-LS	LS- CP	CP- C	C-D	D-E	Beyond E	Total
0	0.00	0.00	48	0	0	0	24	0	0	0	72
1	0.00	155.88	48	0	0	0	24	0	0	0	72
2	0.01	334.32	48	0	0	0	24	0	0	0	72
3	0.02	466.23	48	0	0	0	24	0	0	0	72
4	0.06	707.57	48	0	0	0	24	0	0	0	72
5	0.09	794.38	48	0	0	0	24	0	0	0	72
6	0.11	903.04	48	0	0	0	24	0	0	0	72
7	0.18	1079.06	42	4	2	0	24	0	0	0	72
8	0.22	1175.32	12	4	20	2	34	0	0	0	72
9	0.24	1204.86	4	6	12	6	44	0	0	0	72
10	0.24	1207.83	4	4	8	8	48	0	0	0	72
11	0.25	1222.67	0	4	8	4	56	0	0	0	72
12	0.27	1248.53	0	0	4	2	66	0	0	0	72
13	0.35	1344.76	0	0	0	0	72	0	0	0	72
14	0.37	1360.38	0	0	0	0	72	0	0	0	72
15	0.40	1390.21	0	0	0	0	72	0	0	0	72

Table 4.4 - Numbers of hinges occurred in stages (case2-x)

step	Disp.(ft)	Base Force(kips)	A-B	B-IO	IO-LS	LS- CP	CP- C	C-D	D-E	Beyond E	Total
0	0.01	0	121	0	0	0	0	0	0	0	121
1	0.12	438.82	121	0	0	0	0	0	0	0	121
2	0.38	1518.59	108	2	11	0	0	0	0	0	121
3	0.65	2070.63	99	0	22	0	0	0	0	0	121
4	0.9	2282.48	99	0	22	0	0	0	0	0	121
5	1.15	2429.73	98	1	22	0	0	0	0	0	121
6	1.39	2521.69	65	34	22	0	0	0	0	0	121
7	1.46	2536.67	55	43	23	0	0	0	0	0	121
8	1.71	2570.82	55	22	44	0	0	0	0	0	121
9	1.96	2596.59	55	8	51	7	0	0	0	0	121
10	2.21	2613.61	55	0	55	11	0	0	0	0	121
11	2.46	2631.96	55	0	55	11	0	0	0	0	121
12	2.51	2635.42	55	0	55	11	0	0	0	0	121

Table 4.5 - Numbers of hinges occurred in stages (case2-y)

step	Disp.(ft)	Base Force(kips)	A-B	B-IO	IO-LS	LS- CP	CP- C	C-D	D-E	Beyond E	Total
0	0.00	0.00	121	0	0	0	0	0	0	0	121
1	0.25	737.64	121	0	0	0	0	0	0	0	121
2	0.29	852.26	121	0	0	0	0	0	0	0	121
3	0.44	1294.63	101	20	0	0	0	0	0	0	121
4	0.70	1697.30	99	11	11	0	0	0	0	0	121
5	0.95	2007.72	99	0	22	0	0	0	0	0	121
6	1.20	2248.20	99	0	22	0	0	0	0	0	121
7	1.29	2324.62	88	11	22	0	0	0	0	0	121
8	1.62	2432.10	77	8	36	0	0	0	0	0	121
9	1.69	2452.94	77	7	31	5	0	1	0	0	121
10	1.69	2452.54	77	7	31	5	0	1	0	0	121
11	1.69	2452.52	77	7	31	5	0	1	0	0	121
12	1.69	2453.02	77	7	31	5	0	1	0	0	121

Table 4.6 - Numbers of hinges occurred in stages (case3-x)

step	Disp.(ft)	Base Force(kips)	A-B	B-IO	IO-LS	LS- CP	CP- C	C-D	D-E	Beyond E	Total
0	0	0	298	0	0	0	0	0	0	0	298
1	0.16	1227.36	298	0	0	0	0	0	0	0	298
2	0.25	1740.89	290	0	0	0	0	8	0	0	298
3	0.35	2053.45	282	8	0	0	0	8	0	0	298
4	0.85	2652.97	282	0	0	0	0	16	0	0	298
5	1.14	2981.86	282	0	0	0	0	0	8	8	298
6	1.76	3837.68	282	0	0	0	0	0	0	16	298
7	2.22	4472.59	282	0	0	0	0	0	0	16	298
8	2.71	5106.32	250	0	0	16	0	16	0	16	298
9	2.79	5178.25	250	0	0	0	0	32	0	16	298
10	2.83	5193.37	250	0	0	0	0	32	0	16	298

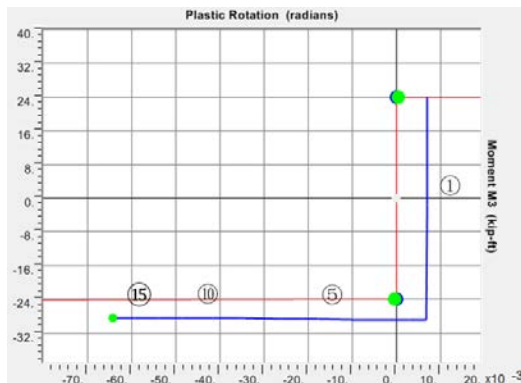
Table 4.7 - Numbers of hinges occurred in stages (case3-y)

step	Disp.(ft)	Base Force(kips)	A-B	B-IO	IO-LS	LS- CP	CP- C	C-D	D-E	Beyond E	Total
0	0	0	298	0	0	0	0	0	0	0	298
1	0.05	667.18	297	1	0	0	0	0	0	0	298
2	0.13	1144.4	296	2	0	0	0	0	0	0	298
3	0.28	1608.04	292	6	0	0	0	0	0	0	298
4	0.3	1643.28	288	9	1	0	0	0	0	0	298
5	0.78	1989.76	280	0	17	0	0	1	0	0	298
6	0.78	1742.98	280	0	17	0	0	0	0	1	298
7	0.78	1744.65	280	0	17	0	0	0	0	1	298
8	0.85	1813.8	280	0	17	0	0	0	0	1	298
9	1.06	1919.72	280	0	16	0	0	1	0	1	298
10	1.06	1919.72	280	0	16	0	0	1	0	1	298

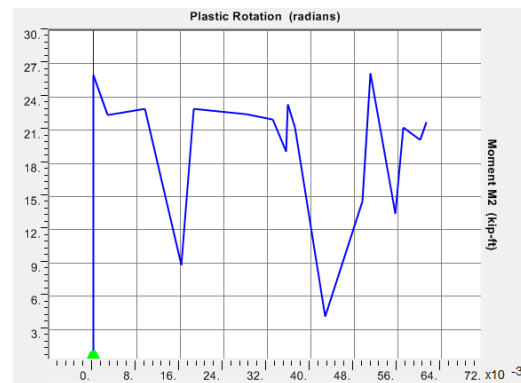
Hinge results:

Development curves of hinges at critical locations are shown in Figures 4.10-4.12.

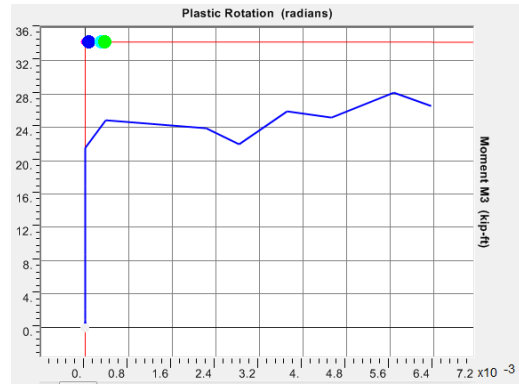
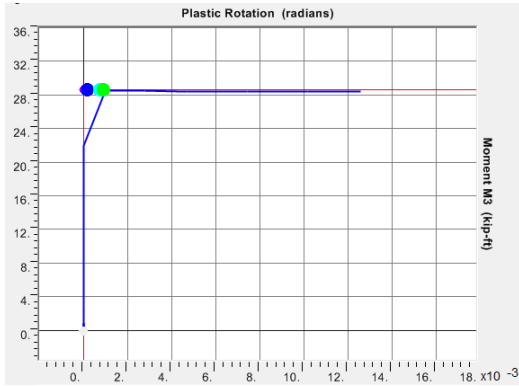
In the elastic stage, the moment and rotation increase linearly; in the plastic stage, the rotation increase along the backbone with constant moment value; after the point of rupture, as shown in Figure 4.12(a)(c), the moment decrease rapidly and the rotation stops increasing.



(a) At pile top x-PM33

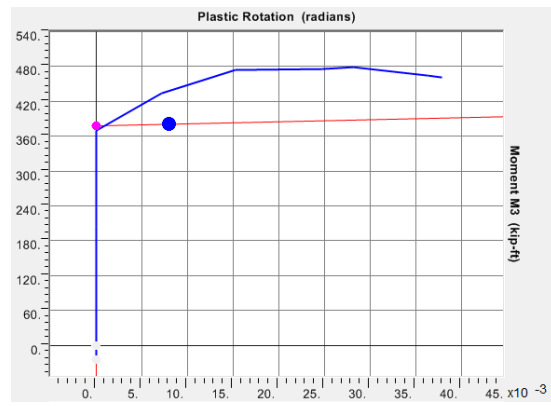


(b) At pile top y-PM22



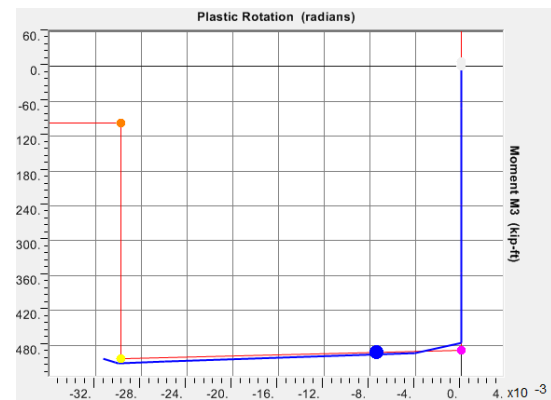
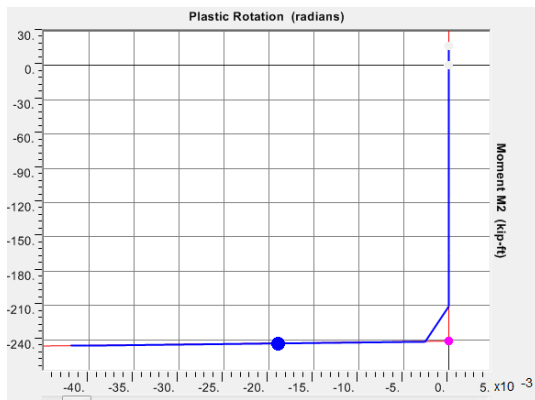
(c) Location with max negative moment (x-PM33) (d) Location with max negative moment (y-PM22)

Figure 4.10 - Case1 hinge results



(a) At pile top x-PM22

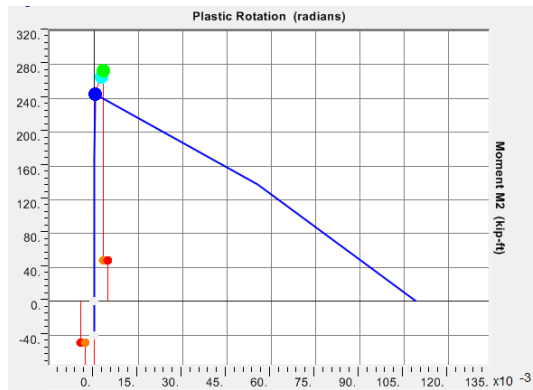
(b) At pile top y-PM33



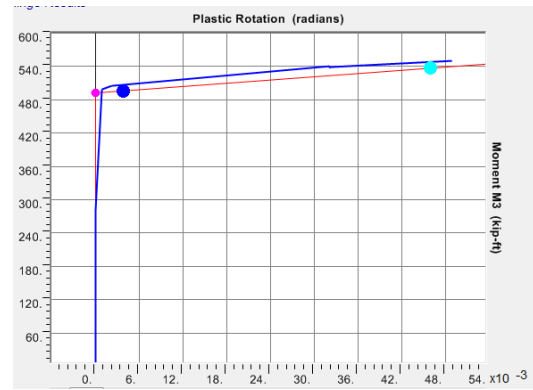
(c) Location with max negative moment (x-PM22)

(d) Location with max negative moment (y-PM33)

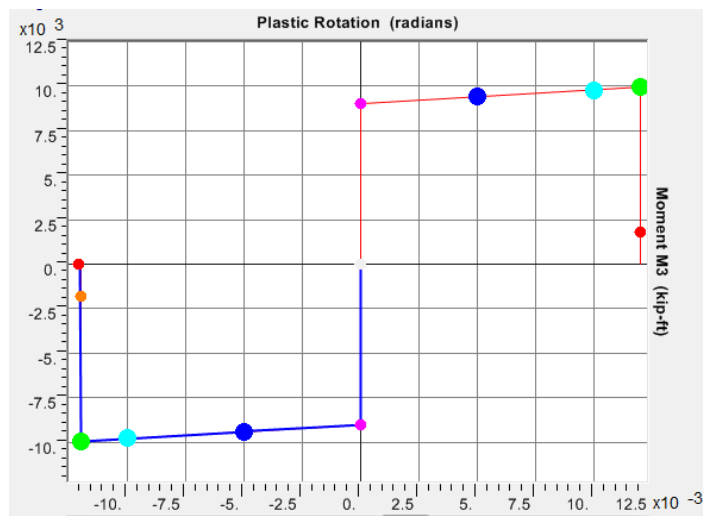
Figure 4.11 - Case2 hinge results



(a) At pile top x-PM22



(b) At pile top y-PM33



(c) Pier bottom y-PM22

Figure 4.12 - Case 3 hinge results

Figures 4.13, 4.15, and 4.17 show the total base shear plotted against the deck displacement from the longitudinal pushover analysis of case1, case2, and case3, respectively. Figures 4.14, 4.16, and 4.18 show the total base shear plotted against the deck displacement obtained from the transverse pushover analysis. In these Figures, the displacements where the hinges start to yield are marked. It can be observed that the system remains generally elastic when the piles started yielding.

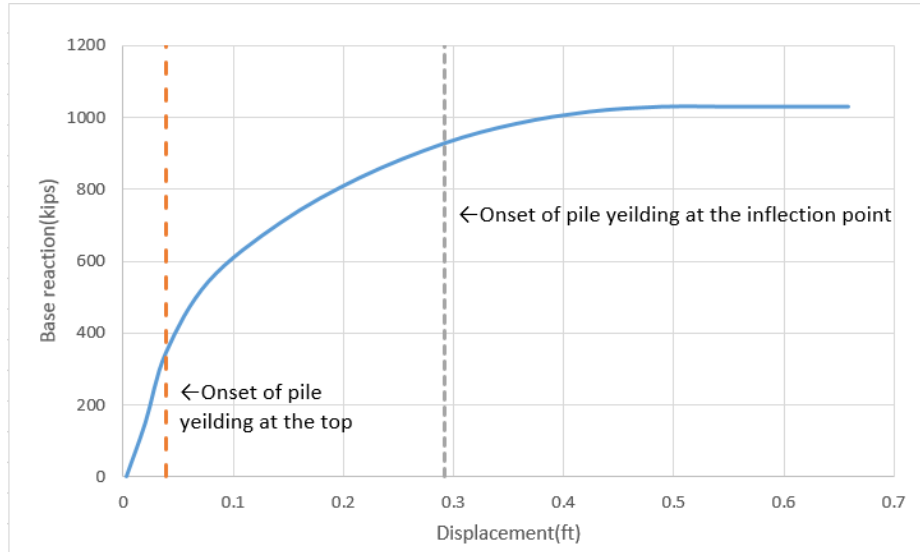


Figure 4.13-Case1 x-direction pushover curve with the mark of hinges yielding

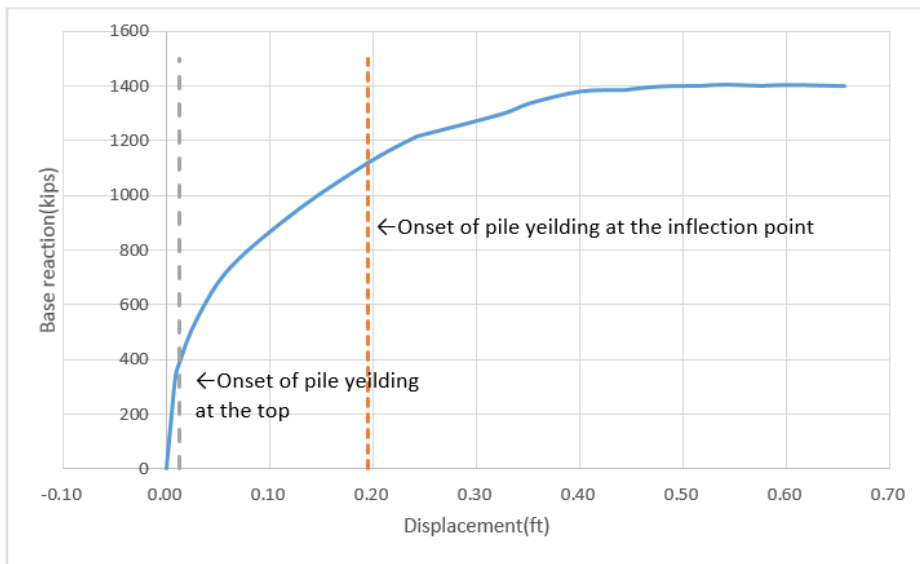


Figure 4.14-Case1 y-direction pushover curve with the mark of hinges yielding



Figure 4.15-Case2 x-direction pushover curve with the mark of hinges yielding

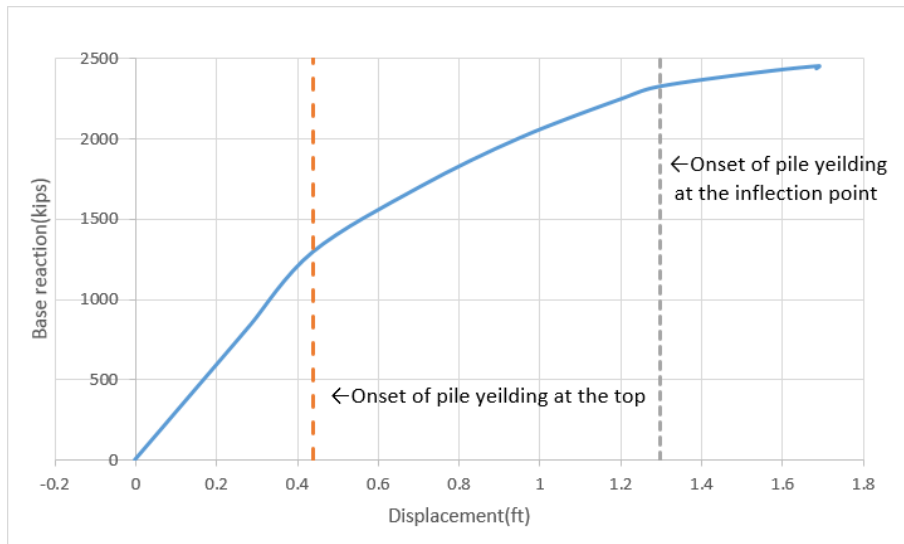


Figure 4.16-Case2 y-direction pushover curve with the mark of hinges yielding

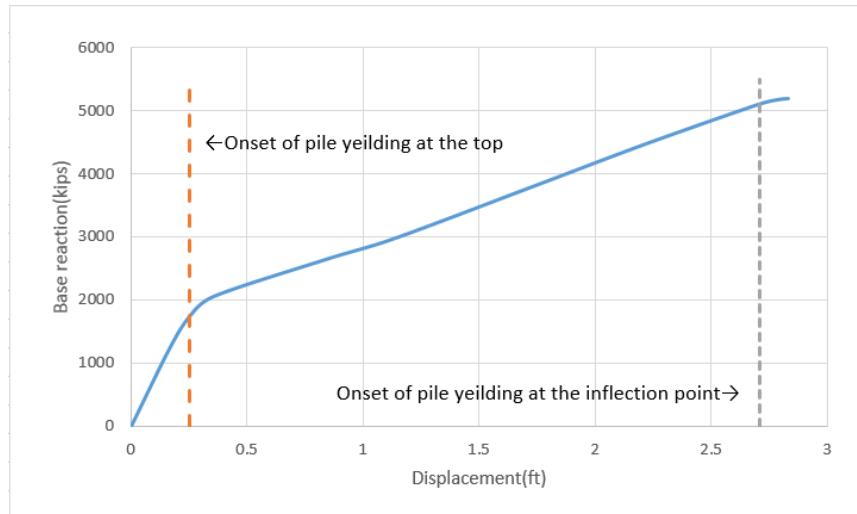


Figure 4.17-Case3 x-direction pushover curve with the mark of hinges yeilding

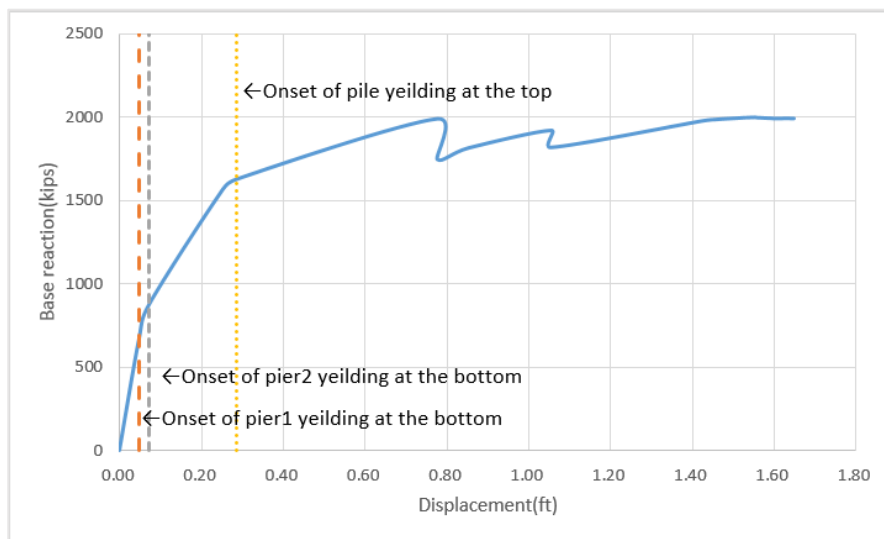


Figure 4.18-Case3 y-direction pushover curve with the mark of hinges yeilding

4.4 Capacity Spectrum method

The force-displacement curves obtained from the pushover analysis display the capacity of the structure. However, from the pushover curves, the response behavior under specify seismic loads cannot be observed, unlike performing the response spectrum

analysis or nonlinear time-history analysis. The capacity spectrum is introduced here for an estimation of the structure response based on the pushover curves.

The capability spectrum method is a simplified structural analysis method developed on the basis of pushover analysis. It is a direct estimation of the elastic-plastic reaction of structures through the structure's capability spectrum and seismic demand spectrum. The demand spectrum is firstly converted from the seismic response spectrum into the elastic demand spectrum by the equivalent single-degree-of-freedom system, and then the inelastic demand spectrum can be obtained with a reduction. Capability spectrum refers to the spectrum acceleration - spectral displacement relation curve of the equivalent single-degree-of-freedom system obtained by the pushover curve transformation. The intersection of the elastic demand spectrum and the capacity spectrum after reduction is called the performance point, which represents the maximum displacement and seismic intensity that the structure can withstand.

Equation (4-1) is used to convert the elastic response spectrum to the elastic demand spectrum.

$$S_{de} = \left(\frac{T}{2\pi} \right)^2 S_{ae} \quad (4-1)$$

In ATC-40 method, the reduced inelastic spectrum was obtained by considering the equivalent damping in equations (4-2) and (4-3).

$$S_{ai} = \frac{S_{ae}}{R_{\mu}} \quad (4-2)$$

$$S_{di} = \frac{\mu}{R_\mu} S_{de} = \mu \left(\frac{T}{2\pi} \right)^2 S_{ai} \quad (4-3)$$

Where S_{ae} , S_{de} are the acceleration and displacement of the elastic response spectrum, respectively; S_{ai} , S_{di} are the acceleration and displacement of the reduced inelastic response spectrum, respectively; R is the reduction factor related to μ and μ is the ductile factor.

Equations (4-4) and (4-5) are used to convert pushover curve to capacity spectrum, which is plotted in acceleration-displacement.

$$S_a = \frac{F_b}{\alpha W} \quad (4-4)$$

$$S_d = \frac{d}{\Gamma \phi_n} \quad (4-5)$$

Where: W is the total weight of the structure

ϕ_n is the model shape location where d is measured

$$\alpha \text{ is the model mass coefficient, } \alpha = \frac{[\sum_{j=1}^n m_j \phi_j]^2}{\sum_{j=1}^n m_j \sum_{j=1}^n m_j \phi_j^2}$$

In this study, the design response spectrum is generated from the USGS Earthquake Hazard Program with the location stated in chapter 2.3, soil class D and risk category I / II / III, as shown in Figure 4.19.

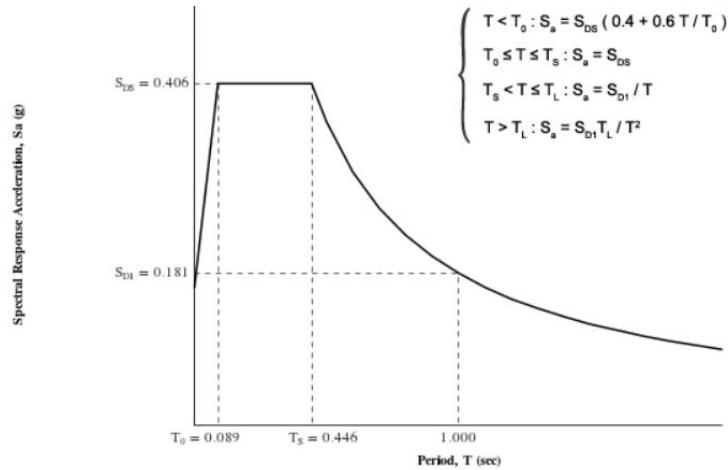
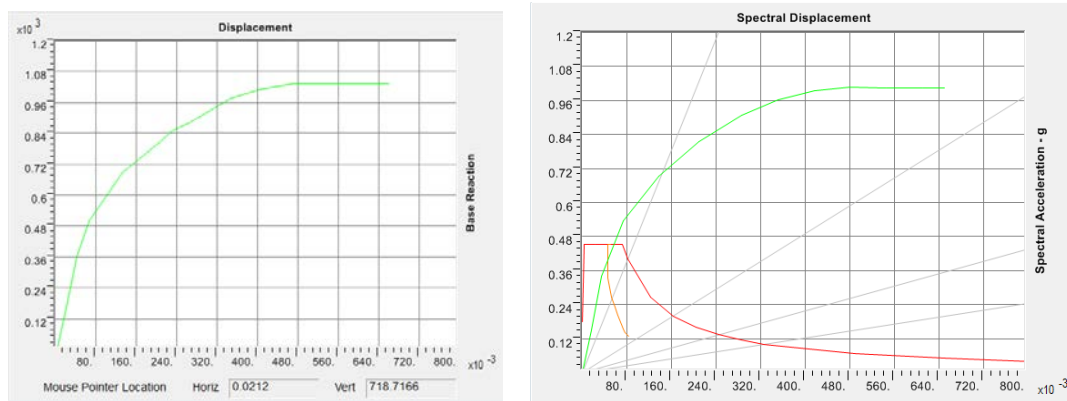


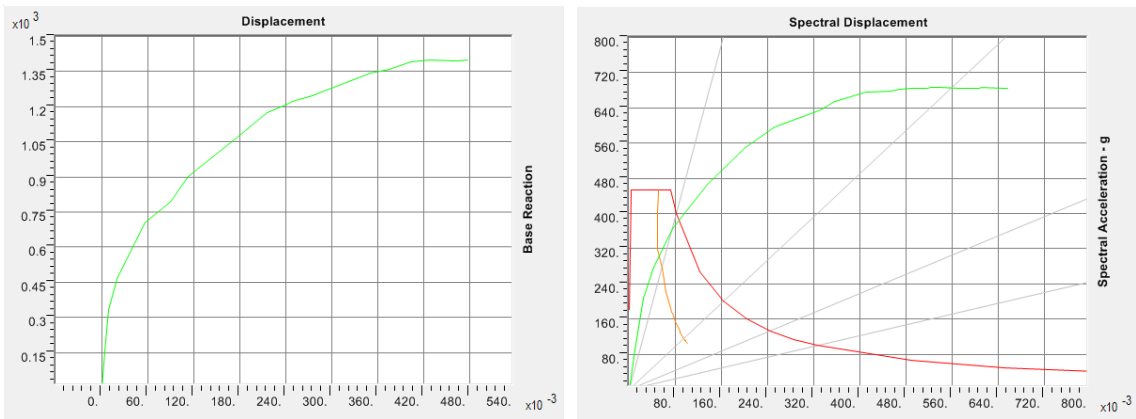
Figure 4.19 - Design response spectrum of bridge site

ATC-40 standard generated from CSiBridge[®] was used to find out the performance point. For the parameters in ATC 40, C_a is the PGA, which equals to 0.181g; C_v relates to the T_s and C_a , as $C_v = 2.5T_s C_a = 2.5 \times 0.446 \times 0.181g = 0.2g$. The 5% damping reduced elastic demand spectrum was used here.

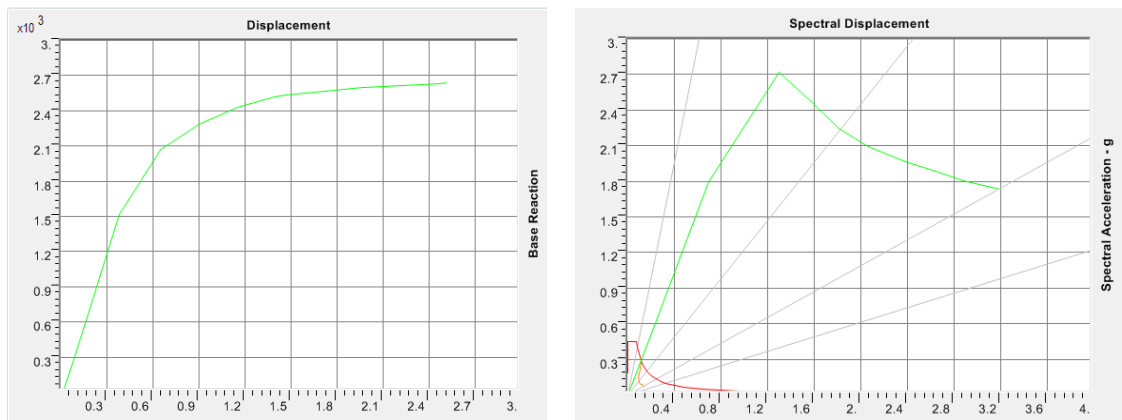
The force-displacement curves and curves from capacity spectrum method are shown in the following Figures 4.10-15. In each Sa-Sd Figure, the capacity spectrum curve is in green, elastic demand spectrum curve is in orange and the red line is the standard response spectrum.



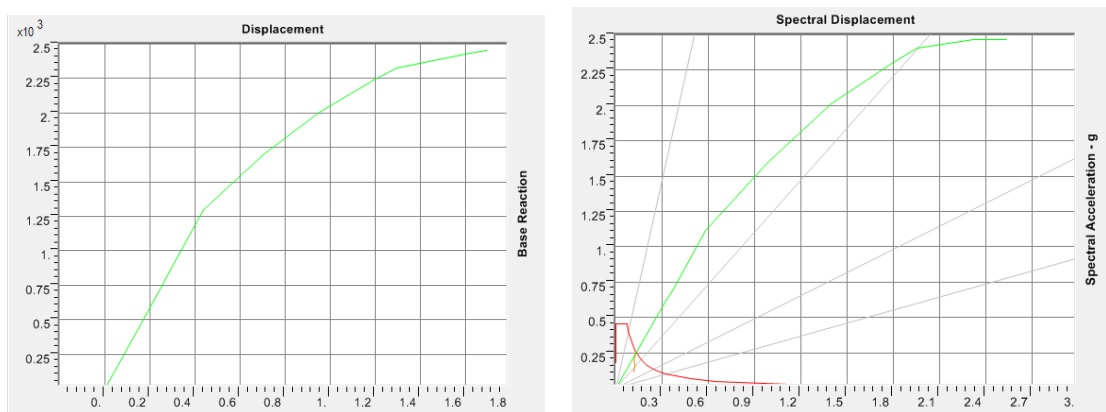
(a) Force-displacement curve (b) Capacity curve and elastic demand spectrum
Figure 4.20 - Case 1 curve results in the longitudinal direction (kips, ft)



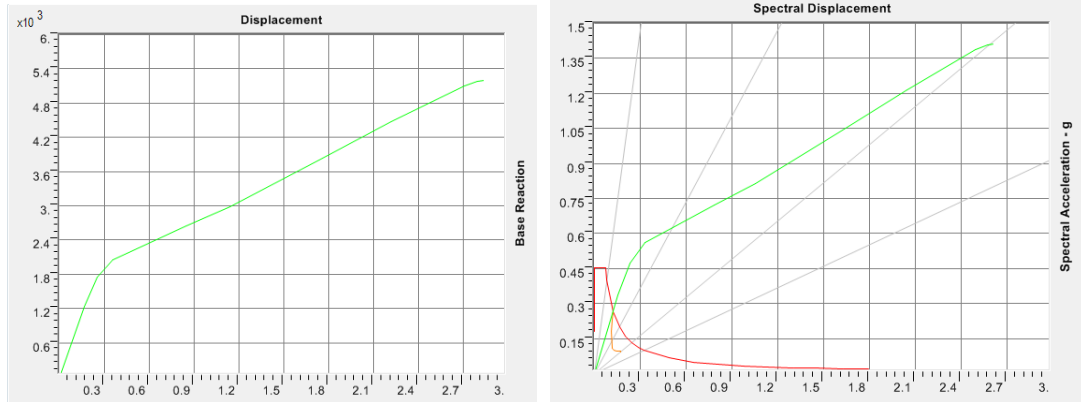
(a) Force-displacement curve (b) Capacity curve and elastic demand spectrum
 Figure 4.21 - Case1 curve results in the transverse direction (kips, ft)



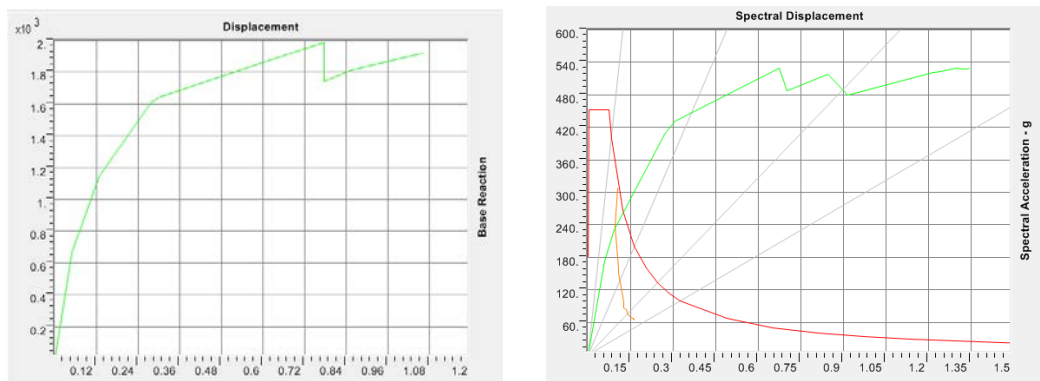
(a) Force-displacement curve (b) Capacity curve and elastic demand spectrum
 Figure 4.22 - Case2 curve results in the longitudinal direction (kips, ft)



(a) Force-displacement curve (b) Capacity curve and elastic demand spectrum
 Figure 4.23 - Case2 curve results in the transverse direction (kips, ft)



(a) Force-displacement curve (b) Capacity curve and elastic demand spectrum
 Figure 4.24 - Case 3 curve results in the longitudinal direction (kips, ft)



(a) Force-displacement curve (b) Capacity curve and elastic demand spectrum
 Figure 4.25- Case 3 curve results in the transverse direction (kips, ft)

The performance point data of three cases are listed in Table 4.8. As the different capacity curves compared to the same demand curve, different seismic capacity is shown. In general, the 3-span IAB is more flexible and has a larger displacement response under the seismic loads.

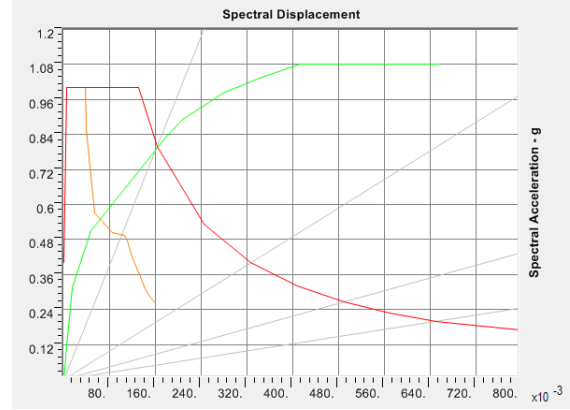
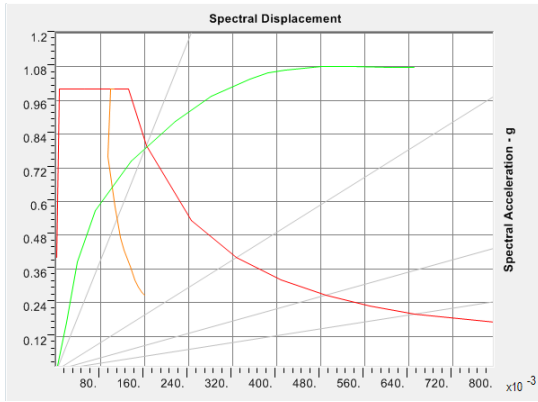
Table 4.8- Performance point data

		Base shear(kips)	Displacement(ft)
Case1	x-direction	403.1	0.050
	y-direction	594.9	0.037
Case2	x-direction	274.9	0.081
	y-direction	301.9	0.101
Case3	x-direction	984.4	0.133
	y-direction	886.9	0.076

4.5 Evaluation by time-history analysis

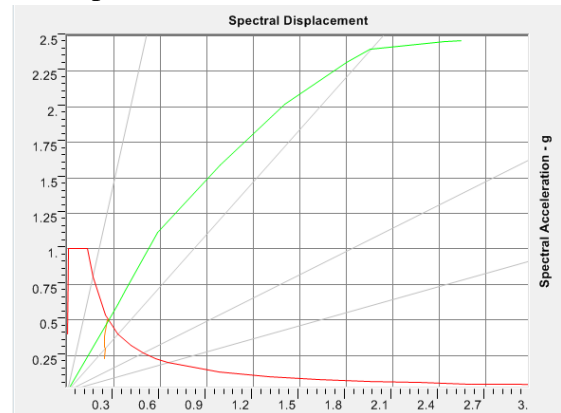
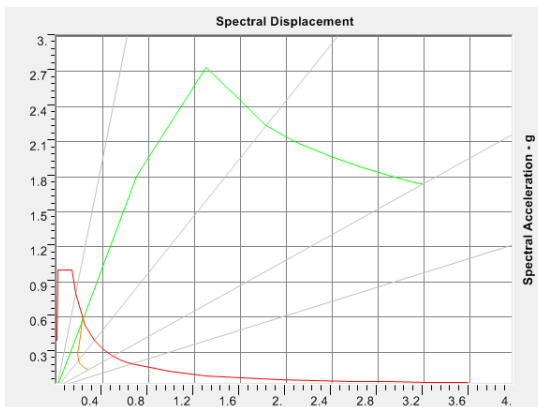
The results obtained from pushover method were compared with those from the nonlinear time history in this case as a verification evaluation. From the nonlinear time history analysis, the displacement response of structure can be found by applying the ground motion.

Based on the capacity spectrum method, the intersection point of the capacity spectrum and the response spectrum indicates the target displacement d of deck calculated from equation (4-5) when subjected to the response spectrum. In this evaluation, the capacity spectrum with $C_a=C_v=0.4g$ was applied. The target displacements are obtained from the software calculation, as shown in Figures 4.32-4.34.



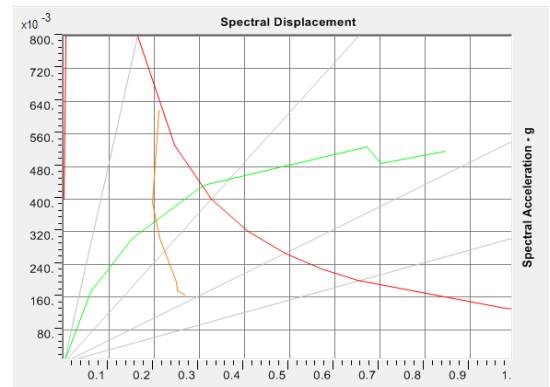
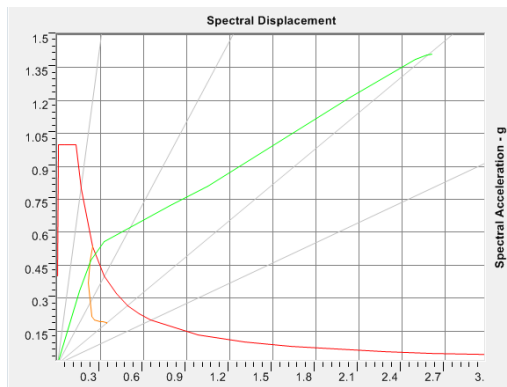
(a) Performance point of Case1 in x direction (b) Performance point of Case1 in y direction

Figure 4.26- Performance point of Case1



(a) Performance point of Case2 in x direction (b) Performance point of Case2 in y direction

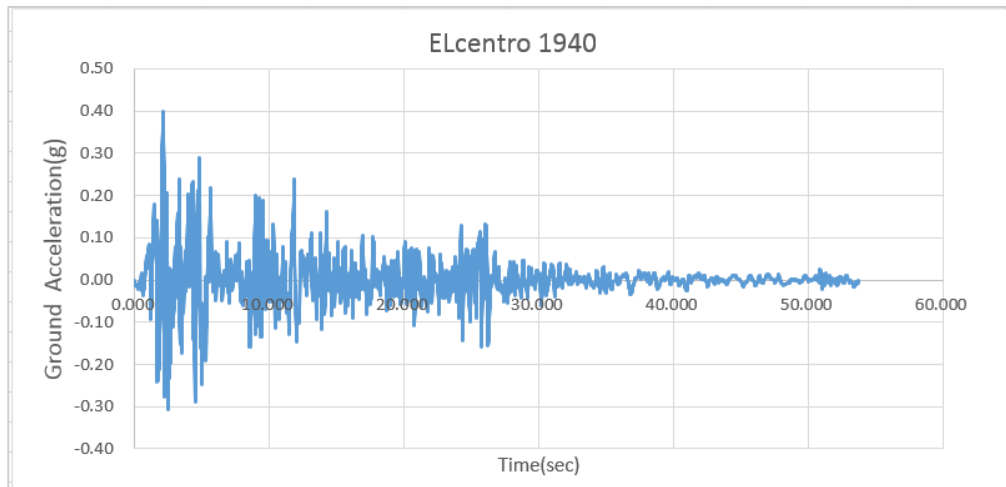
Figure 4.27- Performance point of Case2



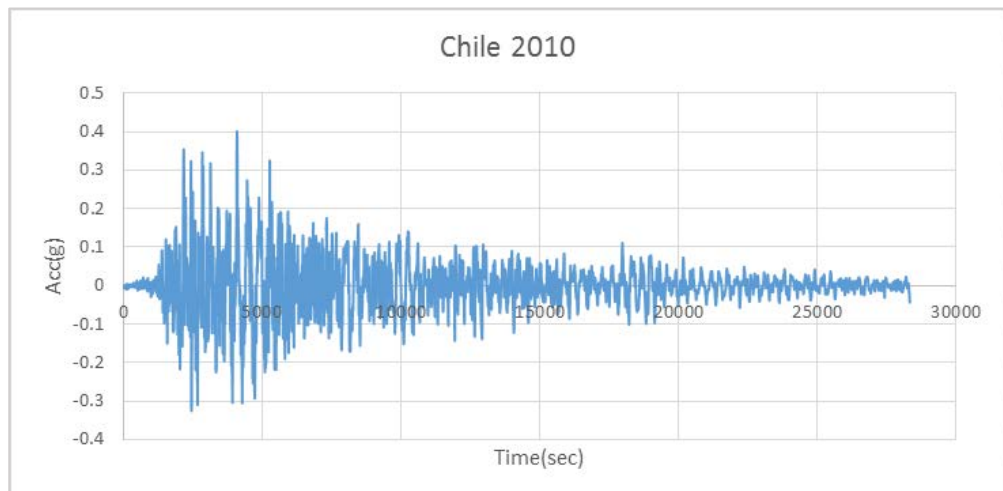
(a) Performance point of Case3 in x direction (b) Performance point of Case3 in y direction

Figure 4.28- Performance point of Case3

For the nonlinear time history analysis, two actual ground motions, Elcentro 1940 and Chile 2010 records, were used in this study and they were adjusted with a PGA of 0.4g to match the design response spectrum.



(a) Time-history record of Elcentro 1940



(b) Time-history record of Chile 2010

Figure 4.29 - Plot of time-history record with scaled 0.4g PGA

Thus, the maximum displacements of decks can be obtained and the results are compared in Table 4.9. The maximum displacements of NLTH are the average values obtained from Elcentro 1994 and Chile 2010. As 20% error is acceptable between results

of response spectrum and time history analysis, the difference between the pushover results and nonlinear time history demonstrated here is reasonable.

Table 4.9 - Comparison of Pushover and NLTH results

	Direction	Case1		Case2		Case3	
		x	y	x	y	x	y
MAX DISP. (in)	NLTH	1.62	1.53	2.47	2.88	3.35	3.82
	PUSHOVER	2.07	1.85	2.11	2.46	3.28	3.52
	Difference (%)	27.78	20.92	14.57	14.58	2.09	7.85

CHAPTER 5: PARAMETRIC STUDY

Different parameters may affect the behavior of IABs under seismic loads. The parameters studied here are bearing condition and planar layout. A series of parametric study has been performed to study the effect of these parameters on the capacity of the bridges.

5.1 Comparison of fully integral abutment and semi-integral abutment bridges

A parametric study was performed on the variation of bearing at the abutment stem. For the three cases studied in chapter 4, case 1 is a fully integral abutment bridge (IAB) and cases 2 and 3 are semi-integral abutment bridges (SIAB). In this study, by changing the bearing restraint, the bridges in the integral abutment and semi-integral abutment of all three cases were analyzed.

The dynamic modes, pushover curves and performance point are compared in this section.

1. Dynamic modes-

The modal analysis was done on the IAB and SIAB bridges. The modal shapes are similar in the same mode. However, the period and frequency of each mode are slightly different, for the bridges with fully integral abutment have a higher stiffness, the period of each mode become smaller. The modal periods and frequencies of three cases are listed in Tables 5.1-5.3.

Table 5.1- Comparison of IAB (Case 1) and SIAB on single span bridges

Modes	IAB		SIAB		Comparison	
No.	T(sec)	f(Hz)	Ts(sec)	fs(Hz)	Ts/T	fs/f
1	0.3386	2.9536	0.3424	2.9202	1.0114	0.9887
2	0.2916	3.4293	0.2983	3.3528	1.0228	0.9777
3	0.2570	3.8909	0.2621	3.8160	1.0196	0.9808
4	0.2174	4.6001	0.2175	4.5972	1.0006	0.9994
5	0.1567	6.3832	0.1567	6.3817	1.0002	0.9998
6	0.1106	9.0387	0.1110	9.0054	1.0037	0.9963
7	0.1062	9.4202	0.1068	9.3677	1.0056	0.9944
8	0.1052	9.5073	0.1062	9.4172	1.0096	0.9905
9	0.0716	13.9714	0.0722	13.8592	1.0081	0.9920
10	0.0626	15.9753	0.0626	15.9728	1.0001	0.9998
11	0.0598	16.7320	0.0598	16.7253	1.0004	0.9996
12	0.0564	17.7395	0.0566	17.6739	1.0037	0.9963

Table 5.2- Comparison of IAB and SIAB (Case 2) on single span skew bridges

Modes	IAB		SIAB		Comparison	
No.	T(sec)	f(Hz)	Ts(sec)	fs(Hz)	Ts/T	fs/f
1	0.5889	1.6980	0.5893	1.6968	1.0007	0.9993
2	0.5163	1.9369	0.5173	1.9331	1.0019	0.9981
3	0.4558	2.1938	0.4570	2.1883	1.0025	0.9975
4	0.4118	2.4286	0.4128	2.4224	1.0026	0.9974
5	0.3167	3.1577	0.3172	3.1523	1.0017	0.9983
6	0.1727	5.7904	0.1728	5.7873	1.0005	0.9995
7	0.1679	5.9551	0.1682	5.9455	1.0016	0.9984
8	0.1284	7.7883	0.1285	7.7813	1.0009	0.9991
9	0.1166	8.5767	0.1166	8.5760	1.0001	0.9999
10	0.1005	9.9550	0.1006	9.9402	1.0015	0.9985
11	0.0974	10.2702	0.0974	10.2692	1.0001	0.9999
12	0.0903	11.0718	0.0904	11.0660	1.0005	0.9995

Table 5.3 - Comparison of IAB and SIAB (Case3) on 3-span bridges

Modes	IAB		SIAB		Comparison	
No.	T(sec)	f(Hz)	Ts(sec)	fs(Hz)	Ts/T	fs/f
1	0.6140	1.6286	0.6141	1.6283	1.0002	0.9998
2	0.5943	1.6825	0.6047	1.6538	1.0174	0.9829
3	0.4488	2.2283	0.4499	2.2225	1.0026	0.9974
4	0.4239	2.3589	0.4241	2.3581	1.0003	0.9997
5	0.4178	2.3932	0.4203	2.3793	1.0058	0.9942
6	0.2866	3.4886	0.2892	3.4581	1.0088	0.9913
7	0.2671	3.7441	0.2735	3.6559	1.0241	0.9765
8	0.2611	3.8300	0.2625	3.8091	1.0055	0.9946
9	0.2499	4.0020	0.2550	3.9222	1.0204	0.9800
10	0.2394	4.1775	0.2395	4.1752	1.0005	0.9995
11	0.2240	4.4646	0.2240	4.4642	1.0001	0.9999
12	0.2181	4.5843	0.2184	4.5796	1.0010	0.9990

2. Pushover curves-

The force-displacement curves of IAB and SIAB in each case were obtained from the pushover analysis in global-x (longitudinal) and global-y (transverse) directions. The pushover curves of IAB and SIAB are plotted in the same figure (Figures 5.1-5.6) for comparison. It can be observed that, comparing to the pushover curve of SIAB in the x direction, the curve of IAB shows a higher force demand when reaches the same displacement. For the bearing pad in SIAB do not restrain in the longitudinal direction, it is reasonable to have larger flexibility in this direction. In the y direction, the effect is not so obvious.

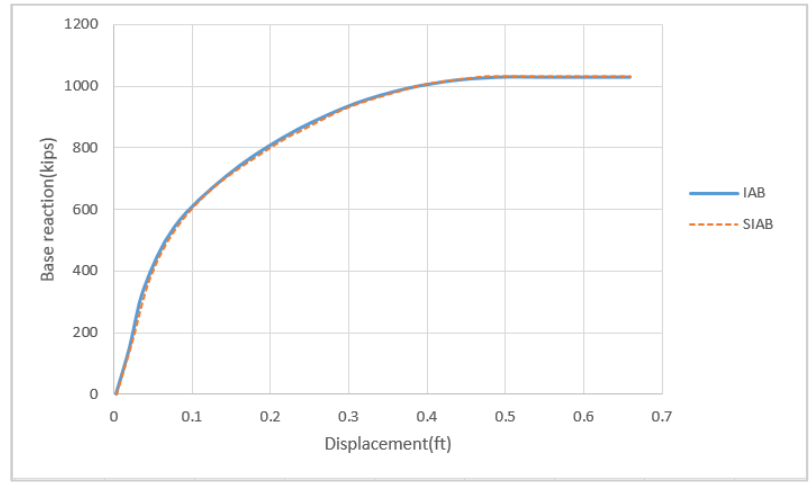


Figure 5.1-Pushover curve comparison in the x-direction of case1

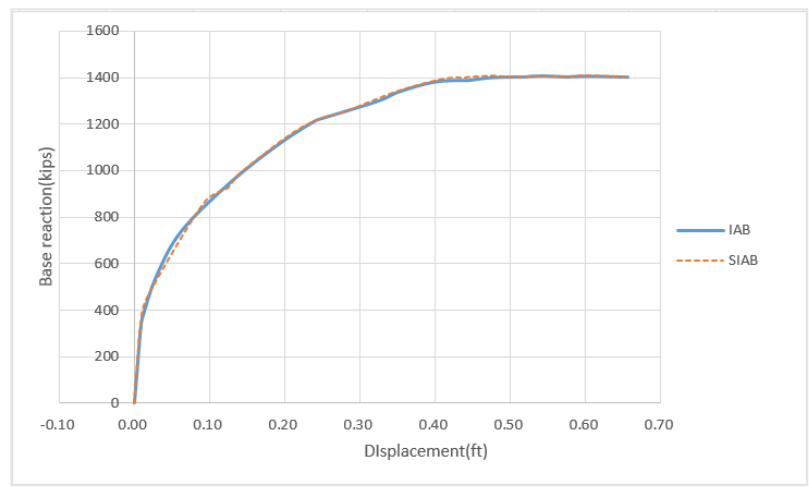


Figure 5.2 - Pushover curve comparison in the y-direction of case1

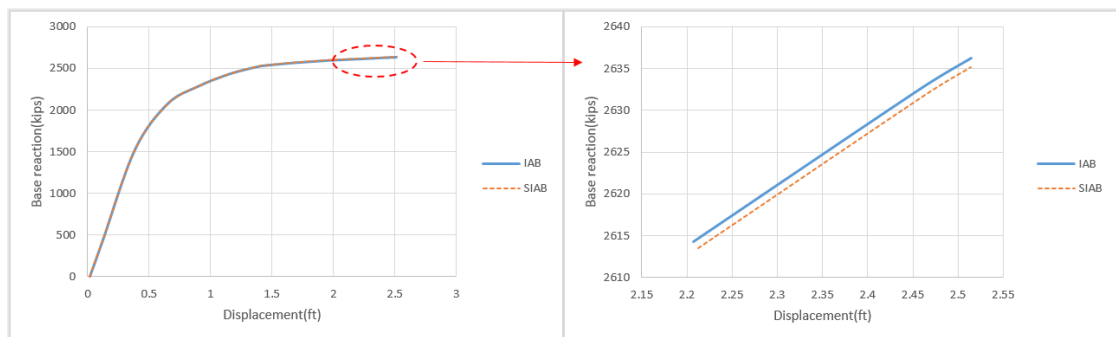


Figure 5.3 - Pushover curve comparison in the x-direction of case2

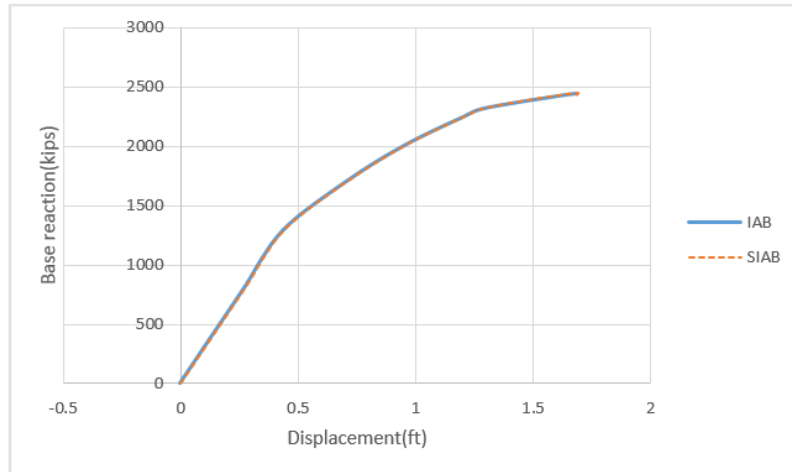


Figure 5.4- Pushover curve comparison in the y-direction of case2

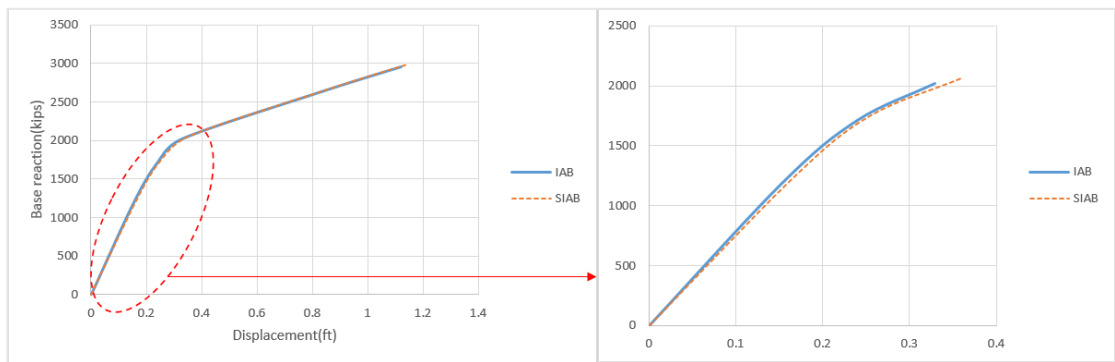


Figure 5.5- Pushover curve comparison in the x-direction of case3

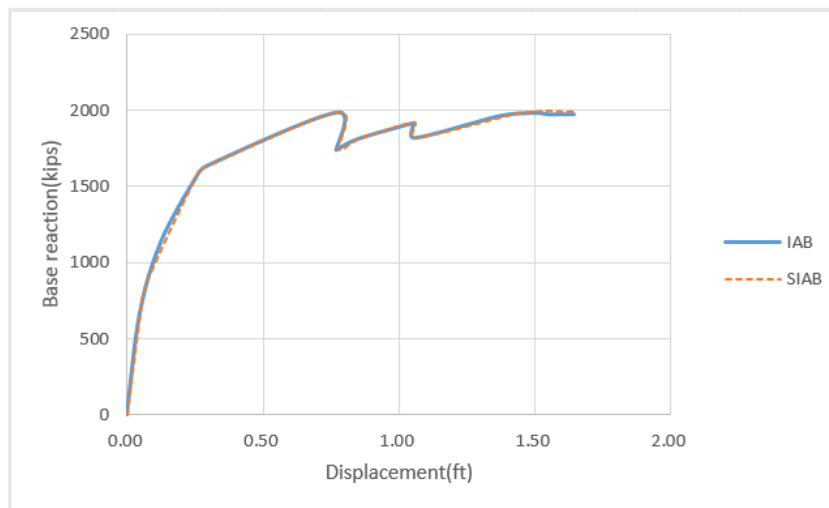


Figure 5.6- Pushover curve comparison in the y-direction of case3

3. Performance point-

The spectrum capacity method was also used to estimate the maximum displacement on deck under the earthquake of various intensities in both IAB and SIAB. In general, the IABs have smaller displacement for the improvement in monolithic stiffness.

Table 5.4 – Performance point value of single span IAB and SIAB (Case1)

Ca&Cv	Pushover direction	IAB		SIAB	
		V (kips)	D(ft)	V (kips)	D(ft)
0.4g	x	624.800	0.110	634.220	0.113
	y	913.884	0.117	913.161	0.119
0.5g	x	705.866	0.143	704.323	0.145
	y	1032.412	0.160	1035.585	0.160
0.6g	x	765.503	0.177	764.260	0.179
	y	1144.310	0.207	1149.653	0.206

Table 5.5 - Performance point value of single skew IAB and SIAB (Case2)

Ca&Cv	Pushover direction	IAB		SIAB	
		V (kips)	D(ft)	V (kips)	D(ft)
0.4g	x	529.135	0.142	535.846	0.144
	y	598.372	0.201	603.702	0.204
0.5g	x	646.804	0.171	655.374	0.173
	y	747.546	0.251	753.572	0.255
0.6g	x	763.964	0.199	774.423	0.202
	y	887.068	0.298	894.195	0.302

Table 5.6 - Performance point value of 3-span IAB and SIAB (Case3)

Ca&Cv	Pushover direction	IAB		SIAB	
		V (kips)	D(ft)	V (kips)	D(ft)
0.4g	x	1724.510	0.244	1726.789	0.250
	y	1306.363	0.177	1290.144	0.181
0.5g	x	1901.587	0.295	1893.913	0.303
	y	1498.979	0.235	1512.377	0.238
0.6g	x	2043.038	0.347	2041.201	0.352
	y	1646.800	0.306	1645.123	0.311

5.2 Comparison of skew and non-skew bridges

To study the effect of skew, a non-skew bridge with same dimensions as the skew bridge in case 2, except of the skew angle of the abutment, was modeled. The 3-D finite element model is shown in Figure 5.7.

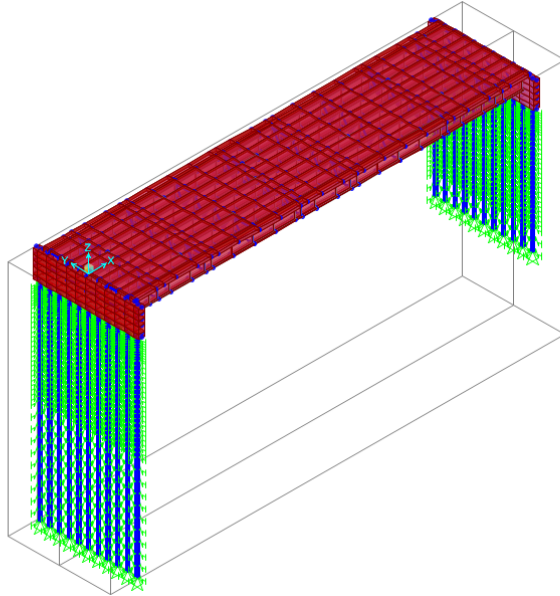


Figure 5.7-3D model of non-skew bridge

1. Dynamic modes-

First, a modal analysis was conducted on the non-skew bridge. Their mode shapes are similar. However, because of the nature of skew, the stiffness in modes is different from that of non-skew bridge. For example, for the second mode, which is mainly in the y direction, the non-skew bridge is more flexible; for the fifth mode, the torsional mode, the skew bridge has a longer period because the skewness always yields a trend of torsion. Thus, compared to the skew bridge, the period of non-skew bridge is lower or higher, depending on different modes. The period and frequency value of the first 10 modes of the two bridges are listed in Table 5.7.

Table 5.7- Comparison of dynamic modes between skew and non-skew bridges

Modes	Skew		Non-skew	
	No.	T1(sec)	f1(Hz)	T2(sec)
1	0.5893	1.6968	0.5810	1.7212
2	0.5173	1.9331	0.5312	1.8827
3	0.4570	2.1883	0.4462	2.2414
4	0.4128	2.4224	0.4099	2.4396
5	0.3172	3.1523	0.3247	3.0800
6	0.1728	5.7873	0.1738	5.7533
7	0.1682	5.9455	0.1702	5.8757
8	0.1285	7.7813	0.1296	7.7154
9	0.1166	8.5760	0.1126	8.8824
10	0.1006	9.9402	0.0972	10.2860

Without the effect of skewness, the locations of plastic hinges are changed, as shown in Table 5.8

The location with maximum negative moment on piles become symmetrical in both directions for non-skew case; the locations of maximum negative moment become lower.

Table 5.8- Comparison of the locations of plastic hinges in skew and non-skew cases

		Skew		Non-skew	
		Pile		Pile	
		First abut.	Last abut.	First abut.	Last abut.
Location (distance in feet from the top of each pile)	x	0	0	0	0
		16	16	18	18
	y	0	0	0	0
		-	16	22	22
		-	18	-	-

The sequence of plastic hinge occurrences in non-skew bridge is slightly different from those in skew bridge, as shown in Figures 5.8 and 5.9. For more detailed

information of plastic hinge status of each step and numbers of hinges are listed in Table 5.9.

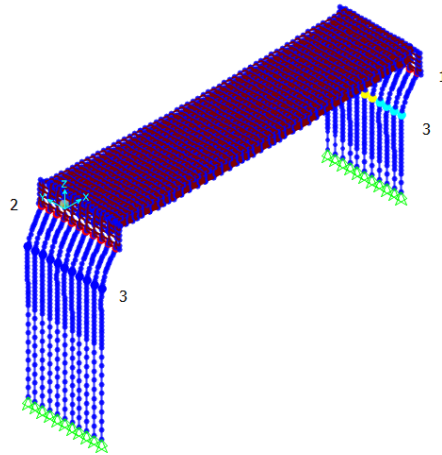


Figure 5.8-Order of occurrence of plastic hinges in the global x direction (non-skew bridge)

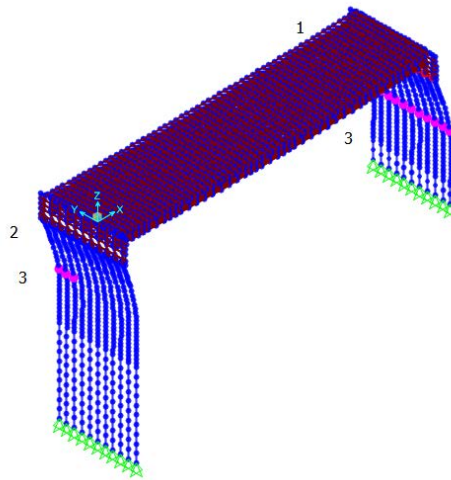


Figure 5.9- Order of occurrence of plastic hinges in the global y direction (non-skew bridge)

Table 5.9- Numbers of hinges occurred in stages (non-skew bridge-x)

step	Disp.(ft)	Base Force(kips)	A-B	B-IO	IO-LS	LS- CP	CP- C	C-D	D-E	Beyond E	Total
0	0	0	110	0	0	0	0	0	0	0	110
1	0.24	1293.36	99	0	11	0	0	0	0	0	110
2	0.3	1663.03	99	0	0	0	0	11	0	0	110
3	0.43	1877.51	99	0	0	0	0	11	0	0	110
4	0.67	2114.87	88	0	0	4	0	18	0	0	110
5	0.68	2116.88	88	0	0	0	0	22	0	0	110
6	0.82	2136.33	88	0	0	0	0	22	0	0	110
7	0.96	2146.21	88	0	0	0	0	22	0	0	110
8	0.99	2147.39	88	0	0	0	0	11	11	0	110
9	0.99	2147.39	88	0	0	0	0	11	0	11	110
10	1.16	2162.25	88	0	0	0	0	11	0	11	110
11	1.38	2212.87	88	0	0	0	0	0	10	12	110
12	1.38	2212.75	88	0	0	0	0	0	0	22	110
13	1.55	2253.36	88	0	0	0	0	0	0	22	110
14	1.94	2377.27	44	0	22	16	0	6	0	22	110
15	1.94	2329.46	44	0	22	16	0	0	0	28	110
16	1.96	2333.55	44	0	22	0	0	16	0	28	110
17	1.97	2205.15	44	0	22	0	0	0	0	44	110
18	2.15	2237.91	44	0	0	0	0	22	0	44	110
19	1.82	2044.08	44	0	0	0	0	22	0	44	110

Table 5.10 - Numbers of hinges occurred in stages (non-skew bridge-y)

step	Disp.(ft)	Base Force(kips)	A-B	B-IO	IO-LS	LS- CP	CP- C	C-D	D-E	Beyond E	Total
0	0	0	110	0	0	0	0	0	0	0	110
1	0.25	690.59	110	0	0	0	0	0	0	0	110
2	0.45	1237.86	106	4	0	0	0	0	0	0	110
3	0.72	1633.25	88	0	22	0	0	0	0	0	110
4	0.97	1900.43	88	0	22	0	0	0	0	0	110
5	1.22	2103.19	88	0	22	0	0	0	0	0	110
6	1.47	2282.5	88	0	18	4	0	0	0	0	110
7	1.74	2451.03	80	8	11	10	0	1	0	0	110
8	1.75	2452.82	80	8	11	8	0	3	0	0	110
9	1.76	2440.75	78	10	11	7	0	4	0	0	110
10	1.77	2416.03	76	12	11	6	0	5	0	0	110
11	1.77	2383.38	72	16	11	5	0	6	0	0	110
12	1.75	1973.82	60	28	11	0	0	5	0	6	110

2. Pushover curves-

The force-displacement curves of skew and non-skew bridge are plotted in the same Figure for comparison in x and y directions in Figures 5.10 and 5.11, respectively. It can be observed that in the x direction, non-skew bridge has a higher stiffness in elastic stage; in plastic stage, its stiffness decreased faster than the stiffness of skew bridge. In the y direction, the skew bridge has a relatively higher stiffness in elastic and inelastic stages.

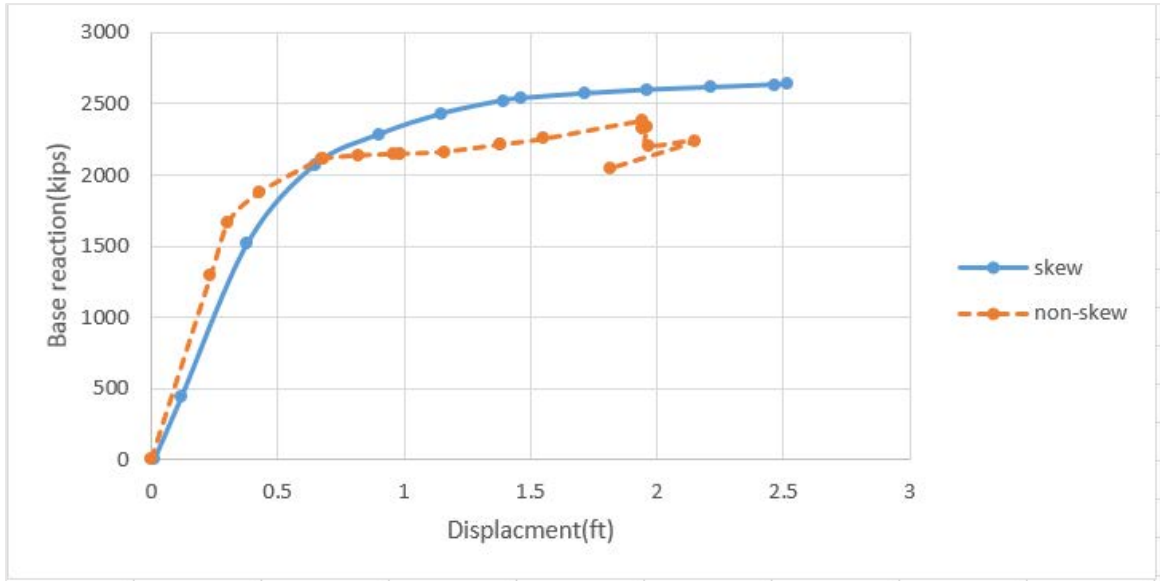


Figure 5.10-Pushover curves of skew and non-skew bridge in the x direction

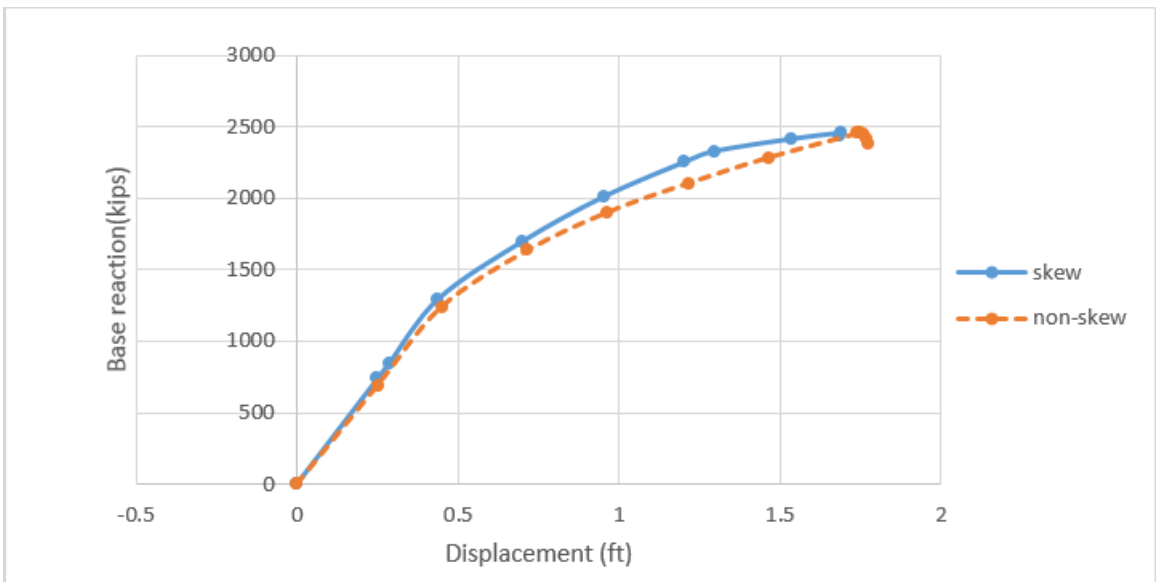


Figure 5.11-Pushover curves of skew and non-skew bridge in the y direction

Performance point-

The spectrum capacity method was conducted to estimate the maximum displacement on deck under the earthquake of various intensities in skew and non-skew bridges. The non-skew bridge is more flexible and has a larger displacement under

specified seismic loads compare to the skew one. Values to performance points are listed in Table 5.11.

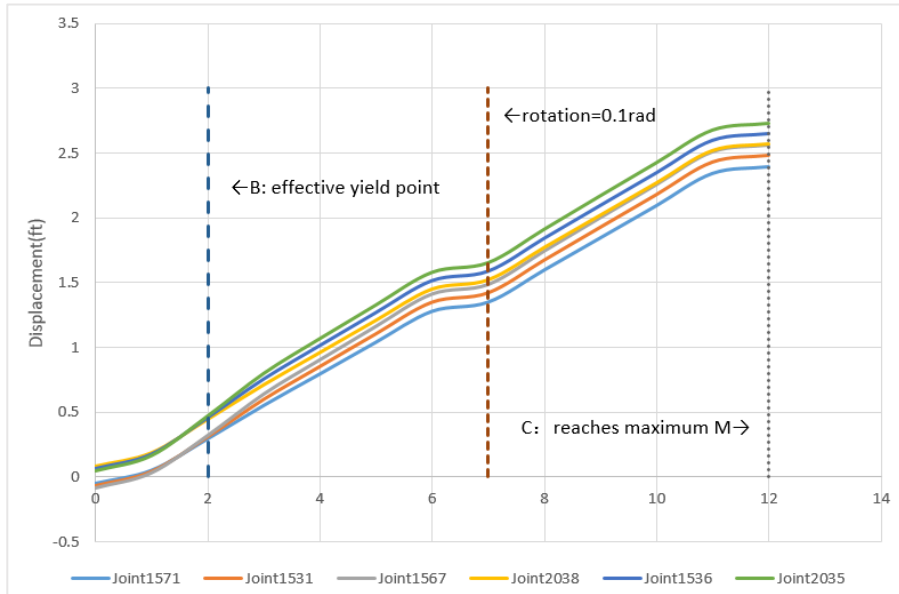
Table 5.11 -Performance point value of skew and non-skew bridges

Ca&Cv	Pushover direction	Skew		non-skew	
		V (kips)	D(ft)	V (kips)	D(ft)
0.4g	x	535.846	0.144	1245.324	0.277
	y	603.702	0.204	907.07	0.329
0.5g	x	655.374	0.173	1500.321	0.283
	y	753.572	0.255	1133.837	0.411
0.6g	x	774.423	0.202	1706.93	0.33
	y	894.195	0.302	1291.586	0.485

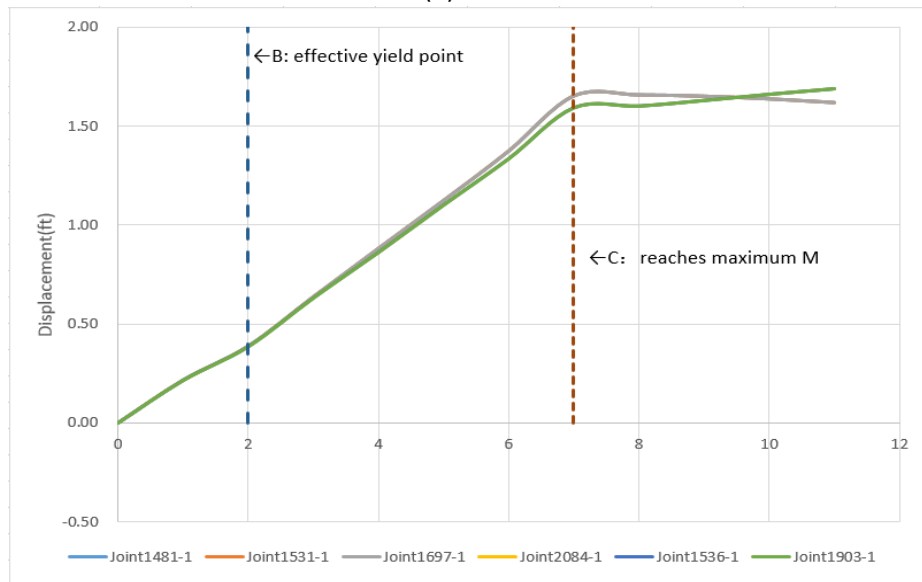
Displacement at the top of piles:

The following figures show the displacements at the top of piles at different locations. Joint 1571, 1531 and 1567 are the joints at the top of pile at the acute angle, midpoint and obtuse angle at the first abutment in skew bridge, respectively; joint 2035, 1536 and 2038 are the joints at the top of pile at the acute angle, midpoint and obtuse angle at the last abutment in skew bridge, respectively. The joint 1481, 1531 and 1697 are the top of pile at the left corner, midpoint and right corner at the first abutment in non-skew bridge, respectively; the joint 2084, 1536 and 1903 are the top of pile at the left corner, midpoint and right corner at the second abutment in non-skew bridge, respectively. The figures are also marked with the displacement of effective yield point (point B), the displacement where the rotation reaches 0.1 rad and the displacement where the section reaches its maximum moment (point C). The displacements at the top of the piles are different in both two directions in the skew bridge due to the skew angle as shown in

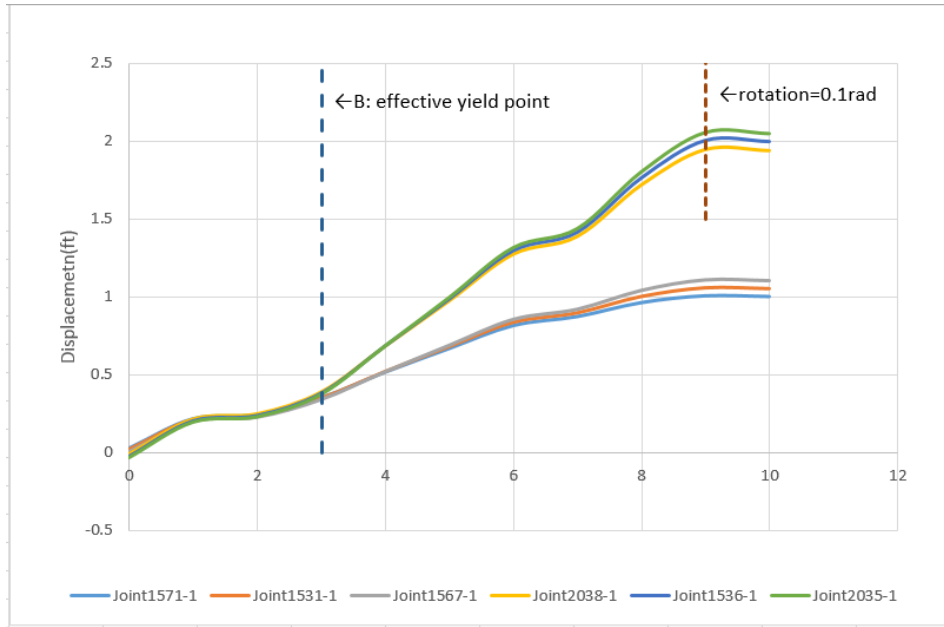
Figure 5.12(a) and 5.13(b). Compare to the displacement in non-skew bridge as shown in Figure 5.12(b) and 5.13(b), the skew bridge has higher capacity displacement.



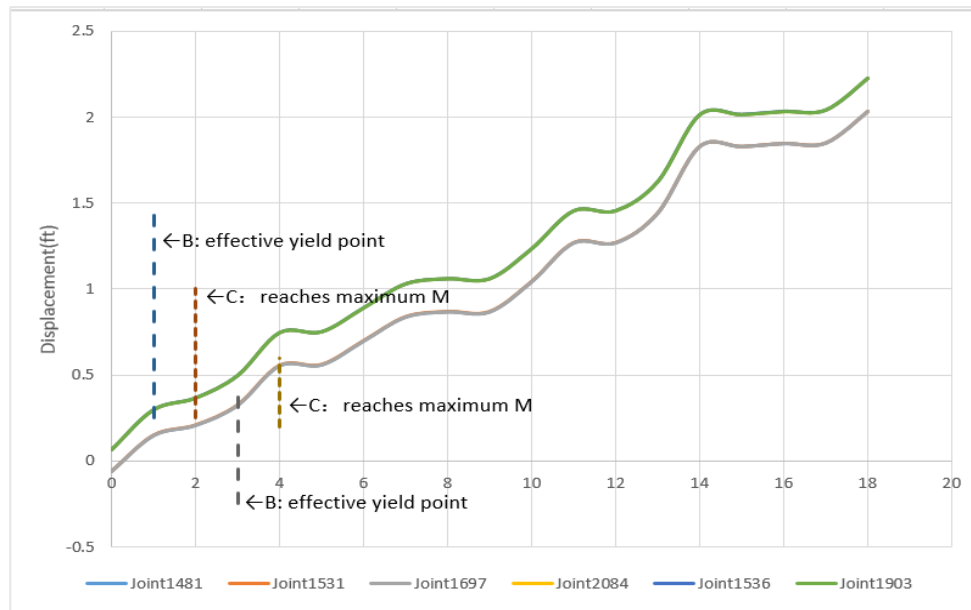
(a) Displacement at the top of piles in skew bridge
(b)



(b) Displacement at the top of piles in non-skew bridge
Figure 5.12-Pile displacement comparison (x-direction)



(a) Displacement at the top of piles in skew bridge



(b) Displacement at the top of piles in non-skew bridge
 Figure 5.13- Pile displacement comparison (y-direction)

CHAPTER 6: CONCLUSIONS

6.1 Conclusions

In this study, the capacity of integral abutment bridges (IABs) in both longitudinal and transverse direction were discussed by performing the pushover analysis in 3-D finite element models. Then the seismic behavior was evaluated by capacity spectrum method. The seismic design procedure for IABs based on capacity spectrum method is provided as a guideline.

1. Pushover results

By performing the pushover analysis on the structures, the elastic design of the structure can be checked and the potential failure mechanism of structure under severe earthquake can be determined.

The location and sequence of plastic hinge occurrences were obtained from the pushover analysis. The sections at the top of piles went into plastic stage first and then the sections at the location with maximum negative moment followed. Locations of maximum negative moment on piles are different in the longitudinal and transverse directions. The whole structure remains elastic when the piles started yielding for these “weak links” protect the structure system.

The parametric study revealed the different response behavior by comparing integral abutment bridge and semi-integral abutment bridges, skew and non-skew bridges. In the comparison of integral abutment bridges and semi-integral abutment bridges, as

expected, IABs have higher stiffness and smaller displacement under the same magnitude of earthquake compared to the SIABs. In the comparison of skew and non-skew bridges,

- (1) Locations of plastic hinges at the maximum negative moment on piles are different;
- (2) In the global x (longitudinal) direction, non-skew bridge has a higher stiffness in elastic stage; in plastic stage, its stiffness lower than the stiffness of skew bridge;
- (3) In the global y (transverse) direction, the skew bridge has a relatively higher stiffness in both elastic and inelastic stages.

2. Seismic Design procedure for IABs based on capacity spectrum method.

Guidelines for the seismic design of integral abutments based on capacity spectrum method were developed. Design procedures were developed to:

Establish structural analysis model with the parameters from shop drawings;

Conduct modal analysis to find out the first multiple longitudinal and transverse modes;

Perform the pushover analysis to obtain the force-displacement curve;

Convert the force-displacement curve into capacity spectrum with the spectrum displacement as the abscissa and spectrum acceleration as the ordinate;

Obtain the acceleration response spectrum from code or time-history record and then convert it to demand spectrum, which is also the relationship between spectrum

acceleration and spectrum displacement;

Find the intersection point (performance point) by overlapping the capacity curve from step (4) and demand curve obtained from step (5); if there is no intersection point, it means the structure does not have collapse resistance;

Identify performance behavior of the structure, if it meets the prescribe target, the design is completed, if not, then turn back to the first step to revise the parameters of the structure to meet the demand of seismic resistance.

A flow chart of the seismic design procedure is shown in in Figure 6.1.

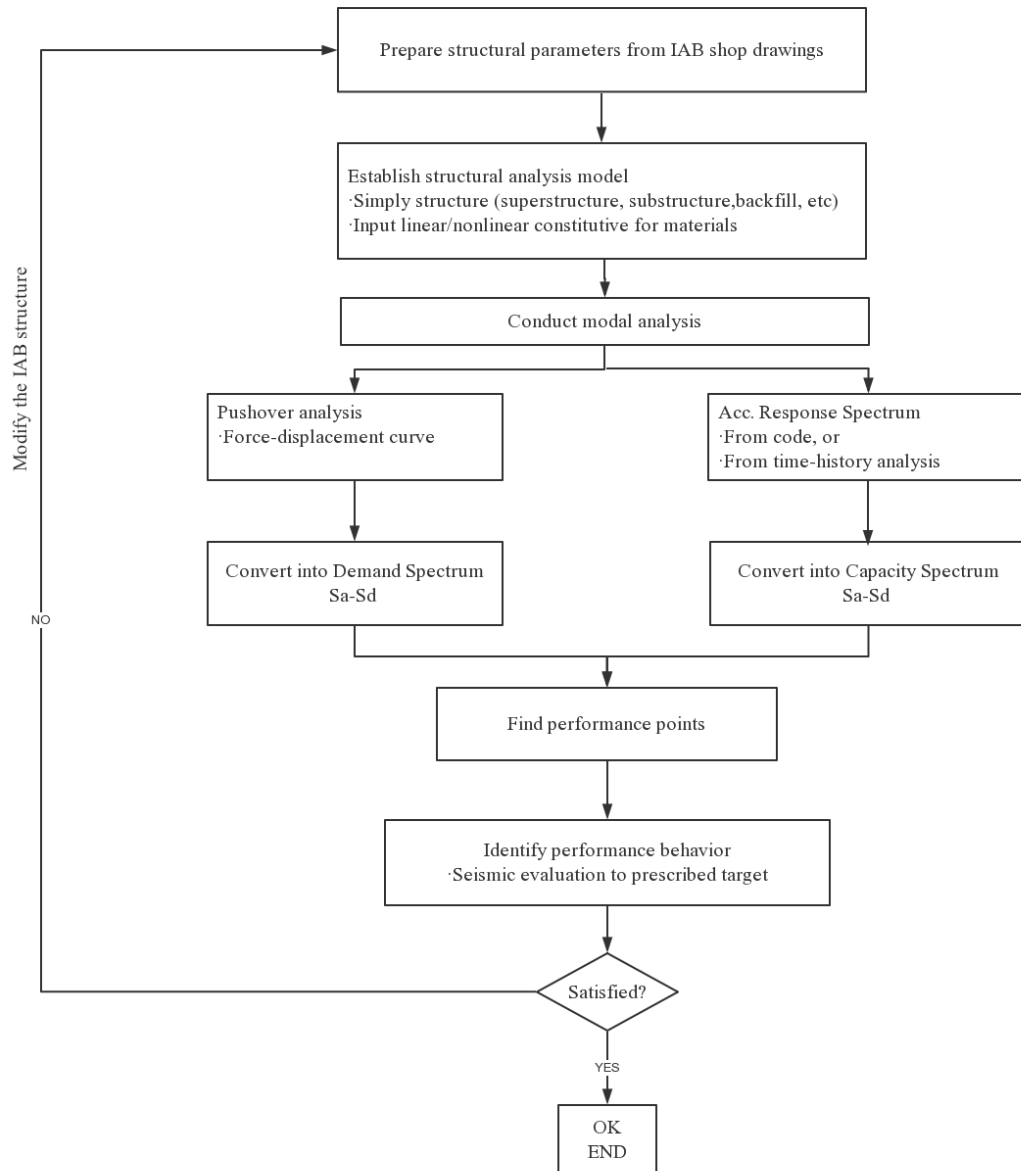


Figure 6.1-Flow chart of seismic design procedure for IABs based on capacity spectrum method

3 Suggestions on seismic design

- (1) The top of piles are the weakest part of the whole structure so it should be well connected with the abutment to make a better performance.
- (2) To guarantee the potential plastic hinges occurred at the top of piles, in high

seismicity region, conventional bearing in semi-integral abutment could be replaced into the earthquake-resistance bearing to absorb earthquake energy.

- (3) While conducting soil-structure interaction analysis, properties of soil springs should be considered carefully in that the soil-structure interaction has significant effect on the structural response. Soil parameters used in simulation should be provided by the geological data from shop drawings if it is available.
- (4) Seismic design should be in consistent with other principal loading cases, such as live load, thermal action.

6.2 Future work

The goal of this study is to investigate the capacity of the integral abutment bridges under the seismic loads and give the guidelines for the seismic design of integral abutments based on capacity spectrum method.

The construction joint on the abutment stem has not been taken into account in this study.

Compared to the complicity of nonlinear time-history analysis method, the simplified capability spectrum method is convenient for seismic design. However, for a more complex structure, multi modal pushover analysis is more accurate, since the influence of high-order mode shapes cannot be ignored. For this type of bridges, the simplified capacity spectrum which based on the fundamental mode is not accurate enough. How to properly consider the influence of high-order mode shapes should be

included for further study.

To obtain the contribution of different part of the structure, the behavior of superstructure and substructures like abutment and piles can be monitored separately to observe the energy dissipation in each part. In this way, the seismic behavior of structures can be observed more accurately and the seismic design could be more economic.

REFERENCE

AASHTO. (2006). *AASHTO LRFD Bridge Design Specifications* (4th ed.). Washington, D.C.: American Association of State Highway and Transportation Officials.

Ahmed, M. S. E. I. (2010). Seismic assessment of curved bridges using modal pushover analysis. University of Maryland, College Park.

Arockiasamy M, Butrieng N, Sivakur M (2004) State-of-the art of integral abutment bridges: design and practice. *J Bridge Eng* 9(5):497–506

Bhowmick A (2003) Design and construction of integral bridges—an innovative concept. *Indian Concr J* 77(7):1203–1209

Briseghella B, Zordan T (2015) An innovative steel-concrete joint for integral abutment bridges. *J Traffic Transp Eng* 2(4):209–222

Broms, M., Lateral Resistance of Piles in Cohesionless Soils. *Journal of the Soil Mechanics and Foundations Division* © ASCE / May 1964

Cristian-Claudiu Comisu. (2005). Integral abutment and jointless bridges. *Bulletin of the Polytechnic Institute of Jassy: Constructions, Architecture Section*,(lv)(1-2), 107-118.

Dicleli M, Erhan S (2011) Live load distribution formulas for single-span prestressed concrete integral abutment bridge girders. *J Bridge Eng* 14(6):472–486

Easazadeh Far, N., & Barghian, M. (2014). Safety identifying of integral abutment bridges under seismic and thermal loads. *The Scientific World Journal*, 2014, 1-12. doi:10.1155/2014/757608

Eberhard, M., Member, ASCE., & Marsh, M., Associate Member, ASCE. (1997). Lateral-Load response of a reinforced concrete bridge. *Journal of Structural Engineering*, 123(4), 451-460. doi:10.1061/(ASCE)0733-9445(1997)123:4(451)

Erhan, S., & Dicleli, M. (2017). Parametric study on the effect of structural and geotechnical properties on the seismic performance of integral bridges. *Bulletin of Earthquake Engineering: Official Publication of the European Association for Earthquake Engineering*, 15(10), 4163-4191. doi:10.1007/s10518-017-0123-9

Franchin, P., & Pinto, P. (2014). Performance-based seismic design of integral abutment bridges. *Bulletin of Earthquake Engineering: Official Publication of the European Association for Earthquake Engineering*, 12(2), 939-960. doi:10.1007/s10518-013-9552-2

Frosch, R. J., Wenning, M., & Chovichien, V. (2005). The in-service behavior of integral abutment bridges: Abutment-pile response. In *Integral Abutment and Jointless Bridges (IAJB 2005)* Federal Highway Administration West Virginia Department of Transportation.

Kalayci, E., Civjan, S., & Breña, S. (2012). Parametric study on the thermal response of

curved integral abutment bridges. *Engineering Structures*, 43, 129-138.

doi:10.1016/j.engstruct.2012.05.007

Marsh, M., Stringer, S., National Research Council (U.S.). Transportation Research Board, National Cooperative Highway Research Program, American Association of State Highway and Transportation Officials, & United States. Federal Highway Administration. (2013). *Performance-based seismic bridge design* (NCHRP synthesis, 440). Washington, D.C.: Transportation Research Board.

Monzon, E. V., Itani, A. M., & Pekcan, G. (2014). Seismic behavior and design of steel girder bridges with integral abutments. *Bridge Structures*, 10(4), 117-128.

Mohebbi, A. (2013). Seismic response of a highway bridge with structural fuses for seismic protection of piers. University of Nevada, Reno

Paraschos, A., & Amde, A. M. (2011). A survey on the status of use, problems, and costs associated with Integral Abutment Bridges. New York City Department of Transportation.

Robert J. Frosch, Michael E. Kreger & Aaron M. Talbott (2008) Earthquake resistance of integral abutment bridge, FHWA/IN/JTRP-2008/11

Song, S. T., Chai, Y. H., & Hale, T. H. (2004, August). Limit state analysis of fixed-head concrete piles under lateral loads. In 13th World Conference on Earthquake Engineering, Vancouver, BC, Canada.

Spyrakos C, Loannidis G (2003) Seismic behaviour of post-tensioned integral bridge including soil-structure interaction. *Soil Dyn Earthq Eng* 23:53–63

Wolde-Tinsae, A., Klinger, J., & Maryland. State Highwa Administration.(1987).*Integral abutment bridge design and construction : [state-of-the-art studies]*(Research report / FHWA/MD-87/07). Baltimore, Md.: Maryland Dept. of Transportation, State Highway Administration.

XTRACT v3.0.8. (2007) Cross-sectional X structural analysis of components.

TRC/Imbsen Software Systems, Rancho Cordova

Zordan, T., Briseghella, B., & Lan, C. (2011). Parametric and pushover analyses on integral abutment bridge. *Engineering Structures*, 33(2), 502-515.

doi:10.1016/j.engstruct.2010.11.009